1-1-2016

Thermoelectric enhancement of different kinds of metal chalcogenides

Chao Han
University of Wollongong, ch861@uowmail.edu.au

Qiao Sun
Soochow University, China, qsun@uow.edu.au

Zhen Li
University of Wollongong, zhenl@uow.edu.au

S X. Dou
University of Wollongong, shi@uow.edu.au

Thermoelectric enhancement of different kinds of metal chalcogenides

Abstract

Due to the urgency of our energy and environmental issues, a variety of cost-effective and pollution-free technologies have attracted considerable attention, among which thermoelectric technology has made enormous progress. Substantial numbers of new thermoelectric materials are created with high figure of merit (ZT) by using advanced nanoscience and nanotechnology. This is especially true in the case of metal-chalcogenide-based materials, which possess both relatively high ZT and low cost among all the different kinds of thermoelectric materials. Here, comprehensive coverage of recent advances in metal chalcogenides and their correlated thermoelectric enhancement mechanisms are provided. Several new strategies are summarized with the hope that they can inspire further enhancement of performance, both in metal chalcogenides and in other materials.

Disciplines

Engineering | Physical Sciences and Mathematics

Publication Details

Han, C., Sun, Q., Li, Z. & Dou, S. X. (2016). Thermoelectric enhancement of different kinds of metal chalcogenides. Advanced Energy Materials, 6 (15), 1600498-1-1600498-36.

DOI: 10.1002/ ((please add manuscript number))
Article type: Review

Thermoelectric enhancement of different kinds of metal chalcogenides

Chao Han, Qiao Sun, Zhen Li, * *and Shi Xue Dou*

Mr. Chao Han, Prof. Qiao Sun, Prof. Zhen Li
Center for Molecular Imaging and Nuclear Medicine, School of Radiation Medicine and Protection, Medical College of Soochow University, Collaborative Innovation Center of Radiation Medicine of Jiangsu Higher Education Institutions, 199 Renai Road, Industrial Park, Suzhou, Jiangsu 215123, P.R. China
Email: zhenli@suda.edu.cn

Mr. Chao Han, Prof. Zhen Li, Prof. Shi Xue Dou
Institute for Superconducting and Electronic Materials, Australian Institute for Innovative Materials, University of Wollongong, Squires Way, North Wollongong, NSW 2500, Australia.

Keywords: metal chalcogenides, thermoelectrics, enhanced *ZT*, energy conversion, new strategies

Abstract: Due to the urgency of our energy and environmental issues, a variety of cost-effective and pollution-free technologies have attracted considerable attention, among which thermoelectric technology has made enormous progress. Substantial numbers of new thermoelectric materials have been created with high figure of merit (*ZT*) by using advanced nanoscience and nanotechnology. This is especially true in the case of metal chalcogenide based materials, which possess both relatively high *ZT* and low cost among all the different kinds of thermoelectric materials. This review provides comprehensive coverage of recent advances in metal chalcogenides and their correlated thermoelectric enhancement mechanisms. Several new strategies are summarized with the hope that they can inspire further enhancement of performance, both in metal chalcogenides and in other materials.

1. Introduction

As might be expected, nowadays, more than half of our primary energy is utilized in the form of heat. Examples include the usage of fossil fuels to power engines; the generation of electricity from steam power generators, etc. Nevertheless, the majority of energy actually produced by humans is lost in the form of waste heat. One example is in vehicles, where only ~10% of the energy produced from burning petrol in the internal combustion engine is converted to useful work, while the rest is wasted.[1] Another example is in steel works. According to the statistics,[2] around 10^9 J of heat would be wasted in the course of producing 1 ton of crude steel. The technologies for recovering waste heat are of great interest, because huge amounts of energy would be saved.

The phenomenon of thermoelectricity (TE), which has been known since the discoveries made by Seebeck, Peltier, and Thomson in the early 1800s, is such a technology that can convert heat into electricity directly via a solid-state conversion. Its basic working mechanism is very simple, i.e. when a material is heated, its charge carriers will flow from the hot side to the cold side to produce a voltage between them. A current will be produced when a load is connected, and the material works as a thermoelectricity generator (TEG); on the other hand, if the material is connected to a power source, the material works as a thermoelectric refrigerator (TER) when the temperature difference is maintained. The main metric for characterizing the performance of thermoelectric materials is the dimensionless "figure of merit" (ZT), which can be expressed by Equation (1):

$$ZT = \frac{S^2\sigma}{\kappa}T \quad (1)$$

In which S is the Seebeck coefficient, σ is the electrical conductivity, κ is the thermal conductivity, and $S^2\sigma$ is defined as the power factor (PF).

Thermoelectric technology has a few distinct advantages, including: (1) it is reliable and operates in silence compared with other energy conversion technologies, as it works without mechanical movement; (2) thermoelectric devices are simple, compact, and safe; (3) it is an environmentally friendly green technology, because no heat, no gases, and no chemical waste are produced during operation; (4) it can be

widely used in places where other energy conversion technologies are unavailable, such as in remote outer space.[3]

Although some typical applications of thermoelectric generators (TEGs) are illustrated in **Figure 1**, their current usage is in niche applications due to their extremely low energy conversion efficiency (η), which is defined in Equation (2):

$$\eta = \eta_c \times \frac{\sqrt{1+ZT}-1}{\sqrt{1+ZT}+T_C/T_H} \quad (2)$$

where η is the conversion efficiency of heat to electricity, T_c and T_h are the temperatures of the cold and the hot sides of a thermoelectric generator, respectively, and η_c represents the Carnot efficiency and can be expressed as $\eta_c = 1\text{-}T_c/T_h$. The equation clearly shows that conversion efficiency could be improved by increasing ZT. Unfortunately, S, σ, and κ are dependent on each other [as shown by Equations (3-5)], and it is very difficult to simultaneously optimize these three factors.

$$\sigma = ne\mu \quad (3)$$

$$S = A \times T \times \frac{m^*}{n^{3/2}} \quad (4)$$

$$\kappa = k_l + L\sigma e \quad (5)$$

n, e, and μ represent the charge carrier density, charge of the electron, and mobility of the charge carriers, respectively. A is a constant and equals to be $\frac{8\pi^2 k_B^2}{3eh^2}$, where k_B, e and h are the Boltzmann constant, charge of electron, and the Plank constant, respectively. m^* is the effective mass of charge carriers near the Fermi level, which is related to the band structure of the material. The thermal conductivity (κ) is composed of the phonon contribution (lattice thermal conductivity $\kappa_{L)}$ and the contribution from the charge carriers ($\kappa_e = L\sigma e$, where L is the temperature dependent Lorenz number). From Equations (3-5), it is easy to conclude that only κ_L is independent on S and σ.

The first generation of bulk thermoelectric materials was developed over four decades ago, with a ZT of ~0.8-1.0 and conversion efficiency (η) of 5-6% (from the 1950s to the 1990s). From a wide variety of research approaches to increase ZT, a near doubling of ZT at high temperatures has emerged and thus given rise to the second generation of bulk thermoelectric materials with ZT ranging from 1.3 to 1.7 and

an efficiency of 10% (1990s to 2010s).[4] The boosting of *ZT* is due to the optimization of existing materials using nanoscale precipitates and compositional inhomogeneity, in which abundant grain boundaries or defects can significantly decrease the lattice thermal conductivity (κ_L) while preserving a relatively high power factor. Continued progress has raised the *ZT* by a factor of 2, with the predicted efficiency increasing to over 20%, a highly exciting prospect which will surely have a large impact in the energy production and conservation fields.[4] There have been many reviews on the development of different kinds of thermoelectric materials, including PbTe,[5] oxides,[6] sulfides,[7] nanostructured thermoelectric materials,[8] etc.

There has been no comprehensive specific review, however, on all the different kinds of metal chalcogenide (MC) based thermoelectric materials despite their varieties, complexity and importance in the field of thermoelectrics. In this review, all kinds of MCs are first categorized based on the recent literatures. Then, their latest developments and the strategies behind their high performances are respectively demonstrated and discussed according to the classification.

2. Merits of metal chalcogenide based thermoelectric materials

The metal chalcogenides, a series of materials composed of both metal and chalcogen elements (S, Se, Te), have been attracting significant attention in a variety of energy applications, including solar cells, light-emitting diodes, sensors, batteries, supercapacitors, thermoelectric devices, etc.[9] Compared with oxides, metal chalcogenide based thermoelectric materials possess a higher power factor (PF = $S^2\sigma$) due to the less covalent nature of their bonds, arising from low electronegativity. Their heavy atomic weight compared to some other thermoelectric materials is of benefit for reducing thermal conductivity. In addition, the chalcogenides are easy to form into different kinds of structures, which offer a good platform for investigating and improving thermoelectric performance. Moreover, the chalcogenides are easily doped into *n*-type (by halides) or *p*-type (by pnictides) materials, which is important for the fabrication of TEGs. It has been proved by many reports that metal chalcogenide based thermoelectric materials possess excellent performance. For example, hitherto, the highest *ZT* value (*ZT* = 3.6 at 580 K)

was obtained in $PbSe_{0.98}Te_{0.02}$/PbTe quantum-dot superlattices (QDSLs) grown by the molecular beam epitaxy (MBE) approach;[10] a *ZT* of 2.6 was obtained at 923 K for a single crystal of SnSe;[11] and Na doped full-scale-structured PbTe exhibited a maximum *ZT* of 2.2 at 915 K.[12]

The superiority of metal chalcogenide based thermoelectric materials also lies in their low cost, both for material fabrication and for operation. As elucidated by **Figure 2**, Yadav et al. calculated the efficiency ratios of different kinds of materials, using their *ZT* values divided by their fabrication cost.[13] The efficiency ratios of metal chalcogenides (typically Bi_2Te_3 and PbTe, which are marked by red circles) are slightly lower than for oxides (e.g. ZnO) and Zn_4Sb_3 (marked by green circle) despite the relatively high price of Te element. ZnO, $NaCoO_2$, and Zn_4Sb_3 are unstable, however, at high temperature or in humid air.[13] LeBlanc et al.[14] evaluated the operating costs for TERs made from different thermoelectric materials under a constant temperature difference. They found that metal chalcogenide based materials possess both the highest *ZT* values and the lowest operating costs, as shown by **Figure 3**.

3. Statistics from reports on MC based TE materials

Due to the large numbers of reports on the thermoelectric performance of metal chalcogenides, we mainly focus on the thermoelectric performance of bulk metal chalcogenides reported since 2009. To give a comprehensive review, according to the statistics from 400 references, we have divided the MCs into nine groups based on their compositions and crystal structures **(Figure 4)**; their thermoelectric performance as well as the strategies used to enhance thermoelectric performance are summarized and discussed.

Groups 1-2 are bismuth and lead chalcogenides, respectively. More than 27% of the selected references are related to the traditional Bi-X (X = S, Se, Te) based thermoelectric materials due to their excellence. More than 12% are related to the Pb-X system, which is another group of traditional high performance thermoelectric materials.[5] Several different new strategies have been developed to enhance their performance, which are summarized in the section of *4.1 "Bi-X and Pb-X thermoelectric materials"*.

Group 3 is from the ternary A-B-X system, in which A is mainly Ag and Cu (group 11 or I_B), B is an element from the III_A, IV_A, and V_A group (groups 13-15, Al, Ga, In, Ge, Sn, As, Sb, Bi), and X is the chalcogen (S, Se, Te in group 16 or VI_A). Group 3 takes up around 14% in the total reports. Due to their complex compositions, the structures of A-B-X thermoelectric materials are varied, and can be generally classified into three types. The first type has diamond-like (or distorted diamond structures) and is usually stoichiometric ABX_2 compounds. The distorted crystal structures lead to relatively low thermal conductivity, and the medium bonding strength offers moderate electrical conductivity. The second type is from "non-stoichiometric" A-B-X (atomic ratio of A:B:X is not 1:1:2) compounds, which own complex crystal structures and behave like the so-called phonon glass electron crystals (PGECs). The third type has an amorphous structure with total random atomic arrangements, which usually shows extremely low thermal and electrical conductivity. By controlling the degree of crystallinity, the electrical conductivity of this type of A-B-X compounds can be improved while preserving relatively low thermal conductivity.

It should be noted that Tl-M-X, Mo-Sb-Te, Chevrel phase, and quaternary Cu-C-B-X compounds (with C another metal element) are also included in this group due to their similar mechanisms for achieving good thermoelectric performance. They take up around 4% of the total reports.

Groups 4-5 are tin and indium based materials, which have rather simple compositions and are newly identified as thermoelectric materials with high *ZT* values. For example, Rhyee et al.[15] reported that single crystal $In_4Se_{2.78}$ was a good *n*-type thermoelectric material with a *ZT* of 1.48 at 705 K. A *ZT* of 2.6 at 923 K was obtained for *p*-type SnSe single crystal.[11] The high *ZT* of these materials is due to their unique zigzag bonding arrangement (i.e. Peierls distortion). About 4% and 3% of the total 400 references are for tin and indium chalcogenides, respectively.

Group 6 consists of materials with layered structure, which have long been identified as excellent thermoelectric materials because there is some separation of charge carriers and phonons by the layer structure. The charge carriers could be effectively transferred within the layers while the phonons may be significantly scattered due to the weak van der Waal bonding between the adjacent layers. The layered

structure materials in this group are mainly sodium cobalt oxides (e.g. $NaCoO_2$), transition metal chalcogenides (such as TiS_2, $MoSe_2$, $ZrSe_2$, MoS_2, WSe_2, etc.), and ternary $ACrX_2$ materials, in which A is Cu, Ag, or Ni. The thermoelectric enhancement of these materials mainly depends on the intercalation of other species into the layers. This group accounts for 6% of the thermoelectric literature.

Group 7 includes binary GeTe, ternary $AgSbTe_2$, and quaternary Ag-Sb-Pb-Te (LAST), Ag-Sb-Ge-Te (TAGS) based materials. The common factor in this group is that the enhancement of their thermoelectric performance (i.e. *ZT*) is due to the formation of nano-inclusions via self-formed inhomogeneities on the nanoscale, driven by phase segregation such as spinodal decomposition, and nucleation and growth. They occupy approximately 9% of reported references.

Group 8 contains the compounds of Cu(Ag)-X system having the "phonon liquid electron crystal (PLEC)" property,[16] which is very similar to the "phonon glass electron crystal (PGEC)" property. The PLEC compounds usually are superionic materials, such as some binary and ternary cuprous and silver chalcogenides. In contrast to the structure of other metal chalcogenides, cuprous and silver chalcogenides have a special structure at higher temperature, where the chalcogen anions form a crystalline lattice and provide pathways for the charge carriers, while the cuprous or silver cations are highly disordered around the chalcogen. Cuprous or silver ions can move fast and behave like a liquid at high temperature, which leads to their extremely low thermal conductivity while preserving good electrical conductivity. As a benefit of this PLEC feature, extremely high *ZT* values are acquired in PLEC materials.[16-17] There are around 8% of thermoelectric references for this group of materials.

In addition to above mentioned metal chalcogenides, there are some other metal chalcogenide thermoelectric materials (around 13% of thermoelectric references), which are included in group 9. These materials are also good candidates as TE materials for several reasons, such as the unique properties of variable bonds of transition metals (e.g. tellurides of rare earth metals), vacancy planes (e.g. gallium chalcogenides), special band structures, tunable modulation, etc.

In the following parts, the thermoelectric enhancement, and the enhancement strategies and mechanisms for these materials will be discussed one by one according to the category.

4. Thermoelectric performance of MCs from different groups

4.1. Bi-X and Pb-X thermoelectric materials

4.1.1. Bi-X compounds (Group 1)

Bismuth telluride based thermoelectric materials

As the most promising thermoelectric materials at room temperature, Bi_2Te_3 and its alloys with Sb and Se, with a *ZT* of 0.6 at 300 K, were commercialized and used in thermoelectric refrigerators several decades ago. Advances in nanotechnology have recently boosted the *ZT* values of these conventional thermoelectric materials to a new record, as demonstrated by a *ZT* of 2.4 at 300 K obtained from a superlattice film of Bi_2Te_3-Sb_2Te_3 in 2000.[18] This breakthrough not only demonstrates the nanoscale effects towards the improvement of thermoelectric performance of conventional materials, but also has led to a burst of research on thermoelectric nanomaterials.

Bi_2Te_3 is a narrow-gap (indirect band gap of 160 meV) layered semiconductor possessing a trigonal unit cell with space group R-3m and lattice constants a = 4.38 Å and c =30.36 Å. The detailed crystal structure is shown in **Figure 5**(a), where Bi_2Te_3 is composed of Te and Bi atomic layers arranged in the order of -Te(1)-Bi-Te(2)-Bi-Te(1)- along the *c*-axis direction. The Bi-Te(2) bond is covalent, while the Bi-Te(1) bond is a covalent–ionic bond. The interaction between two adjacent Te(1) layers is based on weak van der Waals forces. Therefore, Bi_2Te_3 crystals exhibit easy cleavage and high thermoelectric properties along the (00*l*) planes.

The valence and conduction band structures can be described by a many-ellipsoid model with 6 constant-energy ellipsoids that are centered on the reflection planes. Furthermore, the Seebeck coefficient of bulk Bi_2Te_3 becomes compensated, with a sharp rise of thermal conductivity at around room temperature, driving the material used in power generation devices to be an alloy of bismuth, antimony, tellurium, and selenium to further improve its performance.[19] Alloys of $Bi_{0.5}Sb_{1.5}Te_3$ and $Bi_2Se_{0.3}Te_{2.7}$

are the best *p*- and *n*-type thermoelectric materials at room temperature, respectively. The recently reported *ZT* values of BiSbTe and BiSeTe based materials are summarized in **Table 1**, which shows that the maximum *ZT* for bulk *p*-type $Bi_{0.5}Sb_{1.5}Te_3$ and *n*-type $Bi_2Se_{0.3}Te_{2.7}$ reached 1.86 at 320 K and 1.20 at 445 K, respectively.[20]

It should be noted that the enhancement of *ZT* in *p*-type materials is much easier than in their *n*-type analogues due to the strong texture and highly anisotropic properties of *n*-type materials.[21] Several strategies to enhance the thermoelectric performance of Bi-Te based materials can be summarized as follows:

(1) Nanostructuring

Nanostructuring is an effective method to enhance thermoelectric performance due to the decreased thermal conductivity resulting from the presence of abundant grain boundaries. For example, by combining the melt spinning and spark plasma sintering techniques, a high density of nanostructures was achieved in *p*-type $Bi_{0.5}Sb_{1.5}Te_3$, and the maximum *ZT* of 1.56 at 300 K was reached.[22] Flower-like *n*-type Bi_2Te_3 nanostructures were synthesized by a wet chemical method and sintered into a bulk, which exhibited a *ZT* of 1.16 at 420 K.[23]

There are several new developments in the nanostructuring of Bi-X materials. The first development lies in the bottom-up fabrication of nanobulks of Bi-Te based thermoelectric materials.[24] Mehta et al.[24a] reported a microwave assisted synthesis of nanostructured $Bi(Sb)_2Te(Se)_3$, in which thioglycolic acid (TGA) was simultaneously used as a stabilizer and sulphur dopant, with a *ZT* of 1.1 reported for the final product synthesized by this method. From their description, the TGA not only can act as an S dopant for the product, it also could protect the nanostructures from oxidation. They got the highest reported *ZT* for an *n*-type BiSeTe material, and the product could be processed in air, which offers great convenience for further applications of these nanostructures.

The second development is the consolidation method, e.g., the hot pressing or spark plasma sintering (SPS) techniques, which significantly influence the thermoelectric performance of the nanobulks. For

example, although samples were prepared from same batch of $Bi_{0.5}Sb_{1.5}Te_3$ nanopowder, the electrical conductivity of the hot pressed nanobulk decreased with increasing temperature,[25] while in the case of the sample sintered by the SPS technique, an opposite trend was observed. This difference is ascribed to the different features of the two techniques. During the SPS process, the local high temperature from the electric spark causes evaporation of elements and the formation of more defects, which significantly modifies the thermoelectric properties of the final product. On the contrary, the temperature during hot pressing is more controllable and uniform.[25]

The third development is the introduction of nanostructures into the matrix of bulk materials. Several different nanostructures were introduced and their effects are reported in details. One example is that Liu et al.[26] tried to enhance the thermoelectric performance of *n*- and *p*-type Bi_2Te_3 by introducing nanostructured SiC. The *ZT* of *p*-type $Bi_{0.5}Sb_{1.5}Te_3$ was successfully enhanced from 0.88 to 0.97 at 323 K, but the *ZT* of *n*-type $Bi_2Se_{0.3}Te_{2.7}$ was decreased after nano-SiC was introduced into it. This is because SiC is a *p*-type semiconductor, so the mobility of electrons in the *n*-type matrix was strongly decreased by the SiC particles. Besides SiC nanoparticles, many kinds of other nanostructures have been investigated.[27]

Parallel to the experimental progress, several new theories have also been developed based on the introduction of nanostructures into the matrix. An interesting example is a composite made of Cu_3SbSe_4 with *p*-type $Bi_{0.5}Sb_{1.5}Te_3$, in which Cu_3SbSe_4 particles not only played the role of phonon scattering centers, but also significantly increased the Seebeck coefficient due to the energy filtering effect (EFE), as shown in **Figure 6**. Through the embedding of nanostructured impurities with a slightly larger band gap than the matrix, a moderate energy barrier (usually lower than 100 meV) is introduced at the matrix-impurity boundaries. Thus, only the charge carriers with higher energy and larger effective mass (m^*) could pass through these barriers, leading to an increase in the Seebeck coefficient. In addition, the large surface area of nanograins also provides a high density of trap states (or an energy barrier) caused by surface adsorbents.[28] The electrical conductivity could decrease, however, due to the filtering effect and

scattering at grain boundaries. Therefore, there is a trade-off between the benefits from EFE and the detrimental effects from the nanostructure.

(2) Resonant level doping

In the most traditional way, doping with different elements could also lead to enhancement of thermoelectric materials. The doping could result in defects in the matrix, change the carrier concentration (*n*), and decrease the thermal conductivity. Hitherto, the doping effects of many different elements, such as Fe, In, Cu, Ag, Cl, Ga, Sn, and Ag on Bi-Te based thermoelectric materials have been reported.[29] Compared with cases where the same carrier concentration is obtained by doping with other impurities, however, Sn doping remarkably increased the Seebeck coefficient in Bi_2Te_3 single crystal at a given carrier concentration. This phenomenon is ascribed to the effect of resonant level doping, which is illustrated in **Figure 7**. It occurs because tin offers a resonant valence band state, which is 15 meV below the top of the upper valence band of Bi_2Te_3.[29d, 30] The Seebeck coefficient is thus significantly increased by the increased density of states [DOS, g(E)] near the Fermi level (indicated by the solid red line) in comparison with the original DOS of Bi_2Te_3 (indicated by the red dashed line).

As one of the most important strategies of band engineering, resonant level doping shows obvious advantages towards improving the thermoelectric performance, as it distorts the band structure and only increases the Seebeck coefficient without affecting the electrical conductivity. Instead of the resonant effect, however, only normal impurity effects (doping effects) were observed in Sn doped *p*-type BiSbTe and *n*-type BiSeTe materials.[29d, 29e] This is because the formation of a resonant level, which depends critically on the amount of overlap between the impurity states and the band structure of the matrix, is very hard to realize and predict.[31] The distortion of the band must take place near the Fermi level (usually within 0.5 eV) after hybridizing with the impurity band. Too much overlap may distort the band too much and cause a shift in the Fermi level, while too little overlap may not distort the band. Only a few elements or specific materials have been identified as capable of resonant doping, such as Tl and Sb for PbTe, Sn for Bi_2Te_3, and In for SnTe.[29d, 32] Although some dopants are not capable of resonant doping,

they could modify the band structure of the matrix, such as by causing band degeneracy or affecting the band gap, and detailed examples will be discussed in connection with the Pb-X system. Effects that could modify the band structure, including resonant doping, are summarized as another common route to enhance thermoelectric performance in band structure engineering.

(3) Increasing the degree of orientation of the microstructures

Bismuth chalcogenides such as Bi_2Te_3 have a layered structure [Figure 5(a)], so they show anisotropic thermoelectric properties along different crystal directions and a high *ZT* along the plane perpendicular to the *c*-axis. Commonly, Bi_2Te_3 based ingots with high *ZT* values are single crystalline or highly aligned polycrystals fabricated by the Bridgman, Zone melting, and Czochralsky techniques, with a preferred crystal orientation.[33] Therefore, one way to enhance the *ZT* and mechanical properties of the Bi-Te compounds is to increase the degree of orientation of crystals in their polycrystalline bulks, which has attracted considerable attention in recent years. The preferential factor, which is also called the Lotgering Factor (*F*), is employed to characterize the orientation of crystals and can be expressed by the following equations:

$$F = \frac{P - P_0}{1 - P_0} \tag{6}$$

$$P = \frac{I_{(00l)}}{\sum I_{(hkl)}} \tag{7}$$

$$P_0 = \frac{I_{0(00l)}}{\sum I_{0(hkl)}} \tag{8}$$

Where $I(00l)$ and $I_0(00l)$ is the intensity of the $(00l)$ peak for preferentially and randomly oriented samples, respectively. There are several approaches to enhance *F*.

The first approach is hot deformation, which has been proved to be an effective method to increase *F* in the polycrystalline bulk materials.[20a, 33-34] External strains may cause reorientation or induce preferential growth of crystals. For example, by combining the densification of nanostructured powders with two-step hot forging processes, the orientation degree (i.e. *F*) of nanostructured *p*-type $Bi_{0.5}Sb_{1.5}Te_3$ was significantly improved from less than 0.1 to 0.3, and the *ZT* value was increased from 1.0 to 1.5.[35]

The second approach to reorienting the crystals in bulk materials is the use of high magnetic field.[33, 36] When a crystal with anisotropic magnetic susceptibility is placed in a strong magnetic field, it will be rotated to an angle that minimizes the magnetization energy (U) associated with the magnetic anisotropy of the crystal, as given by the following equation[36a]:

$$U = -\frac{\chi_{11}}{2\mu_0^2}B^2 - \frac{(\chi_{33}-\chi_{11})}{2\mu_0}B^2\cos^2\theta \quad (9)$$

where χ_{11} and χ_{33} are the magnetic susceptibilities along the a/b axis and the c axis, respectively; μ_0 is the permeability in vacuum, B is the magnetic field, and Θ is the angle between the direction of the magnetic field and the c-axis of the crystal. For $Bi_{0.4}Sb_{1.6}Te_3$ at room temperature, χ_{11} and χ_{33} are -0.368×10^{-6} cm^3/g and -0.457×10^{-6} cm^3/g, respectively.[36a] Thus, under a high magnetic field, the crystallographic c-axis of single crystal $Bi_{0.6}Sb_{1.4}Te_3$ can be aligned perpendicularly to the direction of an applied magnetic field. Kim et al. fabricated polycrystalline $Bi_{0.6}Sb_{1.4}Te_3$ by a "bottom up" route; e.g. the pellet of nanostructured $Bi_{0.6}Sb_{1.4}Te_3$ was first fabricated under a magnetic field using the slip-casting method and then consolidated by SPS.[36] The obtained bulk material indeed showed preferential orientation under a magnetic field of 10 T, and the maximum ZT reached 1.2 at 323 K, which is a 30% increase over the sample synthesized in the absence of magnetic field.[36b] Luo et al. imposed a variable intensity high static magnetic field during a traditional melt-solidification (MS) process to prepare p-type $Bi_{0.5}Sb_{1.5}Te_3$.[33] A c-axis alignment of the bismuth antimony telluride in the direction perpendicular to the magnetic field was observed in the sample fabricated under 2 T magnetic field, as shown in **Figure 8**. This is related to the enhanced convection of the melt under high magnetic field.[33] Finally, this well aligned material yielded a ZT of 1.71 at 323 K, which is nearly two times higher than for the sample prepared without magnetic field.[33]

The third approach is a combination of chemical exfoliation and spark plasma sintering (CE-SPS). Puneet et al.[21] used this approach to transform bulk n-type Bi_2Te_3 microparticles into well oriented layered nanostructures, which exhibited increased electrical conductivity and ZT. Zhu et al.[37] adopted a similar hydrothermal exfoliation and SPS process (HE-SPS) to obtain well oriented nanostructured p-type

$Bi_{0.48}Sb_{1.52}Te_3$. The maximum *ZT* of *p*-type $Bi_{0.48}Sb_{1.52}Te_3$ increased from 1.2 to 1.4 at 300 K due to the increasing orientation (*F*).

(4) Severe plastic deformation

Severe plastic deformation (SPD) is a "top down" process to achieve materials with ultra-fine grains in the sub-micrometer or nanometer range, which is a general approach to enhancing *ZT* in half-Heusler, skutteridite, and Bi-Te systems.[20a, 34a, 34c, 34e, 35, 38] This method includes several different techniques, such as high pressure torsion, equal-channel angular pressing, direct cold pressing, hot forging, hot extrusion, etc. The extremely large plastic strains induced by the significantly high hydrostatic pressure at the evaluated temperature have a great effect on the microstructure of materials. This method involves several different mechanisms to enhance the thermoelectric properties, including (i) breaking of crystals down to the nanoscale;[35a, 38b] (ii) enhanced formation of lattice defects, vacancies, and especially, dislocations;[20a, 35a] (iii) and re-orientation of the crystals.[35] In addition, the SPD method also improves the mechanical properties of Bi-Te based materials due to the formation of nanocrystallites.[34d] For example, the samples extruded at 360 °C showed the highest Vickers hardness of HV 108, which is 2.5 times higher than that of hot-pressed Bi_2Te_3 compound.[34e]

(5) Defect engineering

Defect engineering is an effective way to modify the thermoelectric performance of Bi-Te compounds. It is well known that antisite defects and anion vacancies play important roles in controlling the conduction type of the Bi-Te system. Although the effects of defects on thermoelectric performance have been investigated in terms of the doping effect, the important effect of point defects on thermoelectric performance has never been fully recognized. Recently, Hu et al.[20a] proposed defect engineering as an effective and important route to enhance the thermoelectric performance of the Bi-Te compounds besides the traditional nanoengineering and band structure engineering. In this report, the defects are well controlled in two ways: (i) the concentration of antisite defects or vacancies in the Bi-Te system strongly depends on the composition and can be adjusted by changing the composition. The smaller the

differences in electronegativity and atomic size between the cation and anion atoms, the less resistance there is to the formation of antisite defects, while by increasing the size difference between the cation and anion atoms, anion vacancies increase. Hence, the composition related formation energies of antisite defects (E_A) and anion vacancies (E_v) follow the order of:

$$E_A(Sb-Te) < E_A(Bi-Te) < E_A(Sb-Se) < E_A(Bi-Se) \quad (10)$$

$$E_V(Sb-Te) < E_V(Bi-Te) < E_V(Sb-Se) < E_V(Bi-Se) \quad (11)$$

(ii) The defect concentration could also be controlled by sample deformation due to induced non-basal slippage across the crystals, which could lead to the formation of $3Te_{(vacancy)}$-$2Bi_{(interstitial)}$ pairs ($V_{Bi}''' - V_{Te}^{\cdot\cdot}$).[20a, 35a] With more Bi vacancies ($Bi_{Bi}^{\times}$), the Bi atoms occupying Te sites (Bi_{Te}') will diffuse backwards to Bi sites to form many Te vacancies ($V_{Te}^{\cdot\cdot}$) and excess electrons (e). The process can be described by Equation (12):

$$2V_{Bi}''' + 3V_{Te}^{\cdot\cdot} + Bi_{Te}' \rightarrow V_{Bi}''' + Bi_{Bi}^{\times} + 4V_{Te}^{\cdot\cdot} + 6e \quad (12)$$

Hu et al.[20a] carefully controlled the concentrations and kinds of defects in these two ways, and achieved the maximum *ZT* values of 1.3 and 1.2 for *p*-type $Bi_{0.5}Sb_{1.5}Te_3$ and *n*-type $Bi_2Se_{0.3}Te_{2.7}$, respectively.

(6) Introduction of dislocation arrays

The *ZT* is reciprocal to the thermal conductivity, which is transferred via vibration of phonons. The heat-carrying phonons cover a broad spectrum of frequencies, and the lattice thermal conductivity can be expressed as a sum of the contributions from different frequencies. According to the Umklapp scattering mechanism and Debye approximation, the lattice thermal conductivity remains constant with increasing temperature.[20b] In the nanostructured Bi-Te system, the point defects are highly efficient for scattering the high frequency phonons, and the grain boundaries, as well as nanoparticles, could be effective for scattering low frequency phonons, while only dislocation arrays are effective for scattering phonons from low to high frequencies [**Figure 9**(a)]. In 2015, Sang et al.[20b] reported a liquid-phase compaction method to create dislocation arrays between adjacent nanostructures to obtain obviously decreased thermal conductivity, as presented in Figure 9(b). The first step of this method is mixing nanoribbons of

$Bi_{0.5}Sb_{1.5}Te_3$ with a 25 wt.% Te powder, followed by sintering the mixture through the SPS technique under 480 °C and 70 MPa. Te powder was melted into a liquid during the SPS sintering, as its melting point is 450 °C. The liquid Te was expelled, which caused the movement of $Bi_{0.5}Sb_{1.5}Te_3$ nanograins. As shown in Figure 9(c), when the sample was cooled, dislocation arrays formed between the grain boundaries, and excess Te was expelled completely due to its extremely low solubility in the $Bi_{0.5}Sb_{1.5}Te_3$ matrix. The maximum *ZT* of 1.86 at 323 K was reached for the liquid-phase compacted samples (Te-MS), and only 1.3 at 323 K was obtained for the solid-phase compacted sample (S-MS).

Bismuth sulfide and selenide based thermoelectric materials

Since the elements Se and S are less expensive and less toxic than Te,[13, 39] great efforts have been made to investigate the thermoelectric performance of Bi-Se and Bi-S systems. Their detailed TE performance is illustrated in **Table 2**.

As presented in Figure 5(b), Bi_2Se_3 has a layered rhombohedral structure (R3m) similar to that of Bi_2Te_3, which is often described as a trigonal structure with 15 atoms per unit cell and lattice parameters *a* = 4.14 Å, *c* = 28.64 Å. In a unit cell, there are two different types of Se layers, denoted as Se(1) and Se(2). The unit cell is packed with two Bi layers and three Se layers in the following pattern: Se(1)–Bi–Se(2)–Bi–Se(1). There are only the van der Waals forces to provide bonding between the neighboring Se(1) planes. Bi_2Se_3 has a similar two-dimensional (2D) structure to that of Bi_2Te_3. It is a narrow-band-gap semiconductor with an energy gap of 0.3 eV. Although they have similar crystal structures, the thermoelectric performance of Bi_2Se_3 is much worse than that of Bi_2Te_3 due to the high thermal conductivity caused by the lighter atomic weight of Se. Hitherto, the highest *ZT* values for *p*-and *n*-type Bi_2Se_3 have reached 0.41 and 0.75, respectively.[40]

Due to the small size and high electronegativity of S, Bi_2S_3 possesses a three-dimensional (3D) orthorhombic structure [Figure 5(c)], which is totally different from that of its analogues, and no van der Waals interaction exists. It is a semiconductor with a 1.3 eV direct band gap, high Seebeck coefficient, and low thermal conductivity at room temperature. The extremely low electrical conductivity of Bi_2S_3,

caused by the high electronegativity of S, is still the main reason for its low thermoelectric properties. Liu et al.[41] fabricated a net-like nanostructured Bi_2S_3 sample via a simple hydrothermal method, and it yielded a *ZT* of 0.5 at 623 K, which is the highest value for a pure Bi_2S_3 sample.

Apart from using pure Bi_2Se_3 and Bi_2S_3, several strategies, including doping with Ag, Cu, Cl, and Br,[42] forming composites with other nanostructures (such as ZnO),[43] and creating a deficiency of the chalcogen element,[44] as well as the formation of solid solutions,[42b, 42e, 45] have been investigated to improve the performance of the Bi-S and Bi-Se compounds. The detailed *ZT* values and mechanisms are listed in Table 2. The highest *ZT* achieved in the Bi-S and Bi-Se systems was 0.8 at 773 K for the alloyed Bi_2SeS_2, which possesses extremely low thermal conductivity. Br doped Bi_2S_3 yielded the maximum *ZT* of 0.72 at 773 K. The improved thermoelectric properties can be attributed to the optimized carrier concentration and the lower thermal conductivity caused by Cu^+ intercalation, Br substitution, and Cu nanoparticles.[42f]

4.1.2 Pb-X compounds (Group 2)

The Pb-X chalcogenides, especially PbTe, are traditional high performance thermoelectric materials for mid-range temperature (600–800 K) applications. They crystallize in the NaCl crystal structure, with Pb atoms occupying the cation sites and X forming the anionic lattice. A small band gap of 0.32 eV for PbTe allows it to be optimized for power-generation applications and easily doped to be either *n*- or *p*-type with appropriate dopants. Although PbTe was one of the first materials investigated for TE generators, with an average *ZT* around 1, the full potential of the Pb-X system for thermoelectric applications has recently been revealed to be far greater than commonly believed, as is listed in **Table 3**. Several strategies to enhance their TE performance are summarized in the following part.

(1) Band engineering

As schematically shown in **Figure 10(a)**, the valence band of PbTe is composed of the orange light hole band (L) and the blue heavy hole band (Σ) (with the heavy band located 0.2 eV below the light band). At lower temperature, the transport properties are dominated by the L band, which possesses 8 valley

pockets with the same energy. This band structure allows easy and effective band structure engineering.[5] With increasing temperature, the energy difference between the L and Σ bands decreases, and once the difference is below k_BT (where k_B is Boltzmann's constant), band degeneracy occurs, and an increasing Seebeck coefficient is observed according to Equation (13), in which

m^*, m_b^* and N_V, are the effective mass after band degeneracy, the effective mass before band degeneracy, and the number of degenerate valley pockets with the same energy [N_V(L) = 4 due to the symmetry structure of PbTe; N_V(Σ) = 12], respectively.[46]

$$m^* = N_V^{2/3} \times m_b^* \tag{13}$$

As shown in Figure 10(b),[5] the degeneracy of the L and Σ bands is also sensitive to carrier concentration, which is easy to adjust by element doping.

With the advantages of this unique band structure, band structure engineering is easy to achieve with different dopants in PbTe, such as Na, K, Cd, Sm, Sb, Ag, etc.[32c, 47] It was found that Na is an effective dopant for the *p*-type Pb-X system. The effects of Na, as well as its solubility in the Pb-X system, were investigated by He et al..[48] Their results show that Na has the highest solubility (2 mol%) in PbS and the lowest solubility (0.5 mol%) in PbTe and that doping with Na not only can lead to band degeneracy by tuning the carrier concentration, but also can introduce point defects and precipitates. In addition, segregation of Na at PbTe/PbS interfaces resulted in cuboidal and truncated cuboidal morphologies for PbS, because Na as a solute in PbTe has a higher energy than in PbS, and its segregation at the (100) PbTe/PbS interface decreased the total energy of the matrix/precipitate system.[49] Besides tuning the carrier concentration to cause the band degeneracy, doping with elements such as K with a big size difference from the original Pb or Se atoms, [47a] may cause distortion of the original cubic lattice and lead to asymmetry of the Brillouin zone, which finally increases N_V and the Seebeck coefficient.

Another important strategy in band structure engineering is resonant doping, which was explained in the case of Sn doped Bi_2Te_3 and elucidated in Figure 7. Tl was first resonantly doped into *p*-type PbTe.[32b] Then, Sb was both theoretically and experimentally proved to be an effective resonant dopant

for *n*-type PbTe.[32c, 50] Al was also resonantly doped into PbSe, leading to a *ZT* of 1.3 at 850 K, which is close to the reported maximum value in the *n*-type Pb-X system.[51]

(2) Formation of endotaxial nanoprecipitates

Compared with previous descriptions of nanostructure engineering in Bi-Te system, endotaxial nanoprecipitates can be easily introduced into Pb-X system by formation of solid solution. The pseudo-binary PbSe−PbS,[52] PbTe-PbS,[31, 47b, 53] and PbTe-PbSe[46] systems have been studied and developed to a state of remarkably high performance. PbTe−PbS exhibits well-defined nanostructures both on the PbTe-rich side and on the PbS-rich side. This system is known to exhibit bulk phase separation by nucleation and growth processes or spinodal decomposition, depending on the relative phase fraction. Similarly, in the PbSe−PbS system,[52c] which was previously believed to be a solid solution, it was discovered that nanostructures did occur and could be used to account for the low expected thermal conductivity.

The PbTe−PbSe system is also a high performance thermoelectric system, but it is believed to be a solid solution due to the lack of nanostructure. Its low lattice thermal conductivity has been explained on the basis of point defects created by the Te/Se mixed occupation in the rock-salt structure and by the presence of dopants.[49, 52a, 53] Besides the pseudo-binary system, the thermoelectric performance of ternary PbTeSeS was also investigated and proved to show high *ZT* over a broad temperature range.[52a, 54]

The endotaxial nanoprecipitates formed by the various compositions of lead chalcogenides can be divided into “coherent” precipitates, which are slightly mismatched with the matrix, and “semi-coherent” and “incoherent” precipitates [**Figure 11**], which show a clear boundary with the host. All kinds of precipitates can significantly reduce the thermal conductivity by different mechanisms and different effects. The coherent precipitates act as point defects and scatter short wavelength phonons due to their slight mismatch with the matrix. They also have a slight effect on the electrical conductivity. Since the incoherent nano-inclusions possess a large mismatch with the matrix, they selectively scatter mid- to long-wavelength phonons. The maximum *ZT* of 2.3 was achieved in 3% Na doped $(PbTe)_{0.8}(PbS)_{0.2}$[53]

due to the extremely low thermal conductivity arising from the various boundaries that ranged from coherent to incoherent, as well as the carrier concentration modulation.[53, 54b]

In addition to binary Pb-X, introducing other materials to form a composite is another important way to modify TE properties. For example, He et al.[55] reported a new approach, displacement of the layered structure ($PbSnS_2$) rather than nanostructures or a solid solution, to enhance phonon scattering in a PbTe based thermoelectric composite. Extremely low lattice thermal conductivity (0.8 W/m·K) was obtained for the composite, which is almost 30% of that of bulk PbTe at room temperature. This is an excellent example of a bulk PbTe thermoelectric material without nanostructures that can still greatly enhance phonon scattering and provide very low thermal conductivity.

(3) Full-scale-length scattering of phonons

Reducing thermal conductivity is a major approach to increase *ZT* values of conventional thermoelectric materials. As mentioned in connection with the Bi-X system, heat carrier phonons have a wide range of vibration frequencies, so carefully controlling the microstructure to form a full-scale scattering center is an effective way to minimize thermal conductivity to enhance *ZT* values.[12, 20b, 56] For example, a *ZT* of 2.2 at 915 K was achieved via a combination of Na doping and nano-inclusions of SrTe in PbTe. As presented in **Figure 12**, in contrast to the concept of decreasing the thermal conductivity by conventional nanostructure scattering, mesoscale structures with a size range of 100-1000 nm are effective for phonon scattering in the Pb-X system. Pei et al. investigated the effective upper limit to the length-scale of microstructures where this effect becomes insignificant.[47e]

4.2 Ternary A-B-X system (Group 3)

Chalcogens can react with metals to form different varieties of complex crystal structures; an example is ternary A-B-X which offers a wealth of thermoelectric properties tuned through the crystal structure engineering. Ternary I_B–III_A–VI_A compounds (I_B = Cu, Ag; III_A = Al, Ga, In; VI_A = S, Se, Te) are usually *p*-type semiconductors with the diamond-like structure (or chalcopyrite structure) derived from the II_B–

VI_A cubic zinc-blende structure. The Zn atom layers in the cubic ZnTe structure are cross-substituted by ordered I_B–III_A atoms, leading to a tetragonal (chalcopyrite) structure with the space group I-42d, as shown in **Figure 13**(a). The I_B–III_A–IV_A atoms are connected mainly by mixed covalent and ionic bonds to form a 3D network, with the chalcogen atoms residing in the tetrahedral voids formed by I_B and III_A atoms, which means that each anion is coordinated by two I_B and two III_A cations, whereas each cation is tetrahedrally coordinated by four anions. The existence of two different cations results in two different bond distances for A−X and B−X, which yields lattice distortion and a smaller band gap than the original ZnTe type structure.[57]

There are no vacancies in the diamond like structure, and the *p*-type conductivity is mainly attributed to the close proximity of the top of valence band to the Fermi level. The low lattice thermal conductivity and electrical conductivity originate from the distortion of the unit cell caused by the structure,[57-58] which could be simply characterized by the parameter δ ($\delta = c/a$, where c and a are lattice parameters). The closer δ is to 2, the less distortion of lattice there is, and the higher the lattice thermal conductivity and electrical conductivity. If δ is around 2, the crystal field splitting energy reaches its minimum state, leading to a cubic-like highly degenerate electronic band-edge state, a large power factor, and a high *ZT* value. For example, the δ (lattice distortion) of $CuInTe_2$ was improved to nearly 2 by prolonging the annealing time, and a higher electrical conductivity and a *ZT* of 1.18 were obtained, which are better than for less annealed counterparts.[58] The maximum *ZT* of 1.4 was first achieved in polycrystalline $CuGaTe_2$ by Plirdpring et al.[59] and later by Massaya et al.[60] via ball milling and hot pressing. The reason for such a high *ZT* value is mainly due to a sudden decrease in the thermal conductivity in the high temperature range. According to theoretical calculations, however, the *ZT* of $CuGaTe_2$ could reach 1.69 at 950 K, with an optimized hole concentration of 3.7×10^{19} cm^{-3}.[61] The thermoelectric performances of I_B–III_A–VI_A compounds are listed in **Table 4**. To further enhance their performance, doping is a widely used as an effective method.[62] A notable example is $CuInTe_2$ doped with Mn, which modifies its band structure.[57]

Deficiency of elements, alloying, and the formation of nanocomposites are also effective routes for enhancing their thermoelectric performance.[62h, 63]

In addition to the formation of stoichiometric compounds, ternary I_B–III_A–VI_A (I_B = Cu, Ag; III_A = Al, Ga, In; VI_A = S, Se, Te) also can form "non-stoichiometric" compounds with complex crystal structures. "Non-stoichiometry" means that the atomic ratio of A:B:X deviates from 1:1:2. One special non-stoichiometric *n*-type semiconductor is $AgIn_5Se_8$,[64] which is not a typical chalcopyrite structure. This material belongs to the I_B-III_{A5}-IV_{A8} family and the defective non-cubic ternary analogs of the III_{A2}-VI_{A3} crystal structure. It is a pseudo-alloy of $AgInSe_2$ and In_2Se_3.[64] Because of the small difference in bonding energies between Se-Ag and Se-In, Se could form bonds with either Ag or In, or both with moderate heat treatment. Therefore, with different heat treatments, different microstructures are achieved in one bulk sample, which is called microstructure modulation. $Cu_2Ga_4Te_7$ is another pseudo alloy of Cu_2Te and Ga_2Te_3 with a sphalerite structure (F-43m) and a band gap of 1.08 eV. In contrast to the chalcopyrite structure, abundant ordered defects exist in this structure.[62a] By doping with Zn, the concentration and type of defects were optimized to achieve a *ZT* of 0.47 at 770 K.[62a]

Ternary I_B–IV_A–VI_A compounds (e.g. Cu_2MSe_3, M = Sn, Ge) also have the diamond-like structure which could be derived from the ZnTe structure by a substitution involving three Zn-Te unit cells (e.g. substituting two Cu atoms for two Zn atoms and one Sn or Ge atom for one Zn atom), while maintaining the ratio of the valence to the number of atoms present in the compound [Figure 13(b)].[65] Cu-Se forms a complex charge carrying network, which has a great influence on the electrical conductivity, and the Ge or Sn atom acts like a filler atom, causing a reduction in lattice thermal conductivity. This structure leads to a low lattice thermal conductivity, moderate electrical conductivity, and thus a high *ZT* value. As Sn or Ge atoms contributes little to electrical conductivity, doping with other elements on this site or Ge substitution for Sn are commonly used to further enhance its thermoelectric performance. For example, maximum *ZT* values of 0.62 in $Cu_2Sn_{0.925}In_{0.075}Se_{2.1}S_{0.9}$, and 1.14 in doped $Cu_2Sn_{0.9}In_{0.1}Se_3$ are reported,[66] which are close to *p*-type commercial Bi_2Te_3-based materials.[58] $Cu_4Sn_7S_{14}$ is an *n*-type A-B-

X semiconductor. It features a large Seebeck coefficient (close to -600 μV/K at room temperature) and a low thermal conductivity, which are benefits of its complex structure. A small *ZT* of 0.2, however, was achieved at 600 K due to its low electrical conductivity.[67]

Contrast to diamond-like structure, I_B–V_A–VI_A compounds $AgSbSe_2$ and $AgBiS_2$ are crystallized in the cubic rock salt structure (Fm-3m) at room temperature with disordered Ag and Sb/Bi positions and ordered Se/S atoms. The lone pair electrons on the V_A elements (such as active $5s^2$ pairs in Sb) would distort the crystal lattice and lead to strong anharmonicity in the V_A-VI_A bond and ultimately, low thermal conductivity, such as in $AgBiS_2$.[68] The thermoelectric performance of $AgSbSe_2$ can be significantly improved by the convergence of the valence band valleys through proper carrier engineering by doping. It has been reported that a *ZT* of above 1 was achieved in $AgSbSe_2$ when it was doped with Pb and Bi.[68a]

Cu_3SbX_4 (X = S, Se) compounds possess a tetragonal structure (I-42d) and have low thermal conductivity due to their complex structure. Substitution of other elements for Sb, doping, and deficiency of elements, as well as the formation of nanocomposites are used to further decrease its thermal conductivity and enhance the *ZT* value.[69] Cu_7PSe_6, as a member of the argyrodite class, is a ternary ionic conductor with an extremely complex structure, which can be described as a cubic close-packing of Se^{2-} anions, with additional Se^{2-} and tetrahedral $[PSe_4]^{3-}$ units alternately occupying the tetrahedral voids.[70] Despite this complex structure and the presence of a light V_A element (P), extremely low thermal conductivity [0.4-0.6 W/(m·K)] is achieved between 300 and 600 K. This value is even lower than the glass limit calculated by Cahill's formulation.[70]

Compared with well crystallized I_B–V_A–VI_A compounds, amorphous analogues usually have lower thermal conductivity. For example, Cu-As-Te compounds can be easily made in pure amorphous form by the conventional quenching method and thus do not need ultrafast-quenching techniques such as melt-spinning. Vaney et al.[71] first synthesized amorphous $Cu_{15}As_{30}Te_{55}$, which possessed extremely low thermal conductivity. They then varied the conditions of heat treatment or consolidation to carefully

adjust the degree of crystallinity to modify the thermoelectric properties of the material. The *ZT* values of this type of material are relative low, however, typically no more than 0.2.[161]

Besides the elements from the III_A-V_A group, replacing the "B" component in A-B-X system with a transition metal, such as Fe, also can from diamond-like structure. The narrow-band-gap semiconductor $CuFeS_2$ (chalcopyrite ore, band-gap energy, E_g = 0.3-0.5 eV), composed of the earth-abundant, non-toxic, and inexpensive elements Cu, Fe, and S, is such a compound with a tetrahedral structure and lattice parameters a = 5.289 Å and c = 10.42 Å.[72] The δ of $CuFeS_2$ is around 1.97, and a low thermal conductivity is expected. The maximum *ZT* of 0.33 was achieved in $Cu_{0.97}Fe_{1.03}S_2$ at 700 K due to the increased lattice defects caused by element deficiency and the diminished carrier−magnetic-moment interactions at high temperature.[72a] Qiu et al. reported the maximum *ZT* of 1.2 at 900 K for a composite of $0.8Cu_8S_4$+$0.2Cu_5Fe_2S_4$.[73]

In addition to above I_B–III_A–VI_A, I_B–IV_A–VI_A and I_B–V_A–VI_A compounds, there are some other A-B-X systems. For example, thallium-M-Te (M = Ag, Bi, Cr, Zr, etc.) has long been investigated as a family of good thermoelectric materials since the 1960s.[74] **Figure 14**, as well as Table 4, presents the thermal conductivities and *ZT* values of some typical compounds in this system,[74b] from which it is found that the *ZT* of Tl_9BiTe_6 and Ag_9TlTe_5 reached 1.2 at 500 and 700 K, respectively.[75] The extremely low thermal conductivities of Tl-M-X compounds originate from two aspects. One is that the Tl-M-X system possesses an extremely well crystallized structure, For example, Tl_9BiTe_6 is a derivative of the isostructural compound Tl_5Te_3 and formed by replacing Tl^{3+} with Bi^{3+} in $2[Tl_5Te_3] = [Tl^+(Tl^+Tl^{3+})Te^{2-}_3]$,[74a] while Ag_9TlTe_5 has a unit cell including 120 atoms.[74b] The second reason is that the heavy atoms in this system greatly contribute to the low thermal conductivity by reducing phonon energies and the speed of sound. If the number of atoms per unit cell is *N*, the ratio of acoustic modes (vibrational modes that effectively transport heat) to the total number of modes will be 1/*N*. A large *N* means a low proportion of acoustic modes, and low lattice thermal conductivity is expected.[74b]

Mo-Sb-Te based compounds are another type of A-B-X, and their structures originate from metallic Mo_3Sb_7 (Im3m, 40 atoms per unit cell). By replacing two Sb atoms with Te, the system changes into a semiconductor with a big cubic void in its crystal structure.[76] Thus in a similar way to the filled skutterudites, introducing other atoms into the big cubic void creates a rattling effect, and a significant decrease in the thermal conductivity could be achieved.[76-77] For example, the maximum *ZT* of 0.93 was achieved in Ni-filled Mo-Sb-Te.[76a] Chevrel phases with a general formula $M_xMo_6X_8$ (M = metal; X = S, Se, Te) are another group of Mo-containing compounds with high potential as thermoelectric materials due to their complex structure. The host structure of a Chevrel phase consists of stacked Mo_6X_8 clusters with metallic cations (M) filling in the spaces between the Mo_6X_8 clusters, which act as rattling centers. In general, Chevrel phases crystallize in a trigonal structure ($R\bar{3}$), and filling in metal ions would distort the hexagonal structure to a triclinic symmetry ($P\bar{1}$). In addition to their low thermal conductivity, another important advantage of Chevrel phases is that their electrical properties appear to be dependent on the number of valence electrons per Mo atom; this number is referred to as the cluster-valence-electron count (cluster-VEC).[78] The cluster-VEC is calculated by adding the valence electrons of the M atoms (V_M) to the valence electrons of the Mo atoms (V_{Mo}), subtracting the number of electrons required to fill the octets of the X atoms (V_X) from the resultant valence electrons, and then dividing the resultant value by the number of Mo atoms (N_{Mo}), e.g. $VEC = \frac{N_{Mo}}{V_M + V_{Mo} - V_X}$. Chevrel phases can have cluster-VECs in the range of 3.3 to 4.0, and the Seebeck coefficient and electrical conductivity could be easily optimized by modifying the cluster-VEC.[78] The TE property of this group is also presented in Table 4.

Derived from A-B-X system, the quaternary Cu-C-B-X system also exists, in which "C" is another metal element from either the transition metal or the main groups, such as Ag, Zn, Fe, Hg, In, Ga, etc.,[79] while "B" is mainly Sn or Ge. These materials are usually used in solar cells due to their wide band gaps. Due to their low thermal conductivity, originating from their extremely complex crystal structures, they have also been widely investigated as thermoelectric materials; such as $Cu_2ZnSnSe_4$, the structure of which can be derived as an analogue of ZnSe, with cross-substitution of other atoms so as to maintain an

electron-to-atom ratio of 4. Every Se atom resides in the tetrahedral voids formed by the cationic elements. The diverse interatomic distances (mainly Se with other atoms) and the electronegativity between the cations result in a natural superlattice structure of the tetragonal type (I-42d; a = 5.449 Å; c = 10.757 Å).[79b] The complex crystal structure could be divided into conducting units and insulating units, such as the tetrahedral [Cu_2X_4] slabs and tetrahedral [$SnZnX_4$] in Cu_2ZnSnX_4 [X = S, Se].[79a] Although a wide band gap is detrimental for electrical conductivity, it can effectively suppress the bipolar effect at high temperature, which occurs very often in the narrow-band-gap materials. The bipolar effect is explained in **Figure 15**. At high temperature, the main charge carriers, such as holes, in narrow-band-gap materials will hop from the valence band (VB) to the conduction band (CB) due to the strengthened random thermal motion and small band gap, which leads to compensation of carriers and changes in the DOS; no such phenomena occur, however, in wide-gap semiconductors. Usually the bipolar effect leads to a decreased Seebeck coefficient and enhanced thermal conductivity. It should be noted that in the presence of the bipolar effect, Equation (5) cannot be used to estimate lattice thermal conductivity.[80] Due to the combination of these two advantages, high ZT values can be expected in the quaternary materials. Typically, ZT values of 0.95 and 0.90 are reported in $Cu_2ZnSn_{0.90}In_{0.10}Se_4$ and $Cu_{2.1}Zn_{0.9}SnSe_4$, respectively.[79a, 79b]

4.3 Sn-X and In-X systems (Groups 4 and 5)

Despite the simple composition and crystal structure of the Sn-X and In-X systems, they are typical thermoelectric materials (**Table 5**) with good performance and low cost. As shown in **Figure 16**(a), SnSe adopts a layered orthorhombic crystal structure at room temperature. Each layer is made up of two-atom-thick SnSe slabs (along the *b*–*c* plane), with strong Sn–Se bonding within the plane of the slabs, which are then linked with weaker Sn–Se bonding along the direction of the *a* axis. The two-atom-thick SnSe slabs are corrugated and create a zig-zag accordion-like projection along the *b* axis.[11] Similarly, the crystal structure of In_4Se_3 is formed by a layered structure of $(In_3)^{5+}$ clusters covalently bonded to Se ions

in the *b*–*c* plane, which are held together by van der Waals interactions along the *a* axis, as shown in Figure 16(b).[15] In contrast to conventional Bi_2Te_3, the layered structure of SnSe and In_4Se_3 is a distorted quasi-one-dimensional chain-like structure. Along this chain-like structure, the charge transport is inherently low dimensional with strong electron-phonon coupling (a structure called the Peierls distortion), leading to a decrease in the thermal conductivity. The occurrence of this phenomenon distorts the chain to form a two-dimensional superlattice structure and charge density wave (CDW) states.[11, 15]

To explain the effects of the Peierls distortion, models with simple arrangements of metallic atoms are used, as shown in **Figure 17**, with distortion of the lattice and electron states of the system also appearing, due to the effects on the periodic arrangement of atoms of additional states [new band B in Figure 17(b)] and a small gap near the Fermi level. These are accompanied by decreased electrical conductivity and an increased Seebeck coefficient, so that the metallic material is transformed to a semiconductor or insulator. Therefore, the zigzag arrangement of different atoms (Peierls distortion structure) leads to a tunable band structure. For example, in the off-stoichiometric In_4Se_{3-x}, the periodical Peierls distortion of the In-Se chains is disturbed by Se vacancies, leading to a big difference in the band structure, as shown in **Figure 18**.[81] The semiconductor type band structure changes into a semi-metallic band with a deficiency of Se, and there is a flat band along the X–Γ and Y–S symmetry lines, indicating that the holes in the *b*-direction are highly localized.[81] The Peierls distortion and charge density wave could also lead to decreased thermal conductivity.[82] In the SnX and In_4Se_3 systems, due to the off-stoichiometric valence of elements, an excess amount of charge carriers usually exists, for example, the hole concentration of SnTe is over 10^{21} cm^{-3}.[83] Thus, the Se vacancies or element doping could simultaneously adjust the band structure and the carrier concentrations.

The thermoelectric performance of Sn-X and In-X can be further enhanced by the off-stoichiometric element ratio or doping effects, such as excess amount of Sn and deficiency of Se.[15, 82-84] Simultaneously, the weak van der Waals bonding between the adjacent layers (along the *a*-axis) is helpful for reducing the thermal conductivity. Due to the combination of these factors, single crystals of SnSe and In_4Se_{3-x} showed

excellent thermoelectric performance, with a *ZT* of 2.6 at 923 K (*p*-type) and 1.48 at 705 K (*n*-type), respectively.[11, 15] A theoretical *ZT* of 3.1 was reported for single-crystal *n*-type SnSe.[85] Despite the effects of the original structure, element doping plays a significant role in the thermoelectric performance of SnTe because it possesses a similar band structure to PbTe, e.g., light and heavy hole bands located close to each other and just below the Fermi level.[83] Thus, it is easy to adjust the band gap via element doping (such as resonant doping with In) and by modifying the band structure with Cd doping.[32a, 83] Reports from Kanatzidis's group demonstrated that compared with single element doping, multi doping can lead to more efficient enhance on *ZT* of SnTe.[83, 86] Very recently, Zhang et al[87] improved the thermoelectric performance of SnTe by rational doping of Gd and Ag together. Doping Gd into SnTe effectively reduced the lattice thermal conductivity close to the theoretical minimum due to the introduction of nanoprecipitates. Further doping Ag into optimized $Gd_{0.06}Sn_{0.94}Te$ significantly improved the Seebeck coefficient and power factor by tuning its composition to reduce the carrier density. It is very interesting that Ag doping led to the homogenous distribution of Gd in SnTe. The low thermal conductivity and large Seebeck coefficient in optimized sample (e.g. $Ag_{0.11}Gd_{0.06}Sn_{0.94}Te$) resulted in the maximum *ZT* of ~1.1 at 873 K.

4.4 Layered structure materials (Group 6)

Layered structure materials have long been recognized as good thermoelectric materials due to their special crystal structure and the possibility of manipulating charge carrier transport and phonon transport by modulation of different crystal planes. In addition to the aforementioned Bi-Te and Bi-Se systems, recent progress on the thermoelectric performance of layered $ACrX_2$ (A = Ni, Cu, or Ag; X = S, Se), transition metal dichalcogenides (TMD), as well as the Bi-O-X system, is listed in **Table 6**. A good comprehensive review on layered structure metal chalcogenides materials by Jood et al. was published in 2015.[7] Here, we mainly focus on the following materials, which are not described in detail.

4.4.1 Ternary $ACrX_2$ layered structure

As a group of magnetic materials, $ACrX_2$ (A = Ni, Cu, or Ag; X = S, Se) compounds possess a trigonal layered structure (R3m), which can be described as CdI_2-type layers of CrX_2^- in which the Cr^{3+} cations are in a distorted octahedral coordination to X^{2-} anions, with the interlayer spaces being filled by the copper or silver ions occupying tetrahedral sites, such as in the structure shown in **Figure 19**(a). The atoms inside the triple layers of CrX_2 are bound to each other by strong ionic bonds, while the neighboring triple layers are bound to each other by weak van der Waals forces. Thus, $CuCrX_2$ and $AgCrX_2$, which show an order–disorder transition of Cu or Ag atoms around 400°C, are also PLEC materials.[88] Thus, they show excellent thermoelectric performance. Tewari et al. and Gascoin et al. reported the maximum *ZT* of 2 at 300 K and 1 at 848 K for $CuCrS_2$ and $AgCrS_2$, respectively.[88] A *ZT* of 1.4 was achieved in sandwich-like $(AgCrSe_2)_{0.5}(CuCrSe_2)_{0.5}$ at 773 K.[89] The thermoelectric performance of this group of materials strongly depends on their synthesis, however. For example Tewari et al.[88a] obtained highly textured $CuCrS_2$ via a specific heat treatment process, which finally led to high electrical conductivity in the sample, but the $CuCrS_2$ sample fabricated by ball-milling and SPS methods exhibited poor thermoelectric performance with a *ZT* of 0.11.[90]

4.4.2 Layered transition metal dichalcogenides

As one kind of transition metal dichalcogenide (TMD), TiS_2 also has a layered structure with a trigonal space group (P3m1). As shown in Figure 19(b), the most stable form of TiS_2 (1T-TiS_2, crystallizing in a layered CdI_2-like structure) consists of sheets of face-sharing TiS_6 octahedra forming S-Ti-S sandwich layers, where a Ti sheet is sandwiched between two sulfur sheets. Atoms within the S-Ti-S sheets are bound by strong covalent interactions, whereas the bonding between the layers is only due to the weak van der Waals forces. Therefore, as a layer-structured compound with a van der Waals gap, TiS_2 is well known for its capability of intercalation by a wide range of both organic and inorganic materials to adjust its performance.[91] Detailed performances of TiS_2 related materials have been reported by Jood et al.[7]

Because of the wide van der Waals gap, excess Ti atoms can also be inserted into the layers, leading to the formation of $Ti_{1+x}S_2$. The Seebeck coefficient and electrical resistivity of $Ti_{1+x}S_2$ decrease with

increasing titanium content because the carrier concentration increases with *x*. A high power factor was found for a near-stoichiometric composition.[92] Hence, despite the merits of its low cost, low toxicity, low density, and simple composition, the main difficulty for the wide application of this material is the synthesis of stoichiometric TiS_2, which is usually prepared by sulfurization of TiO_2 by CS_2.[7, 92-93] The atmosphere, pressure, temperature, and synthesis conditions can seriously affect sulfurization. Besides TiS_2, other transition metal disulfides (TMD) have also been investigated, such as MoS_2, WSe_2, TiS_3, etc.[94]

4.4.3 Bi-O-X system

The Bi-O-X system features another new type of layered structure with complex crystal structure. As an example, the crystal structure (I4/mmm) of Bi_2O_2Se is illustrated in Figure 19(c), which consists of tetragonal $(BiO)_n$ layers with Se occupying interlayer positions.[95] This system has a moderate negative Seebeck coefficient but rather low electrical conductivity due to the strong electronegativity of O atoms. As an important route towards tuning electrical conductivity, deficiency of Bi is reported to be an effective approach for increasing the thermoelectric performance of the Bi-O-Se system.[96]

4.5 AST, LAST, TAGS and GeTe based systems (Group 7)

Binary GeTe, ternary Ag-Sb-Te (AST), and quaternary Ag-Sb-Pb-Te (LAST) and Ag-Sb-Ge-Te (TAGS) based materials are grouped together because their thermoelectric properties can be enhanced through the formation of endotaxial nanoprecipitates via self-formed inhomogeneities due to spinodal decomposition. Spinodal decomposition is an atomic level mechanism in which a metastable single phase (i.e., a solid solution) generates a bi-phase nanoscale structure by phase segregation. It can occur when the phase diagram exhibits a miscibility gap. Moreover, the spinodal decomposition does not result in a nucleation-growth process; instead, coherent nanodomains are uniformly created throughout the whole matrix via a diffusion-segregation procedure. Therefore, both the composition and temperature play significant roles in the spinodal decomposition.

The thermoelectric performance of these materials is very sensitive to their compositions and syntheses. Even for the same composition, the *ZT* values always vary with different synthesis routes. Therefore, their application has long been hindered by the issues of the reproducibility, stability, and complex composition. **Table 7** summarizes the thermoelectric properties of materials from group 7.

4.5.1 Ag-Sb-Te (AST) system

$AgSbTe_2$ features the cubic rock salt structure (Fm-3m), with disordered Ag and Sb atoms randomly occupying the Na sites. With a certain degree of Ag and Sb atomic ordering and different ratios, however, the symmetry can be broken, and the tetragonal P4mmm or the primary cubic Pm-3m structure can be formed.[97] The disordered lattice structure makes the dominant contribution to low lattice thermal conductivity through Umklapp and intrinsic phonon-phonon scattering processes, without a substantial reduction in its electrical conductivity.[98] This special structure makes this material extremely attractive for thermoelectric application. Moreover, $AgSbTe_2$ can be recognized as a solid solution between Ag_2Te and Sb_2Te_3. Spinodal decomposition could also occur in it with changes in composition. Single-phase $AgSbTe_2$ can only be fabricated in a certain composition range with a ratio of Ag_2Te/Sb_2Te_3 smaller than 1.[97] Accordingly, Zhang et al.[97] synthesized composites in situ with Ag_2Te or Sb_2Te_3 embedded in the $AgSbTe_2$ matrix, by utilizing the change in solid solubility near the single-phase region boundaries. The nanodomain boundaries led to a further decrease in the thermal conductivity and a *ZT* of 1.53 was obtained in this material.

4.5.2 Ag-Pb-Sb-Te (LAST) system

The LAST system refers to the solid solutions of PbTe and $AgSbTe_2$ (both NaCl type crystals, Fm-3m) because their lattice parameters follow the Vegard law. The nanoscale inclusions of minor phase in LAST-m exhibit coherent or semi-coherent interfaces with the matrix. This seems to be a consequence of the unique properties of spinodal decomposition as well as their similar crystal structures. Therefore, these nanodomains are only minimally detrimental to the charge carriers. The nanodomains in LAST show a preferential orientation along the (001) planes, with a high degree of lattice strain at the interface, which

is still not fully understood.[4] Although these materials possess complicated compositions, their crystal structures can be derived from simple cubic phase PbTe or $AgSbTe_2$. Hence, with a less distorted lattice or intrinsic defects, this material offers moderate to high electrical conductivity. The symmetry of the crystal structure and the special band structure are responsible for the high Seebeck coefficient. Thus, it is reasonable to expect high *ZT* values in these materials, e.g. Hsu et al.[99] reported a high *ZT* value (*ZT* = 2.20 at 800 K, *n*-type) for $AgPb_{18}SbTe_{20}$ alloys (LAST-18). As an example of the effects of material processing, Li et al.[100] synthesized $AgPb_{21}SbTe_{20}$ by combining mechanical alloying and the spark plasma sintering process. With the advantages of the refined grains and nanostructures produced by repeating milling and SPS processes, simultaneous enhancement of the electrical conductivity and the Seebeck coefficient could be achieved, leading to a 50% increase in *ZT* value.

4.5.3 Ag-Ge-SbTe (TAGS) system

$(GeTe)_m(AgSbTe_2)_{100-m}$ compounds, commonly referred to as 'TAGS-m', can be considered as pseudo-binary compounds of $AgSbTe_2$ and GeTe, and they represent some of the best traditional thermoelectric materials.[101] This material system possesses high electrical conductivity, a high Seebeck coefficient, and relatively low thermal conductivity on the GeTe-rich side, especially for TAGS with 80 and 85 mol% GeTe (denoted as TAGS-80 and TAGS-85). The high power factor originates from the coexistence of the high carrier concentration and the high Seebeck coefficient. Both theoretical and experimental investigations indicate that TAGS are highly degenerate semiconductors similar to PbTe,[102] and their valence bands consist of two sub-bands with different effective masses. This suggests that the presence of a second, heavy valence band causes the dependence of the Seebeck coefficient on the hole density, also known as the Pisarenko relation [Equation (4)], to undergo a deviation when the carrier concentration increases and the Fermi level moves further into the heavy band. Above about 500 K, TAGS are in a face-centered-cubic Fm-3m phase; below that temperature, they are in a rhombohedral R3m phase.[101] Thus, with increasing temperature, band degeneracy appears due to the improved symmetry of the crystal structure. Based on LAST and TAGS materials, several similar systems with

spinodal decomposition have been developed, such as $AgPb_mSn_nSbTe_{2+m+n}$ (LASTT-m), $NaPb_mSbTe_{2+m}$ (SALT-m), $NaPb_mSn_nSbTe_{m+2+n}$ (SALTT-m), KPb_mSbTe_{2+m} (PLAT-m), etc., which possess a similar crystal structure and exhibit spinodal decomposition at moderate temperatures and compositions, as described in a comprehensive review by the Kanatzidis group.[4] The progress on this type of material from 2010 is also summarized in Table 7.

4.5.4 GeTe system

GeTe features a large deviation from stoichiometry towards tellurium and a high density of defects that exist as doubly ionized metal vacancies. As a result, GeTe always exhibits *p*-type conductivity with a high carrier concentration (10^{20} cm^{-3} to 10^{21} cm^{-3}),[103] which leads to high electrical conductivity and thermal conductivity. Element doping is an effective way to improve the thermoelectric properties of GeTe by reducing its hole concentration and/or introducing a secondary phase into the matrix to reduce its thermal conductivity, e.g. Mn, Yb doped GeTe.[104] At ambient temperature, the thermodynamically stable pseudo-binary compounds of the homologous series $Ge_nSb_2Te_{n+3}$ consist of tetradymite-type Sb_2Te_3 slabs that are formally enlarged by *n* layers of additional GeTe. The crystal structure of these compounds consists of layer-like distorted rock-salt-type building blocks separated by van der Waals gaps between the Te atomic layers terminating the individual slabs.[105] These distorted octahedral voids are surrounded by Te atoms, so that the van der Waals gaps can be viewed as layer-like ordered cationic defects, which become randomly disordered in a cubic phase, where Ge, Sb, and vacancies occupy the cation positions, and Te atoms occupy the anion positions. Moreover, for GeTe rich samples with $n \geq 3$, quenching their high temperature cubic phase yields a metastable pseudo-cubic phase, which easily undergoes spinodal decomposition.[105-106]

Another big issue for utilizing GeTe based materials lies in their narrow optimum operating temperature, ranging from 680 K to 780 K, because a phase transition between the rhombohedral lattice (R3m) and the cubic phase (Fm-3m) occurs at about 700 K. The instability of the cubic phase is probably due to their high concentration of vacancies, which involves “incomplete” coordination spheres and a

large energy gain when ordered structures are formed.[107] Therefore, decreasing the vacancies, such as by replacing Ge^{2+} with double monovalent cations, gives a cation/anion ratio closer to 1 and increases the temperature range in which the materials can be applied, as demonstrated by $(GeTe)_{11}(LiSbTe_2)_2$.[107] The maximum *ZT* of 1.90 at 773 K for a *p*-type heterostructure consisting of a Ge-Sb-Te matrix and $CoGe_2$ precipitates was achieved with good reproducibility.[108] The pseudo-binary PbTe-GeTe phase diagram shows unlimited mutual solubility of its end members in both liquid and solid states at high temperature, but phase separation driven by spinodal decomposition (miscibility gap) exists below 860 K.[103, 109]

4.6 Binary and ternary PLEC chalcogenides (Group 8)

The concept of the phonon liquid electron crystal (PLEC)[16] is very similar to that of the phonon glass electron crystal (PGEC), which can simultaneously exhibit high electrical conductivity and low thermal conductivity. This is mainly composed by binary or ternary chalcogenides of Cu or Ag. Although this concept was proposed in 2012, investigations of this type of materials have a long history.[110] The TE properties of PLEC crystals are summarized in **Table 8**; and several PLEC materials (such as $AgBiSe_2$ and Cu_7PSe_6) have already been described in other series.[70, 111] Cu_2Se is chosen as an example to describe the mobility of cations at high temperature. The crystal structure of high temperature cubic Cu_2Se is presented in **Figure 20**, in which the Se atoms are stacked in a close-packed arrangement, with the layers in the sequence of ABC. The Cu1 position is located exactly at the center of the tetrahedral interstice, whereas the Cu2 and Cu3 atoms are located close to a triangular face of the tetrahedron. Each tetrahedron is always occupied by a copper atom, although the copper atom can be disordered in a static or dynamic manner, which means that the Cu^+ ions can easily drift among the Cu1, Cu2, and Cu3 positions inside the tetrahedron.[112] The PLEC compounds show outstanding thermoelectric performance, as demonstrated by the *ZT* of Cu_2Se and Cu_2S. Liu et al.[17] reported a *ZT* value of 2.3 at 400 K for an I-doped Cu_2Se sample due to the critical scattering of electrons and phonons, which means the simultaneous achievement of the minimum thermal conductivity and the maximum electrical conductivity.

Due to the liquid behavior of Cu^+, even for polycrystalline bulk $Cu_{1.97}S$ fabricated by a simple melt-solidification method, a maximum *ZT* of 1.9 at 970 K was achieved.[113] Nevertheless, the thermoelectric performance of their analogue, $Cu_{2-x}Te$, is rather low,[114] which is attributed to its thermal instability arising from the loss of Te element, which leads to changes in the composition and crystal structure.

In addition to binary I_B-VI_A chalcogenides, some ternary I_B–V_A–VI_A materials are also good PLEC crystals. For example, as shown in Figure 10(c), $AgBiSe_2$ is a *p*-type semiconductor and crystallizes in the hexagonal phase with parameters a = 4.18 Å and c =19.67 Å (space group $P\bar{3}m1$) at room temperature. This material undergoes a reversible hexagonal-rhombohedral-cubic phase transition,[111] and in the cubic structure, the Se atoms form a rigid crystal lattice, while the Ag and Bi ions can change places with each other or move. This order-disorder phase transition leads to drastic changes in the electrical and/or thermal properties. For example, the thermal conductivity of the material was decreased due to the enhanced phonon scattering by highly moveable cations, and a maximum *ZT* of 1.5 was reported at 700 K.[111] Nb doping could transform $AgBiSe_2$ into an *n*-type semiconductor and enhance the thermal power by increasing the carrier concentration. A maximum *ZT* of 1 was obtained at 773 K for Nb doped $AgBiSe_2$.[115]

4.6.1 Anomalous TE properties during phase transition of PLEC materials

There is a notable effect of the phase transition on the thermoelectric properties of these PLEC materials.[17, 111, 116] As phase transitions usually involve changes in the atomic configuration, big transformations of the electronic or the thermal transport properties could take place and give rise to unexpected physical properties of solids. PLEC materials usually undergo an order (low temperature rigid phase)-disorder (high temperature PLEC phase) phase change. In the rigid ordered structure, the rigid crystal lattice yields relatively high electrical conductivity and thermal conductivity, while the highly movable ions in the disordered phase strongly suppress the thermal conductivity and slow the transport of charge carriers. There have been some reports that the maximum *ZT* point appeared near the phase transition temperature because of the simultaneously optimized power factor and thermal conductivity,[17,

[116a] although the phase transition temperature window is rather narrow and there are difficulties in the accurate measurement of thermal conductivity during the phase change. The thermoelectric performance at the phase transition temperature has rarely been investigated.

Another typical phenomenon is a transition of the conduction type arising from the change in the crystal structure.[111, 116b, 116c] As a typical example, Han et al.[116b] prepared CuAgSe nanoparticles using a low-cost, effective wet chemical method and found that this material underwent a sudden conductivity transition from *n*-type to *p*-type because the crystal structure was transformed from a mixture of orthorhombic and tetragonal to a pure high temperature cubic PLEC phase, as shown in **Figure 21**(a). This transition was further explained by band structure calculations [Figure 21(b-c)]. Figure 21(b) illustrates the calculated band structure of the tetragonal phase at the Γ point near the Fermi level. It clearly shows that one of conduction bands crosses the Fermi level along the Z−Γ and Γ−X lines, while the top of the valence band is located just below the Fermi level. Therefore, the low-temperature tetragonal CuAgSe should possess two kinds of charge carriers. The main charge carriers are electrons, however, and the conductivity is *n*-type. For the high temperature cubic phase [Figure 21(c)], however, the band gap has disappeared, and two valence bands with positive charge carrier effective mass and one conduction band with negative charge carrier effective mass have appeared near the Fermi level. The estimated total effective mass is positive because of the presence of both valence bands and the bigger curvature, resulting in a positive Seebeck coefficient.

4.6.2 Effects of element deficiency on PLEC materials

The effects on thermoelectric performance of defects formed due to non-stoichiometric elemental ratio are also notable.[116d, 117] Typically, in the binary Cu_2X system, it is easy to form Cu vacancies, and the composition changes from stoichiometric Cu_2X to non-stoichiometric $Cu_{2-x}X$. The vacancies caused by Cu deficiency play several significant roles in the thermoelectric properties: (i) the vacancies as point defects directly tune the carrier concentration and conduction type of a PLEC;[116d, 117b] (ii) the order-disorder phase transition temperature could also vary with *x*, because the vacancies may offer diffusion

paths and accelerate the diffusion process;[118] (iii) the existence of these vacancies leads to a percolation effect on electrical conductivity, as charge carriers could also pass through them,[117a] which is very similar to the concept of the energy filtering effect (EFE, Figure 6). The vacancies can be regarded as a conductive medium with an energy barrier, and the conductivity of the vacancies could be described by the percolation law presented in the literature.[117a] Thereby element deficiency is an efficient way to adjust thermoelectric performance of PLEC materials.

4.6.3 Mosaic crystals of PLEC materials

Besides the conventional routes (e.g. nanostructuring,[119] alloying,[120] forming nanocomposites[121] and full-scale scattering[122]) used to further enhance thermoelectric performance, He et al.[123] proposed the concept of a "mosaic crystal" to explain the enhanced thermoelectric performance of $Cu_2S_{0.5}Te_{0.5}$ bulk materials with a *ZT* of 2.2 at 1000 K. As presented in **Figure 22**, in most cases, bulk thermoelectric crystals are composed of many crystallites with various sizes and random orientations, which are referred to as polycrystalline specimens. Especially in the case of polycrystalline nanobulks, the presence of a huge amount of grain boundaries leads to a simultaneous decrease in thermal conductivity and electrical conductivity. On the contrary, in a large bulk single-crystal material, the electrical conductivity and thermal conductivity are both relatively high due to the lack of grain boundaries. In contrast to the random orientations in polycrystalline or nanocrystal materials, the blocks in a mosaic crystal exhibit a nearly identical orientation, and the bulk appears to be a single crystal from the macroscale point of view, but it contains a number of small-angle grain boundaries. Therefore, the mosaic crystal is much like a single crystal with grain boundaries, and an effect similar to critical scattering is achieved,[17] e.g. phonons could be scattered by the presence of the grain boundaries, while charge carriers are seldom affected by small angle grain boundaries.

The formation of mosaic crystals is not easy, however. To form a mosaic crystal, a fast cooling speed is usually necessary to suppress the diffusion and accumulation of structural defects at the surface. In the meantime, possible compositional variation is more important, because it results in large internal stress to

further underscore the imperfection of the crystals, such as in the case of $Cu_2S_{0.5}Te_{0.5}$. Although the cooling speed is not high, the big size difference between S (1.04 Å) and Te (1.70 Å) ions causes large internal stress in the crystal, which needs to be released by the formation of sub-grain boundaries.[123]

4.6.4 Stability of PLEC materials

Despite the high thermoelectric performance of Cu/Ag based PLECs, a big obstacle hindering their wide application is their poor stability at high temperature. In virtue of the high mobility of Cu^+, degradation of the composition and performance appear after several cycles of heating and cooling, even in a protective atmosphere.[124] One efficient way to increase thermal stability is to take advantage of the pinning effect of Fe atoms on the Cu sites, which can greatly suppress the migration of copper ions.[73] Because Fe atoms are more reactive than Cu atoms and are randomly located at the same crystallographic sites as the mobile Cu ions, the migration of Cu ions can be blocked or interrupted.[73] However, it is very interesting that CuAgSe shows intrinsically good cycling stability.[116b]

4.7 Other metal chalcogenides (Group 9)

4.7.1 Ga-Te system

Ga_2Te_3 is one of the typical defective semiconductors containing atoms from the III_{A2} and VI_{A3} groups, with a band gap of 1.65 eV. It has the same crystal structure as a defective zinc-blende cubic crystal [F-43m, **Figure 23**(a)]. Due to the valence mismatch between the cations and anions, two thirds of the ordered Ga atoms occupy the 4c Wyckoff positions (1/4, 1/4, 1/4), and the remaining one third of 4c positions are vacancies,[125] so that the chemical formula of Ga_2Te_3 can be described as $Ga_2V_{A1}Te_3$, where V_A means vacancy. Moreover, there are periodical self-assembled 2D vacancy planes [(111) planes] that wrap the nanostructured domains, as shown in Figure 23. Thus, Ga_2Te_3 shows low thermal conductivity.[126] The engineering of the vacancy planes via doping or alloying has been found to be an effective way to control the thermoelectric performance of this kind of material.[125-127] For example, because the difference in electronegativity (0.09) between Cu and Ga is much smaller than that between

Cu and Te (0.2), Cu tends to occupy the Ga lattice sites or vacancies rather than Te sites to form covalent bonds with Te. As a consequence, the periodicity of the self-assembled 2D vacancy planes is disturbed, releasing the wrapped nanostructured domains, which can scatter phonons on a large scale.[126b]

4.7.2 Non-layered transition metal chalcogenides

Besides the aforementioned layered metal chalcogenides, other non-layered metal chalcogenides, such as MnTe, Ce_3Te_4, $CeSe_2$, FeS_2, Re-Gd-S (Re = rare earth element), etc. have also proved to be promising thermoelectric materials because of either their complex crystal structures or their special band structures originating from the unique properties of transition metals.[128] The relevant thermoelectric performances of these materials are summarized in **Table 9**. $ReGd_{1+x}S_3$ compounds feature quite high performance as *n*-type thermoelectric materials because of their special properties such as their self-doping ability, which originates from the formation of their cubic structures with abundant metal vacancies. These compounds can be written as $Re_2V_{A0.25}S_3$ (or $Re_{2.67}V_{A0.33}S_4$, where Re is a rare-earth metal and V_A is a metal vacancy). These vacancies can be filled with Re atoms. The carrier concentration increases with the Re content. These materials also have low thermal conductivity due to their complex crystal structure.[128a, 128g]

4.8 Others

4.8.1 Modulation doping

Modulation doping (MD), another important way to enhance thermoelectric performance, is a well-developed technique that is widely used in thin-film devices in order to improve the electrical conductivity. A typical thin film device utilizing the concept of modulation doping consists of three active layers, i.e. a doped layer which provides charge carriers, an undoped layer, which serves as a charge transport channel without interruptions from impurity atoms, and a thin spacer layer which spatially separates the above two layers.[128r] Extending this concept to 3D bulk materials, Wu et al.[128r] mixed dopant particles ($BiAgSeS_{0.97}Cl_{0.03}$) with undoped matrix material (BiAgSeS) and consolidated the powder into bulks, which showed increased electrical conductivity and decreased thermal conductivity

due to the modulation doping effect. A schematic illustration of 3D modulation doping is shown in **Figure 24**. Compared with traditional uniform doping, the dopants offer extra charge carriers to the whole bulk, while the scattering between the charge carriers and the ionized dopants is greatly reduced, as the dopants are localized in the doped grains. Hence, this method provides a new approach to increasing the concentration of charge carriers while reducing the loss of carrier mobility. Moreover, it is a general method to enhance the thermoelectric performance of other kinds of materials, such as in the SiGe and Pb-X systems.[54b, 129]

4.8.2 Surface engineering of thermoelectric nanomaterials prepared by the wet chemical method

Although nanostructuring has long been identified as the most widely used and effective method to enhance thermoelectric performance, its application is strongly hindered by the lack of a large-scale fabrication method with both low cost and high controllability of the nanostructures. As one of most important bottom-up routes used to fabricate nanobulk materials, the wet chemical method has been used to fabricate nanostructured thermoelectric materials.[130] The merits of this method are obvious: (i) the morphology, composition, and crystallinity of nanostructured metal chalcogenides can be well controlled via the reaction parameters;[9a] (ii) it is a facile and low-cost method compared with other methods, such as solid-state reaction and melt-spinning;[20b, 131] (iii) the product has relatively high purity compared with ball milling. Due to their large surface area, the nanostructures may be covered, however, by non-conductive solvents or ligands, which are hard to remove and very fatal for the electrical conductivity of the sintered bulk.[24, 132] The yield of the wet chemical method is also relatively low.[9a] In addition, sometimes the cost of wet chemical method is high if expensive solvents or ligands are used.[9a, 133]

Although the wet chemical method has advantages in tuning the size and morphology of nanostructures,[130] the resultant nanostructures may be covered by non-conductive solvents or ligands due to their large surface area, which are hard to remove and fatal for the electrical conductivity of the sintered bulk. An alternative is the development of surfactant-free chemical synthesis routes. Recently, Han et al.[116b, 131] developed a low-cost wet chemical method to synthesize different kinds of surfactant-

free binary and ternary metal chalcogenide nanostructures. As presented in **Figure 25**, the method is based on the extremely low solubility of metal chalcogenides in aqueous solution, and includes a reduction of the chalcogen source by $NaBH_4$ and a precipitation of the obtained chalcogen ions with metal ions. The whole synthesis is conducted under ambient conditions, no surfactants are used, and it is easy to scale up. The thermoelectric performance of consolidated nanobulks from the obtained nanostructures is comparable to those of the corresponding bulk analogues.[116b, 131]

Another important method to enhance the thermoelectric performance of nanostructures obtained by wet chemical methods is the surface engineering of nanocrystals by using other inorganic materials to replace the capping ligands and absorbed organic solvents.[45a, 52b, 134] As the simplest agent for surface modification, hydrazine is already widely used to remove residual ligands in the wet chemical method.[24a, 130a] Simply replacing surface oleic acid of PbS nanocrystals with NH_4SCN led to a strong increase in the electrical conductivity in the low temperature range compared with the original oleic acid covered PbS nanocrystals.[52b] Stirring oleic acid covered PbS with HCl can simultaneously replace the non-conductive oleic acid and promote doping with Cl ions, leading to a significant increase in the electrical conductivity over the whole temperature range.[52b] Talapin et al. simply replaced non-conductive organics with inorganic materials and proposed the concept of "nanocrystal glue" or "semiconductor solder" for mesoscale particles of thermoelectric materials. [45a, 134] The nanocrystal glue can form a semiconducting material after heat treatment, which is structurally and compositionally matched to the bonded semiconductors. Because the electronic properties of semiconductor interfaces are much more sensitive to impurities and structural defects than those of metals, the misalignment of the Fermi energy levels or the trapping of charge carriers at the interface creates a Schottky barrier.[134b] Details of fabrication of nanocrystal glues can be found in their report.[134b] The benefits of using nanocrystal glue are: (i) there is a depressed melting point for nanocrystals, which permits the consolidation of grains at lower temperature; (ii) the usage of glue can improve the quality of the sintered body and lead to higher density at lower temperature, as shown in **Figure 26**; (iii) selective modification of the grain boundaries can be by tuning

the chemistry of the nanocrystal glue, offering an additional degree of control over charge and heat transport in thermoelectric materials. For example, due to the structurally and compositionally matched interfaces, the decrease in charge carrier mobility was minimized with an extremely small amount of the solder (1-3 wt.%).[45a, 134] CdSe nanocrystals capped with $Na_2Cd_2Se_3$ solder were used as a soluble precursor for CdSe films, with electron mobility exceeding 300 $cm^2/(V \cdot s)$.[134b]

4.8.3 Other approaches used for defect engineering

As mentioned previously,[20a, 35a] defect engineering has been an important route to tuning the properties of thermoelectric materials in the Bi-Te system. Actually, it is a general method that can be used for other metal chalcogenides, as the defects can affect carrier concentrations and lower thermal conductivity. Besides hot deformation, the defects engineering can be achieved in several different ways; such as by hydraulic pressure together with ion beams,[135] bombardment by ion beams or high energy electromagnetic radiation, such as with He^{2+}, Ar^+, neutrons, γ-rays, X-rays, etc., which are widely used for improving the thermoelectric performance of films, etc.[135b, 136] Joonki et al.[135b] used He^{2+} ion beam to induce native defects that dramatically enhanced the thermoelectric properties in Bi_2Te_3 film by simultaneously modifying all of them towards the desired direction. This was enabled by the multiple functions of native defects, which act beneficially as electron donors, energy-dependent charge scattering centers, and phonon blockers.

Hydrogenation is another approach to improve the performance of thermoelectric materials. The introduction of hydrogen atoms onto the surface or into the lattice of the target materials can be performed in several ways, such as hydrogenation at high temperature in the presence of an H source; bombardment with a high energy H^+ ion beam, direct hydrogenation using HCl, etc.[135a] Besides the introduction of point defects, the injected electrons from the doped hydrogen atoms greatly influence the density of states (DOS), which leads to increased charge density across the Fermi surface to improve the electrical conductivity. Meanwhile, due to their very small ionic radius, the incorporation of protons can avoid large-scale structural distortion and maintain the lattice thermal conductivity. For example, in the

case of VO_2, after hydrogen incorporation, electrons from the hydrogen atoms were injected into the V–V chains, resulting in obviously enhanced electron–electron correlation effects. The hydrogenated VO_2 with the highest hydrogen concentration had a *ZT* value of about 0.12 at 210 K, which was much higher than for the other two samples with less or no hydrogen incorporation.[137]

5 Summary and outlook

Metal chalcogenides, which possess many different structures with different compositions (e.g. layered structures, diamond-like structures, complex cage structures, etc.), and relatively low fabrication costs, offer a good platform for either searching for new thermoelectric materials or discovering new theories that can lead to high thermoelectric performance. Significant advances in improving the thermoelectric performance of metal-chalcogenide-based materials have been made in the last few decades.

5.1 Summary

In the field of materials, besides the conventional thermoelectric materials, such as Bi-X, Pb-X, etc., many new kinds of metal chalcogenides have been proved to be effective thermoelectric materials, such as PLEC materials with an order-disorder transition (Cu, Ag chalcogenides), layered structures with quasi-one-dimensional structures (In-X, Sn-X system), structures with extremely complex lattices (Tl-M-Te system, Chevrel phase), structures with vacancy planes (Ga_2Te_3), etc. The development of metal-chalcogenide-based thermoelectric materials mainly shows the following features: (i) The materials with simple compositions but complex structures have attracted ever increasing attention, such as SnSe,[11] In_4Se_3,[15] $CsBi_4Te_6$,[29a] etc. (ii) The formation of nanocomposites has been a widely used method to obtain high *ZT* due to the decreased thermal conductivity and possible energy filtering effect (EFE).[121, 138] (iii) Composition fluctuations from using solid solutions, substitution of atoms, self-doping, or deficiency of elements can introduce defects and decrease thermal conductivity, and lead to high performance thermoelectric materials.[128f, 128g, 128k] (iv) Formation of heterostructures has been another way to produce new thermoelectric materials.[45a, 130a, 130b, 139] (v) Precise intercalation into the gaps

between adjacent layers of layered materials is an important route to producing new types of thermoelectric materials.[89, 91e, 91g] (vi) Phase separation and the formation of nanostructured precipitates, induced by composition control; representing another important direction in the search for new thermoelectric materials.[27j, 97, 140]

For the strategies and methodologies used to enhance the thermoelectric performance of metal chalcogenides, they also exhibit several new trends including: (i) tuning of distorted structure, unit cells, and mobility of atoms;[141] (ii) band engineering through resonant doping[32b] and band degeneracy,[46] which can increase the DOS near the Fermi level to optimize the power factor; (iii) engineering intrinsic defects, which can act as both charge carrier donors and phonon scattering centres;[20a] (iv) full-scale scattering originating from composition engineering;[12, 122] (v) dislocation arrays formed by the pressure-assisted liquid phase sintering technique;[20b] (vi) phonon liquid electron crystals, showing both high electrical conductivity and low thermal conductivity;[16] (vii) formation of mosaic crystals, which possess well oriented grains and grain boundaries;[123] (viii) 3D modulation doping, which can localize ionized impurities to increase charge carrier mobility;[54b, 128r] (ix) surface engineering, such as utilizing nanocrystal glues to improve connections between nanocrystals and decrease the sintering temperature of nanobulks;[45a, 52b, 134] (x) deformation as an important way to enhance thermoelectric performance, because it can both refine crystal grains and introduce defects, as well as improving mechanical properties;[34e, 38b, 142] and (xi) enhancement of orientation for materials with anisotropic thermoelectric performance along different crystal directions, as an effective way to improve their thermoelectric performance, such as in the Bi-Te system and SnSe.[11, 33, 37] Among these strategies, methods involving nanoscience and nanotechnology[4, 74a, 110, 143] represent the most significant and most widely used strategy.

5.2 Outlook

Although metal chalcogenide based thermoelectric materials shows relatively higher *ZT* values than other materials and significant progress has been achieved in recent years, several problems still need to be resolved. (i) Many high-*ZT* metal chalcogenides such as bulk SnSe single crystal,[11] full scale

structured PbTe bulk,[12] bulk CuSTe system,[123] etc. are produced in the laboratory, they face many difficulties for making commercialization. For instance, it is more difficult and expensive to grow a single crystal or a Mosaic crystal than fabrication of a polycrystalline SnSe. (ii) Most metal chalcogenides (e.g. Pb-X based materials) with high thermoelectric performance show poor mechanical properties,[144] which limits their real application. (iii) Due to the intrinsic volatility of chalcogen elements (S, Se, Te), some metal chalcogenides possess poor thermal stability, especially for those nanoscale metal chalcogenides fabricated from bottom up processes.[131] For PLEC materials, the fast movement of liquid like metal ions could also lead to their instability. The chalcogenide nanostructures originated from spinodal decomposition are also not stable during operation because spinodal decomposition is sensitive to temperature. (iv) Most high thermoelectric performance metal chalcogenides have the environmental issue or fabrication cost due to the use of toxic elements (e.g. Pb) or expensive precursors (e.g. Ag and Te).[145] To fully develop the potential of thermoelectric materials for wide commercial applications in the near future, parallel development on both materials and thermoelectric devices are needed.

From the viewpoint of materials, traditional Bi-Te and Pb-Te systems would continue dominate the commercial market because of their better performance than other metal chalcogenides and mature processing technologies. However, more and more efforts would be devoted to enhancing their mechanical strength, reducing fabricating cost and optimizing thermoelectric generators. In addition, low dimensional metal sulphides and selenides would attract considerable attention due to the possibility of simultaneous optimization of the thermal and electrical conductivity via separating the transfer of charge carriers from that of phonons, and their lower cost, environmental friendliness, as well as simple composition. Moreover, the stable PLEC materials with high performance would be a focus for future research.

Meanwhile careful tailoring of nanostructures including shape, size, and interface would be still an important and efficient way to further enhance thermoelectric properties in near future. Partially introducing rationally designed nanostructures into bulk matrix would be a major development because of

its distinct advantages. It can improve the thermal stability of metal chalcogenides, and the scattering of charge carriers can be supressed. The hybrid of nanostrcutures and bulk may lead to full scale phonon scattering compared with single size of nanostructure. The introduced nanostructures could also lead to energy filtering effect. Chen et al.[146] designed a core-shell structure to simultaneously achieve total non-scattering of charge carriers and enhance the Seebeck coefficient. This effect is called "anti-resonant doping" or "invisible dopants" effect.

Besides nanostructure engineering, defect engineering is another new highlight in the near future to further enhance thermoelectric performance of metal chalcogenides, because defects could effectively decrease their thermal conductivity and tune their carrier concentrations. Compared with traditional hot deformation method, irradiation could be a better way to introduce defects in thermoelectric materials because defects can be well controlled with different beams and their dosage. The effects of induced defects on thermoelectric properties of bulk materials have been rarely reported.

For practical applications, more efforts should be devoted to fabricate efficient thermoelectric devices. An important development on thermoelectric devices is fabrication of flexible thin film thermoelectric generators (TEGs), which has several merits in comparison with rigid bulk modules.[147] It can be easily integrated into unusual topologies and maximize the heat absorbing area, leading to an enhanced practical efficiency compared to rigid TE devices. More importantly, the cost of thin film TEGs is low because the screen printing, inkjet printing or the roll to roll manufacturing have been widely used. The thin film TEGs can be used to supply power for small electronics due to their high power density. Their weight is also low. These supreme features of thin film TEGs have attracted considerable attentions[147] and remarkable progress has been achieved. However, most of thin film TEGs are fabricated from Bi-Te system and polymers, and used at room temperature.[148] A major problem of thin films TEGs is their much lower *ZT* compared with that of bulk materials, due to the less density of film and low sintering temperature.

To further opens up new market for metal chalcogenides based thermoelectric materials, one of the important developments of their application forms is combine the thermoelectric devices with other energy harvest devices such as solar cells. Many metal chalcogenide based thermoelectric materials can also be used in solar cells, such as the Pb-X system, Cu-X system, Cu-In-Ga-Se system, etc.[9b, 9c, 149] Recently, Kraemer et al.[150] reported a flat-panel solar thermoelectric generator (STEG) with a system efficiency of 4.6%-5.2% generated from a temperature difference of 180 ˚C (T_c = 20 ˚C, T_h = 200 ˚C). The thermoelectric legs are made from *p*-type and *n*-type ZnSb compound. The efficiency is 7-8 times higher than the best value previously reported.[150]

With the development of nanotechnology and fabrication technology, with the discovery of new metal chalcogenide structures, as well as new theories leading to high thermoelectric performance, the *ZT* values of metal chalcogenides could be further enhanced to yield a comparable efficiency to conventional heat engines, and thus make greater contributions to energy saving and environmental protection.

Acknowledgements
C. Han gratefully acknowledges the Chinese Scholarship Council (CSC) for his scholarship. Z. Li acknowledges support from the Australian Research Council (ARC) through the Discovery Projects DP130102699 and DP130102274, and support from the National Natural Science Foundation of China (81471657, 81527901), the 1000 Talents Plan, and Jiangsu Specially Appointed Professorship. S. Dou is grateful for support from the Baosteel-Australia Research Centre (BARC) through the project BA110011 and from the ARC through the Linkage Project LP120200289. The authors are grateful for the support from ISEM at UOW, Jiangsu Provincial Key Laboratory of Radiation Medicine and Protection, and the Priority Academic Program Development of Jiangsu Higher Education Institutions (PAPD). The authors would like to thank Dr. Tania Silver for polishing the manuscript.

Received: ((will be filled in by the editorial staff))
Revised: ((will be filled in by the editorial staff))
Published online: ((will be filled in by the editorial staff))

[1] A. P. Gonçalves, C. Godart, *Eur. Phys. J. B* **2014**, *87*, 42.
[2] T. Kuroki, K. Kabeya, K. Makino, T. Kajihara, H. Kaibe, H. Hachiuma, H. Matsuno, A. Fujibayashi, *J. Electron. Mater.* **2014**, *43*, 2405.
[3] C. Han, Z. Li, S. Dou, *Chin. Sci. Bull.* **2014**, *59*, 2073.
[4] M. G. Kanatzidis, *Chem. Mater.* **2010**, *22*, 648.
[5] A. D. LaLonde, Y. Pei, H. Wang, G. Jeffrey Snyder, *Mater. Today* **2011**, *14*, 526.

[6] J. He, Y. Liu, R. Funahashi, *J. Mater. Res.* **2011**, *26*, 1762.
[7] P. Jood, M. Ohta, *Mater. Today* **2015**, *8*, 1124.
[8] a) K. Nielsch, J. Bachmann, J. Kimling, H. Böttner, *Adv. Energy Mater.* **2011**, *1*, 713; b) Z. Li, Q. Sun, X. D. Yao, Z. H. Zhu, G. Q. Lu, *J. Mater. Chem.* **2012**, *22*, 22821.
[9] a) C. Han, Z. Li, W.-j. Li, S.-l. Chou, S.-x. Dou, *J. Mater. Chem. A* **2014**, *2*, 11683; b) Y. Bai, C. Han, X. Chen, H. Yu, X. Zong, Z. Li, L. Wang, *Nano Energy* **2015**, *13*, 609; c) M.-R. Gao, Y.-F. Xu, J. Jiang, S.-H. Yu, *Chem. Soc. Rev.* **2013**, *42*, 2986; d) J. Xiong, C. Han, Z. Li, S. Dou, *Chi. Sci. Bull.* **2015**, *60*, 2083; e) J. Xiong, C. Han, W. Li, Q. Sun, J. Chen, S. Chou, Z. Li, S. Dou, *CrystEngComm* **2016**, *18*, 930; f) Y. B. Chao Han, Qiao Sun, Shaohua Zhang, Zhen Li, Lianzhou Wang, Shixue Dou, *Adv. Sci.* **2016**, DOI: DOI: 10.1002/advs.201500350; g) X. Q. Chen, Y. Bai, Z. Li, L. Z. Wang, S. X. Dou, *ChemPlusChem* **2016**, *81*, 414; h) X. Q. Chen, Z. Li, Y. Bai, Q. Sun, L. Z. Wang, S. X. Dou, *Chem. A. Europ. J.* **2015**, *21*, 1055; i) W.-J. Li, C. Han, S.-L. Chou, J.-Z. Wang, Z. Li, Y.-M. Kang, H.-K. Liu, S.-X. Dou, *Chem. A. Europ. J.* **2016**, *22*, 590.
[10] T. C. Harman, P. J. Taylor, M. P. Walsh, B. E. LaForge, *Science* **2002**, *297*, 2229.
[11] L.-D. Zhao, S.-H. Lo, Y. Zhang, H. Sun, G. Tan, C. Uher, C. Wolverton, V. P. Dravid, M. G. Kanatzidis, *Nature* **2014**, *508*, 373.
[12] K. Biswas, J. He, I. D. Blum, C.-I. Wu, T. P. Hogan, D. N. Seidman, V. P. Dravid, M. G. Kanatzidis, *Nature* **2012**, *489*, 414.
[13] G. G. Yadav, J. A. Susoreny, G. Zhang, H. Yang, Y. Wu, *Nanoscale* **2011**, *3*, 3555.
[14] S. LeBlanc, S. K. Yee, M. L. Scullin, C. Dames, K. E. Goodson, *Renew. Sustain. Energy Rev.* **2014**, *32*, 313.
[15] J.-S. Rhyee, K. H. Lee, S. M. Lee, E. Cho, S. I. Kim, E. Lee, Y. S. Kwon, J. H. Shim, G. Kotliar, *Nature* **2009**, *459*, 965.
[16] H. Liu, X. Shi, F. Xu, L. Zhang, W. Zhang, L. Chen, Q. Li, C. Uher, T. Day, G. J. Snyder, *Nat Mater* **2012**, *11*, 422.
[17] H. Liu, X. Yuan, P. Lu, X. Shi, F. Xu, Y. He, Y. Tang, S. Bai, W. Zhang, L. Chen, Y. Lin, L. Shi, H. Lin, X. Gao, X. Zhang, H. Chi, C. Uher, *Adv. Mater.* **2013**, *25*, 6607.
[18] R. Venkatasubramanian, E. Siivola, T. Colpitts, B. O'Quinn, *Nature* **2001**, *413*, 597.
[19] C. B. Satterthwaite, R. W. Ure, *Phys. Rev.* **1957**, *108*, 1164.
[20] a) L. Hu, T. Zhu, X. Liu, X. Zhao, *Adv. Funct. Mater.* **2014**, *24*, 5211; b) K. H. L. Sang Il Kim, Hyeon A. Mun, Hyun Sik Kim, Sung Woo Hwang, Jong Wook Roh, Dae Jin Yang, Weon Ho Shin, Xiang Shu Li, Young Hee Lee, G. Jeffrey Snyder, Sung Wng Kim, *Science* **2015**, *348*, 109.
[21] P. Puneet, R. Podila, M. Karakaya, S. Zhu, J. He, T. M. Tritt, M. S. Dresselhaus, A. M. Rao, *Sci. Rept.* **2013**, *3*, 3212.
[22] W. Xie, X. Tang, Y. Yan, Q. Zhang, T. M. Tritt, *J. Appl. Phys.* **2009**, *105*, 113713.
[23] F. Wu, H. Song, F. Gao, W. Shi, J. Jia, X. Hu, *J. Electron. Mater.* **2013**, *42*, 1140.
[24] a) R. J. Mehta, Y. Zhang, C. Karthik, B. Singh, R. W. Siegel, T. Borca-Tasciuc, G. Ramanath, *Nat Mater* **2012**, *11*, 233; b) A. Soni, Z. Yanyuan, Y. Ligen, M. K. K. Aik, M. S. Dresselhaus, Q. Xiong, *Nano Lett.* **2012**, *12*, 1203.
[25] H. Li, H. Jing, Y. Han, G.-Q. Lu, L. Xu, *Intermetallics* **2013**, *43*, 16.
[26] D.-W. Liu, J.-F. Li, C. Chen, B.-P. Zhang, *J. Electron. Mater.* **2011**, *40*, 992.
[27] a) N. Gothard, J. E. Spowart, T. M. Tritt, *Phys. Status Solidi (a)* **2010**, *207*, 157; b) J. H. Sun, X. Y. Qin, H. X. Xin, D. Li, L. Pan, C. J. Song, J. Zhang, R. R. Sun, Q. Q. Wang, Y. F. Liu, *J. Alloys Compd.* **2010**, *500*, 215; c) Y. H. Zhang, G. Y. Xu, F. Han, Z. Wang, C. C. Ge, *J. Electron. Mater.* **2010**, *39*, 1741; d) F. Li, X. Huang, Z. Sun, J. Ding, J. Jiang, W. Jiang, L. Chen, *J. Alloys Compd.* **2011**, *509*, 4769; e) D.-H. Park, M.-Y. Kim, T.-S. Oh, *Curr. Appl. Phys.* **2011**, *11*, S41; f) K.-C. Je, B. Ko, C. Kim, H. Kim, D.-H. Kim, *J. Alloys Compd.* **2012**, *517*, 75; g) H. Fang, T. Feng, H. Yang, X. Ruan, Y. Wu, *Nano Lett.* **2013**, *13*, 2058; h) L. P. Tan, T. Sun, S. Fan, L. Y. Ng, A. Suwardi, Q. Yan, H. H. Hng, *Nano Energy* **2013**, *2*, 4; i) J.-H. Yim, S.-H. Baek, H.-Y. Shin, D. Hyun, J.-S. Kim, *J. Electron. Mater.* **2013**, *42*, 2178; j) Y. Zhai, T. Zhang, Y. Xiao, J. Jiang, S.

Yang, G. Xu, *J. Alloys Compd.* **2013**, *563*, 285; k) T. Zhang, J. Jiang, Y. Xiao, Y. Zhai, S. Yang, G. Xu, *Appl. Mater. Interface* **2013**, *5*, 3071; l) M. Keshavarz, D. Vasilevskiy, R. Masut, S. Turenne, *J. Electron. Mater.* **2014**, *43*, 2239; m) Y. Xiao, G. Chen, H. Qin, M. Wu, Z. Xiao, J. Jiang, J. Xu, H. Jiang, G. Xu, *J. Mater. Chem. A* **2014**, *2*, 8512; n) Q. Zhang, X. Ai, W. Wang, L. Wang, W. Jiang, *Acta Mater.* **2014**, *73*, 37; o) Y. Li, D. Li, X. Qin, X. Yang, Y. Liu, J. Zhang, Y. Dou, C. Song, H. Xin, *J. Mater. Chem. C* **2015**, *3*, 7045; p) Z. Li, S. Zheng, Y. Zhang, H. Chen, T. Huang, G. Lu, *J. Electron. Mater.* **2015**, *44*, 2061; q) Q. Lognoné, F. Gascoin, *J. Alloys Compd.* **2015**, *635*, 107; r) S. Hwang, S.-I. Kim, K. Ahn, J. Roh, D.-J. Yang, S.-M. Lee, K.-H. Lee, *J. Electron. Mater.* **2013**, *42*, 1411; s) C.-L. Hsin, Y.-Y. Tsai, *Nano Energy* **2015**, *11*, 647; t) D. K. Misra, S. Sumithra, N. S. Chauhan, W. M. Notling, P. F. P. Poudeu, K. L. Stokes, *Mater. Sci. Semicond. Process.* **2015**, *40*, 453.

[28] M. Scheele, N. Oeschler, I. Veremchuk, S.-O. Peters, A. Littig, A. Kornowski, C. Klinke, H. Weller, *ACS Nano* **2011**, *5*, 8541.

[29] a) D.-Y. Chung, T. Hogan, P. Brazis, M. Rocci-Lane, C. Kannewurf, M. Bastea, C. Uher, M. G. Kanatzidis, *Science* **2000**, *287*, 1024; b) V. A. Kulbachinskii, V. G. Kytin, P. M. Tarasov, N. A. Yuzeeva, *Phys. Solid State* **2010**, *52*, 1830; c) X. Zhang, X.-y. Ma, Q.-m. Lu, F.-p. Zhang, Y.-q. Liu, J.-x. Zhang, L. Wang, *J. Electron. Mater.* **2011**, *40*, 773; d) V. A. Kulbachinskii, V. G. Kytin, A. A. Kudryashov, R. A. Lunin, *J. Solid State Chem.* **2012**, *193*, 83; e) M. K. Fuccillo, S. Jia, M. E. Charles, R. J. Cava, *J. Electron. Mater.* **2013**, *42*, 1246; f) M.-K. Han, H. Ryu, S.-J. Kim, *J. Electron. Mater.* **2013**, *42*, 2758; g) K.-H. Lee, S. Hwang, B. Ryu, K. Ahn, J. Roh, D. Yang, S.-M. Lee, H. Kim, S.-I. Kim, *J. Electron. Mater.* **2013**, *42*, 1617; h) H. Kitagawa, T. Matsuura, T. Kato, K.-y. Kamata, *J. Electron. Mater.* **2015**, *44*, 1870; i) H. Mun, K. Lee, S. Kim, J.-Y. Kim, J. Lee, J.-H. Lim, H. Park, J. Roh, S. Kim, *Mater. Today* **2015**, *8*, 959.

[30] V. A. Kulbachinskii, H. Negishi, M. Sasaki, Y. Giman, M. Inoue, P. Lostták, J. Horák, *Phys. Status Solidi (b)* **1997**, *199*, 505.

[31] C. M. Jaworski, B. Wiendlocha, V. Jovovic, J. P. Heremans, *Energy Environ. Sci.* **2011**, *4*, 4155.

[32] a) Q. Zhang, B. Liao, Y. Lan, K. Lukas, W. Liu, K. Esfarjani, C. Opeil, D. Broido, G. Chen, Z. Ren, *Proceed. Nation, Academy Sci. U. S. A.* **2013**, *110*, 13261; b) J. P. Heremans, V. Jovovic, E. S. Toberer, A. Saramat, K. Kurosaki, A. Charoenphakdee, S. Yamanaka, G. J. Snyder, *Science* **2008**, *321*, 554; c) H. S. Dow, M. W. Oh, B. S. Kim, S. D. Park, B. K. Min, H. W. Lee, D. M. Wee, *J. Appl. Phys.* **2010**, *108*, 113709.

[33] Y. Luo, J. Yang, Q. Jiang, L. Fu, Y. Xiao, W. Li, D. Zhang, Z. Zhou, Y. Cheng, *Nano Energy* **2015**, *15*, 709.

[34] a) H. Kitagawa, A. Kurata, H. Araki, S. Morito, E. Tanabe, *J. Electron. Mater.* **2010**, *39*, 1692; b) R. Srinivasan, N. Gothard, J. Spowart, *Mater. Lett.* **2010**, *64*, 1772; c) X. Yan, B. Poudel, Y. Ma, W. S. Liu, G. Joshi, H. Wang, Y. Lan, D. Wang, G. Chen, Z. F. Ren, *Nano Lett.* **2010**, *10*, 3373; d) A. M. Dehkordi, D. Vashaee, *Phys. Status Solidi (a)* **2012**, *209*, 2131; e) Y. Nagami, K. Matsuoka, T. Akao, T. Onda, T. Hayashi, Z.-C. Chen, *J. Electron. Mater.* **2014**, *43*, 2262.

[35] a) T. Zhu, Z. Xu, J. He, J. Shen, S. Zhu, L. Hu, T. M. Tritt, X. Zhao, *J. Mater. Chem. A* **2013**, *1*, 11589; b) Q. Jiang, H. Yan, J. Khaliq, H. Ning, S. Grasso, K. Simpson, M. J. Reece, *J. Mater. Chem. A* **2014**, *2*, 5785.

[36] a) D. H. Kim, C. Kim, K.-C. Je, G. H. Ha, H. Kim, *Acta Mater.* **2011**, *59*, 4957; b) H. Kim, D. H. Kim, C. Kim, S. Park, *AIP Confer. Proceeds.* **2012**, *1449*, 139.

[37] W.-T. Zhu, W.-Y. Zhao, H.-Y. Zhou, J. Yu, D.-G. Tang, Z.-Y. Liu, Q.-J. Zhang, *J. Electron. Mater.* **2014**, *43*, 1768.

[38] a) G. Rogl, A. Grytsiv, P. Rogl, E. Royanian, E. Bauer, J. Horky, D. Setman, E. Schafler, M. Zehetbauer, *Acta Mater.* **2013**, *61*, 6778; b) J.-J. Shen, T.-J. Zhu, X.-B. Zhao, S.-N. Zhang, S.-H. Yang, Z.-Z. Yin, *Energy Environ. Sci.* **2010**, *3*, 1519; c) X. Guo, X. Jia, T. Su, K. Jie, H. Sun, H. Ma, *Chem. Phys. Lett.* **2012**, *550*, 170; d) D. I. Bogomolov, V. T. Bublik, S. Y. Skipidarov, N. Y. Tabachkova, *Inorg. Mater.* **2013**, *49*, 758; e) S.-J. Jung, J.-H. Kim, D.-I. Kim, S. K. Kim, H.-H.

Park, J.-S. Kim, D.-B. Hyun, S.-H. Baek, *Phys. Chem. Chem. Phys.* **2014**, *16*, 3529; f) Z. J. Xu, L. P. Hu, P. J. Ying, X. B. Zhao, T. J. Zhu, *Acta Mater.* **2015**, *84*, 385.
[39] R. Amatya, R. J. Ram, *J. Electron. Mater.* **2012**, *41*, 1011.
[40] a) Z. Ali, S. Butt, C. Cao, F. K. Butt, M. Tahir, M. Tanveer, I. Aslam, M. Rizwan, F. Idrees, S. Khalid, *AIP Advances* **2014**, *4*, 117129; b) S. Gupta, N. Vijayan, A. Krishna, K. Thukral, K. K. Maurya, S. Muthiah, A. Dhar, B. Singh, G. Bhagavannarayana, *J. Appl. Crystallogr.* **2015**, *48*, 533.
[41] W. Liu, C. F. Guo, M. Yao, Y. Lan, H. Zhang, Q. Zhang, S. Chen, C. P. Opeil, Z. Ren, *Nano Energy* **2014**, *4*, 113.
[42] a) Y.-Q. Yu, B.-P. Zhang, Z.-H. Ge, P.-P. Shang, Y.-X. Chen, *Mater. Chem. Phys.* **2011**, *131*, 216; b) K. Biswas, L.-D. Zhao, M. G. Kanatzidis, *Adv. Energy Mater.* **2012**, *2*, 634; c) Z.-H. Ge, B.-P. Zhang, Y.-Q. Yu, P.-P. Shang, *J. Alloys Compd.* **2012**, *514*, 205; d) X. Du, F. Cai, X. Wang, *J. Alloys Compd.* **2014**, *587*, 6; e) L. Li, Y. Liu, J. Y. Dai, H. X. Zhu, A. J. Hong, X. H. Zhou, Z. F. Ren, J. M. Liu, *Nano Energy* **2015**, *12*, 447; f) Z. Liu, Y. Pei, H. Geng, J. Zhou, X. Meng, W. Cai, W. Liu, J. Sui, *Nano Energy* **2015**, *13*, 554; g) G. Sun, X. Qin, D. Li, J. Zhang, B. Ren, T. Zou, H. Xin, S. B. Paschen, X. Yan, *J. Alloys Compd.* **2015**, *639*, 9.
[43] X. Du, R. Shi, Y. Ma, F. Cai, X. Wang, Z. Yuan, *RSC Advances* **2015**, *5*, 31004.
[44] H. Iwasaki, I. Kimura, T. Murakami, H. Kim, *Physica B: Condensed Matter* **2015**, *472*, 91.
[45] a) M.-K. Han, S. Kim, H.-Y. Kim, S.-J. Kim, *RSC Advances* **2013**, *3*, 4673; b) W. Liu, K. C. Lukas, K. McEnaney, S. Lee, Q. Zhang, C. P. Opeil, G. Chen, Z. Ren, *Energy Environ. Sci.* **2013**, *6*, 552; c) L.-J. Zhang, B.-P. Zhang, Z.-H. Ge, C.-G. Han, *Solid State Commun.* **2013**, *162*, 48.
[46] Y. Pei, X. Shi, A. LaLonde, H. Wang, L. Chen, G. J. Snyder, *Nature* **2011**, *473*, 66.
[47] a) J. Androulakis, I. Todorov, D.-Y. Chung, S. Ballikaya, G. Wang, C. Uher, M. Kanatzidis, *Phys. Rev. B* **2010**, *82*, 115209; b) S. N. Girard, J. He, X. Zhou, D. Shoemaker, C. M. Jaworski, C. Uher, V. P. Dravid, J. P. Heremans, M. G. Kanatzidis, *J. Am. Chem. Soc.* **2011**, *133*, 16588; c) Y. Pei, N. A. Heinz, A. LaLonde, G. J. Snyder, *Energy Environ. Sci.* **2011**, *4*, 3640; d) M. Guch, C. Raj Sankar, J. R. Salvador, G. P. Meisner, H. Kleinke, *J. Appl. Phys.* **2012**, *111*, 063706; e) Y. Pei, A. D. LaLonde, N. A. Heinz, G. J. Snyder, *Adv. Energy Mater.* **2012**, *2*, 670; f) F. F. Aliev, H. A. Hasanov, *Indian J. Phys.* **2013**, *87*, 345; g) H. Wang, J. Hwang, M. L. Snedaker, I.-h. Kim, C. Kang, J. Kim, G. D. Stucky, J. Bowers, W. Kim, *Chem. Mater.* **2015**, *27*, 944.
[48] J. He, L.-D. Zhao, J.-C. Zheng, J. W. Doak, H. Wu, H.-Q. Wang, Y. Lee, C. Wolverton, M. G. Kanatzidis, V. P. Dravid, *J. Am. Chem. Soc.* **2013**, *135*, 4624.
[49] J. He, I. D. Blum, H.-Q. Wang, S. N. Girard, J. Doak, L.-D. Zhao, J.-C. Zheng, G. Casillas, C. Wolverton, M. Jose-Yacaman, D. N. Seidman, M. G. Kanatzidis, V. P. Dravid, *Nano Lett.* **2012**, *12*, 5979.
[50] S. Ahmad, S. D. Mahanti, K. Hoang, M. G. Kanatzidis, *Phys. Rev. B* **2006**, *74*, 155205.
[51] a) Q. Zhang, H. Wang, W. Liu, H. Wang, B. Yu, Q. Zhang, Z. Tian, G. Ni, S. Lee, K. Esfarjani, G. Chen, Z. Ren, *Energy Environ. Sci.* **2012**, *5*, 5246; b) A. D. LaLonde, Y. Pei, G. J. Snyder, *Energy Environ. Sci.* **2011**, *4*, 2090.
[52] a) R. J. Korkosz, T. C. Chasapis, S.-h. Lo, J. W. Doak, Y. J. Kim, C.-I. Wu, E. Hatzikraniotis, T. P. Hogan, D. N. Seidman, C. Wolverton, V. P. Dravid, M. G. Kanatzidis, *J. Am. Chem. Soc.* **2014**, *136*, 3225; b) M. Ibáñez, R. J. Korkosz, Z. Luo, P. Riba, D. Cadavid, S. Ortega, A. Cabot, M. G. Kanatzidis, *J. Am. Chem. Soc.* **2015**, *137*, 4046; c) J. Androulakis, I. Todorov, J. He, D.-Y. Chung, V. Dravid, M. Kanatzidis, *J. Am. Chem. Soc.* **2011**, *133*, 10920.
[53] D. Wu, L.-D. Zhao, X. Tong, W. Li, L. Wu, Q. Tan, Y. Pei, L. Huang, J.-F. Li, Y. Zhu, M. G. Kanatzidis, J. He, *Energy Environ. Sci.* **2015**, *8*, 2056.
[54] a) S. Aminorroaya Yamini, H. Wang, Z. M. Gibbs, Y. Pei, D. R. G. Mitchell, S. X. Dou, G. J. Snyder, *Acta Mater.* **2014**, *80*, 365; b) S. A. Yamini, D. R. G. Mitchell, Z. M. Gibbs, R. Santos, V. Patterson, S. Li, Y. Z. Pei, S. X. Dou, G. Jeffrey Snyder, *Adv. Energy Mater.* **2015**, DOI: 10.1002/aenm.201501047, n/a.

[55] J. He, S. N. Girard, J.-C. Zheng, L. Zhao, M. G. Kanatzidis, V. P. Dravid, *Adv. Mater.* **2012**, *24*, 4440.
[56] Y. Lee, S.-H. Lo, J. Androulakis, C.-I. Wu, L.-D. Zhao, D.-Y. Chung, T. P. Hogan, V. P. Dravid, M. G. Kanatzidis, *J. Am. Chem. Soc.* **2013**, *135*, 5152.
[57] J. Yao, N. J. Takas, M. L. Schliefert, D. S. Paprocki, P. E. R. Blanchard, H. Gou, A. Mar, C. L. Exstrom, S. A. Darveau, P. F. P. Poudeu, J. A. Aitken, *Phys. Rev. B* **2011**, *84*, 075203.
[58] R. Liu, L. Xi, H. Liu, X. Shi, W. Zhang, L. Chen, *Chem. Commun.* **2012**, *48*, 3818.
[59] T. Plirdpring, K. Kurosaki, A. Kosuga, T. Day, S. Firdosy, V. Ravi, G. J. Snyder, A. Harnwunggmoung, T. Sugahara, Y. Ohishi, H. Muta, S. Yamanaka, *Adv. Mater.* **2012**, *24*, 3622.
[60] K. K. Masaya Kumagai, Yuji Ohishi,, S. Y. Hiroaki Muta, *Mater. Trans.* **2014**, *55*, 1215.
[61] V. Kumar Gudelli, V. Kanchana, G. Vaitheeswaran, A. Svane, N. E. Christensen, *J. Appl. Phys.* **2013**, *114*, 223707.
[62] a) S. Chen, W. Ren, Q. Meng, X. Liu, J. Yang, J. Cui, *Phys. Status Solidi (a)* **2014**, *211*, 618; b) N. Cheng, R. Liu, S. Bai, X. Shi, L. Chen, *J. Appl. Phys.* **2014**, *115*, 163705; c) R. L. N. Cheng, S. Bai, Xun Shi, Lidong Chen, *J. Appl. Phys.* **2014**, *115*, 163705(1; d) L. Wang, P. Ying, Y. Deng, H. Zhou, Z. Du, J. Cui, *RSC Advances* **2014**, *4*, 33897; e) J. Zhang, X. Qin, D. Li, H. Xin, C. Song, L. Li, Z. Wang, G. Guo, L. Wang, *J. Alloys Compd.* **2014**, *586*, 285; f) W. D. Carr, D. T. Morelli, *J. Alloys Compd.* **2015**, *630*, 277; g) V. Kucek, C. Drasar, J. Navratil, T. Plechacek, L. Benes, *J. Phys. Chem. Solids* **2015**, *83*, 18; h) J. Zhang, X. Qin, D. Li, C. Song, X. Zhu, Y. Liu, H. Xin, L. Chen, T. Zou, *Intermetallics* **2015**, *60*, 45.
[63] a) K. K. Aikebaier Yusufu, Atsuko Kosuga, Tohru Sugahara, Yuji Ohishi, Hiroaki Muta, Shinsuke Yamanaka, *Appl. Phys. Lett.* **2011**, *99*, 061902(1; b) J. Zhang, X. Qin, D. Li, H. Xin, C. Song, L. Li, X. Zhu, Z. Wang, G. Guo, L. Wang, *J. Mater. Chem. A* **2014**, *2*, 2891; c) A. H. Reshak, *J. Phys. Chem. Solids* **2015**, *78*, 46.
[64] J. L. Cui, Y. Y. Li, Y. Deng, Q. S. Meng, Y. L. Gao, H. Zhou, Y. P. Li, *Intermetallics* **2012**, *31*, 217.
[65] C. H. L. Goodman, *J. Phys. Chem. Solids* **1958**, *6*, 305.
[66] a) X. Shi, L. Xi, J. Fan, W. Zhang, L. Chen, *Chem. Mater.* **2010**, *22*, 6029; b) E. Skoug, J. Cain, D. Morelli, *J. Electron. Mater.* **2012**, *41*, 1232.
[67] C. Bourgès, P. Lemoine, O. I. Lebedev, R. Daou, V. Hardy, B. Malaman, E. Guilmeau, *Acta Mater.* **2015**, *97*, 180.
[68] a) S. N. Guin, A. Chatterjee, D. S. Negi, R. Datta, K. Biswas, *Energy Environ. Sci.* **2013**, *6*, 2603; b) S. N. Guin, K. Biswas, *Chem. Mater.* **2013**, *25*, 3225.
[69] a) A. Suzumura, M. Watanabe, N. Nagasako, R. Asahi, *J. Electron. Mater.* **2014**, *43*, 2356; b) T.-R. Wei, F. Li, J.-F. Li, *J. Electron. Mater.* **2014**, *43*, 2229; c) T. H. Zou, X. Y. Qin, D. Li, G. L. Sun, Y. C. Dou, Q. Q. Wang, B. J. Ren, J. Zhang, H. X. Xin, Y. Y. Li, *Appl. Phys. Lett.* **2014**, *104*, 013904.
[70] K. S. Weldert, W. G. Zeier, T. W. Day, M. Panthöfer, G. J. Snyder, W. Tremel, *J. Am. Chem. Soc.* **2014**, *136*, 12035.
[71] a) J. B. Vaney, G. Delaizir, E. Alleno, O. Rouleau, A. Piarristeguy, J. Monnier, C. Godart, M. Ribes, R. Escalier, A. Pradel, A. P. Goncalves, E. B. Lopes, G. J. Cuello, P. Ziolkowski, E. Muller, C. Candolfi, A. Dauscher, B. Lenoir, *J. Mater. Chem. A* **2013**, *1*, 8190; b) J. B. Vaney, A. Piarristeguy, A. Pradel, E. Alleno, B. Lenoir, C. Candolfi, A. Dauscher, A. P. Gonçalves, E. B. Lopes, G. Delaizir, J. Monnier, M. Ribes, C. Godart, *J. Solid State Chem.* **2013**, *203*, 212.
[72] a) Y. Li, T. Zhang, Y. Qin, T. Day, G. Jeffrey Snyder, X. Shi, L. Chen, *J. Appl. Phys.* **2014**, *116*, 203705; b) N. Tsujii, T. Mori, Y. Isoda, *J. Electron. Mater.* **2014**, *43*, 2371.
[73] P. Qiu, T. Zhang, Y. Qiu, X. Shi, L. Chen, *Energy Environ. Sci.* **2014**, *7*, 4000.
[74] a) J. R. Sootsman, D. Y. Chung, M. G. Kanatzidis, *Angew. Chem. Int. Ed.* **2009**, *48*, 8616; b) K. Kurosaki, S. Yamanaka, *Phys. Status Solidi (a)* **2013**, *210*, 82.

[75] a) B. Wölfing, C. Kloc, J. Teubner, E. Bucher, *Phys. Rev. Lett.* **2001**, *86*, 4350; b) K. Kurosaki, A. Kosuga, H. Muta, S. Yamanaka, *Mater. Trans.* **2005**, *46*, 1502.
[76] a) H. Zhang, J. He, B. Zhang, Z. Su, T. Tritt, N. Soheilnia, H. Kleinke, *J. Electron. Mater.* **2007**, *36*, 727; b) C. Candolfi, B. Lenoir, C. Chubilleau, A. Dauscher, E. Guilmeau, *J. Phys.: Condens. Matter* **2010**, *22*, 025801.
[77] H. Xu, K. M. Kleinke, T. Holgate, D. Rossouw, G. Botton, T. M. Tritt, H. Kleinke, *J. Alloys Compd.* **2010**, *504*, 314.
[78] a) M. Ohta, A. Yamamoto, H. Obara, *J. Electron. Mater.* **2010**, *39*, 2117; b) T. Zhou, B. Lenoir, C. Christophe, A. Dauscher, P. Gall, P. Gougeon, M. Potel, E. Guilmeau, *J. Electron. Mater.* **2011**, *40*, 508; c) R. Al Rahal Al Orabi, P. Gougeon, P. Gall, B. Fontaine, R. Gautier, M. Colin, C. Candolfi, A. Dauscher, J. Hejtmanek, B. Malaman, B. Lenoir, *Inorg. Chem.* **2014**, *53*, 11699.
[79] a) M.-L. Liu, F.-Q. Huang, L.-D. Chen, I.-W. Chen, *Appl. Phys. Lett.* **2009**, *94*, 202103; b) X. Y. Shi, F. Q. Huang, M. L. Liu, L. D. Chen, *Appl. Phys. Lett.* **2009**, *94*, 122103; c) F.-J. Fan, Y.-X. Wang, X.-J. Liu, L. Wu, S.-H. Yu, *Adv. Mater.* **2012**, *24*, 6158; d) K. Suekuni, M. Kunii, H. Nishiate, M. Ohta, A. Yamamoto, M. Koyano, *J. Electron. Mater.* **2012**, *41*, 1130; e) H. Yang, L. A. Jauregui, G. Zhang, Y. P. Chen, Y. Wu, *Nano Lett.* **2012**, *12*, 540; f) K. Suekuni, K. Tsuruta, H. Fukuoka, M. Koyano, *J. Alloys Compd.* **2013**, *564*, 91; g) J. Navrátil, V. Kucek, T. Plecháček, E. Černošková, F. Laufek, Č. Drašar, P. Knotek, *J. Electron. Mater.* **2014**, *43*, 3719.
[80] J.-S. Rhyee, E. Cho, K. H. Lee, S. I. Kim, E. S. Lee, S. M. Lee, Y. S. Kwon, *J. Appl. Phys.* **2009**, *105*, 053712.
[81] J.-S. Rhyee, E. Cho, K. H. Lee, S. M. Lee, S. I. Kim, H.-S. Kim, Y. S. Kwon, S. J. Kim, *Appl. Phys. Lett.* **2009**, *95*, 212106.
[82] J.-S. Rhyee, J. Kim, *Mater. Today* **2015**, *8*, 1283.
[83] G. Tan, L.-D. Zhao, F. Shi, J. W. Doak, S.-H. Lo, H. Sun, C. Wolverton, V. P. Dravid, C. Uher, M. G. Kanatzidis, *J. Am. Chem. Soc.* **2014**, *136*, 7006.
[84] a) K. Ahn, E. Cho, J.-S. Rhyee, S. Il Kim, S. Mock Lee, K. Hyoung Lee, *Appl. Phys. Lett.* **2011**, *99*, 102110; b) J.-S. Rhyee, K. Ahn, K. H. Lee, H. S. Ji, J.-H. Shim, *Adv. Mater.* **2011**, *23*, 2191; c) G. H. Zhu, Y. C. Lan, H. Wang, G. Joshi, Q. Hao, G. Chen, Z. F. Ren, *Phys. Rev. B* **2011**, *83*, 115201; d) J.-Y. Yang, J. Wu, G. Li, J.-S. Zhang, J. Peng, *J. Electron. Mater.* **2012**, *41*, 1077; e) Y. Zhai, Q. Zhang, J. Jiang, T. Zhang, Y. Xiao, S. Yang, G. Xu, *J. Alloys Compd.* **2013**, *553*, 270; f) J. H. Kim, M. J. Kim, S. Oh, J.-S. Rhyee, *J. Alloys Compd.* **2014**, *615*, 933.
[85] J. Yang, G. Zhang, G. Yang, C. Wang, Y. X. Wang, *J. Alloys Compd.* **2015**, *644*, 615.
[86] G. Tan, F. Shi, J. W. Doak, H. Sun, L.-D. Zhao, P. Wang, C. Uher, C. Wolverton, V. P. Dravid, M. G. Kanatzidis, *Energy Environ. Sci.* **2015**, *8*, 267.
[87] Z. Li, L. Zhenag, J. Wang, Z. X. Cheng, Q. Sun, S. Dou, *J. Mater. Chem. A* **2016**, DOI: 10.1039/C6TA01994C.
[88] a) G. Tewari, T. S. Tripathi, A. K. Rastogi, *J. Electron. Mater.* **2010**, *39*, 1133; b) F. Gascoin, A. Maignan, *Chem. Mater.* **2011**, *23*, 2510.
[89] S. Bhattacharya, A. Bohra, R. Basu, R. Bhatt, S. Ahmad, K. N. Meshram, A. K. Debnath, A. Singh, S. K. Sarkar, M. Navneethan, Y. Hayakawa, D. K. Aswal, S. K. Gupta, *J. Mater. Chem. A* **2014**, *2*, 17122.
[90] Y.-X. Chen, B.-P. Zhang, Z.-H. Ge, P.-P. Shang, *J. Solid State Chem.* **2012**, *186*, 109.
[91] a) E. Guilmeau, Y. Bréard, A. Maignan, *Appl. Phys. Lett.* **2011**, *99*, 052107; b) J. Zhang, X. Y. Qin, H. X. Xin, D. Li, C. J. Song, *J. Electron. Mater.* **2011**, *40*, 980; c) R. Nunna, F. Gascoin, E. Guilmeau, *J. Alloys Compd.* **2015**, *634*, 32; d) C. Wan, X. Gu, F. Dang, T. Itoh, Y. Wang, H. Sasaki, M. Kondo, K. Koga, K. Yabuki, G. J. Snyder, R. Yang, K. Koumoto, *Nat Mater* **2015**, *14*, 622; e) C. Wan, Y. Wang, N. Wang, K. Koumoto, *Mater. Today* **2010**, *3*, 2606; f) T. Holgate, Y. Liu, D. Hitchcock, T. Tritt, J. He, *J. Electron. Mater.* **2013**, *42*, 1751; g) P. Jood, M. Ohta, H. Nishiate, A. Yamamoto, O. I. Lebedev, D. Berthebaud, K. Suekuni, M. Kunii, *Chem. Mater.* **2014**, *26*, 2684.

[92] M. Ohta, S. Satoh, T. Kuzuya, S. Hirai, M. Kunii, A. Yamamoto, *Acta Mater.* **2012**, *60*, 7232.
[93] M. Beaumale, T. Barbier, Y. Bréard, G. Guelou, A. V. Powell, P. Vaqueiro, E. Guilmeau, *Acta Mater.* **2014**, *78*, 86.
[94] a) T. P. Swastibrata Bhattacharyya, Abhishek K Singh, *Nanotechnology* **2014**, *25*, 465701(1; b) S. Kumar, U. Schwingenschlögl, *Chem. Mater.* **2015**, *27*, 1278; c) P. R. N. Misse, D. Berthebaud, O. I. Lebedev, A. Maignan, E. Guilmeau, *Materials (1996-1944)* **2015**, *8*, 2514.
[95] P. Ruleova, C. Drasar, P. Lostak, C. P. Li, S. Ballikaya, C. Uher, *Mater. Chem. Phys.* **2010**, *119*, 299.
[96] B. Zhan, Y. Liu, X. Tan, J.-l. Lan, Y.-h. Lin, C.-W. Nan, *J. Am. Ceram. Soc.* **2015**, *98*, 2465.
[97] S. N. Zhang, T. J. Zhu, S. H. Yang, C. Yu, X. B. Zhao, *J. Alloys Compd.* **2010**, *499*, 215.
[98] R. Mohanraman, R. Sankar, F. C. Chou, C. H. Lee, Y.-Y. Chen, *J. Appl. Phys.* **2013**, *114*, 163712.
[99] K. F. Hsu, S. Loo, F. Guo, W. Chen, J. S. Dyck, C. Uher, T. Hogan, E. K. Polychroniadis, M. G. Kanatzidis, *Science* **2004**, *303*, 818.
[100] Z.-Y. Li, J.-F. Li, *Adv. Energy Mater.* **2014**, *4*, n/a.
[101] C. M. J. Y Chen, Y B Gao, H Wang, T J Zhu, G J Snyder, J P Heremans, X B Zhao, *New J. Phys.* **2014**, *16*, 013057(1.
[102] S. K. Plachkovka, T. I. Georgiev, *J. Phys.: Condens. Matter* **1993**, *5*, 67.
[103] J. Q. Li, J. F. Deng, S. K. Li, Y. Li, F. S. Liu, W. Q. Ao, *Intermetallics* **2015**, *56*, 63.
[104] a) J. F. Deng, J. Q. Li, R. F. Ye, X. Y. Liu, F. S. Liu, W. Q. Ao, *J. Alloys Compd.* **2014**, *585*, 173; b) J. K. Lee, M. W. Oh, B. S. Kim, B. K. Min, H. W. Lee, S. D. Park, *Electron. Mater. Letters* **2014**, *10*, 813; c) Z. W. Lu, J. Q. Li, C. Y. Wang, Y. Li, F. S. Liu, W. Q. Ao, *J. Alloys Compd.* **2015**, *621*, 345.
[105] T. Rosenthal, P. Urban, K. Nimmrich, L. Schenk, J. de Boor, C. Stiewe, O. Oeckler, *Chem. Mater.* **2014**, *26*, 2567.
[106] a) T. Rosenthal, S. Welzmiller, O. Oeckler, *Solid State Sci.* **2013**, *25*, 118; b) R. Sankar, D. P. Wong, C.-S. Chi, W.-L. Chien, J.-S. Hwang, F.-C. Chou, L.-C. Chen, K.-H. Chen, *CrystEngComm* **2015**, *17*, 3440.
[107] T. Schröder, S. Schwarzmüller, C. Stiewe, J. de Boor, M. Hölzel, O. Oeckler, *Inorg. Chem.* **2013**, *52*, 11288.
[108] F. Fahrnbauer, D. Souchay, G. Wagner, O. Oeckler, *J. Am. Chem. Soc.* **2015**, *137*, 12633.
[109] J. Q. Li, Z. W. Lu, H. J. Wu, H. T. Li, F. S. Liu, W. Q. Ao, J. Luo, J. Q. He, *Acta Mater.* **2014**, *74*, 215.
[110] C. J. Vineis, A. Shakouri, A. Majumdar, M. G. Kanatzidis, *Adv. Mater.* **2010**, *22*, 3970.
[111] C. Xiao, X. Qin, J. Zhang, R. An, J. Xu, K. Li, B. Cao, J. Yang, B. Ye, Y. Xie, *J. Am. Chem. Soc.* **2012**, *134*, 18460.
[112] M. D. Lubomir GULAY, Oksana STROK, Adam PIETRASZKO, *Chem. Metal Alloys* **2011**, *4*, 200.
[113] L. Zhao, X. Wang, F. Y. Fei, J. Wang, Z. Cheng, S. Dou, J. Wang, G. J. Snyder, *J. Mater. Chem. A* **2015**, *3*, 9432.
[114] C. Nethravathi, C. R. Rajamathi, M. Rajamathi, R. Maki, T. Mori, D. Golberg, Y. Bando, *J. Mater. Chem. A* **2014**, *2*, 985.
[115] L. Pan, D. Bérardan, N. Dragoe, *J. Am. Chem. Soc.* **2013**, *135*, 4914.
[116] a) D. R. Brown, T. Day, K. A. Borup, S. Christensen, B. B. Iversen, G. J. Snyder, *APL Materials* **2013**, *1*, 052107; b) C. Han, Q. Sun, Z. X. Cheng, J. L. Wang, Z. Li, G. Q. Lu, S. X. Dou, *J. Am. Chem. Soc.* **2014**, *136*, 17626; c) A. J. Hong, L. Li, H. X. Zhu, X. H. Zhou, Q. Y. He, W. S. Liu, Z. B. Yan, J. M. Liu, Z. F. Ren, *Solid State Ionics* **2014**, *261*, 21; d) W. Mi, P. Qiu, T. Zhang, Y. Lv, X. Shi, L. Chen, *Appl. Phys. Lett.* **2014**, *104*, 133903.
[117] a) Q. Jiang, H. Yan, J. Khaliq, Y. Shen, K. Simpson, M. J. Reece, *J. Mater. Chem. A* **2014**, *2*, 9486; b) P. Q. Xiaobei Wang, Tiansong Zhang, Dudi Ren, Lihua Wu, Xun Shi, Jihui Yang, Lidong Chen, *J. Mater. Chem. A* **2015**, *3*, 13662.

[118] X.-X. Xiao, W.-J. Xie, X.-F. Tang, Q.-J. Zhang, *Chin. Phys. B* **2011**, *20*, 087201.
[119] a) H. Wang, W. Chu, D. Wang, W. Mao, W. Pan, Y. Guo, Y. Xiong, H. Jin, *J. Electron. Mater.* **2011**, *40*, 624; b) D. Li, X. Y. Qin, Y. F. Liu, C. J. Song, L. Wang, J. Zhang, H. X. Xin, G. L. Guo, T. H. Zou, G. L. Sun, B. J. Ren, X. G. Zhu, *RSC Advances* **2014**, *4*, 8638; c) X. Q. Chen, Z. Li, S. X. Dou, *Appl. Mater. Interface* **2015**, *7*, 13295; d) K. Tyagi, B. Gahtori, S. Bathula, M. Jayasimhadri, N. K. Singh, S. Sharma, D. Haranath, A. K. Srivastava, A. Dhar, *J. Phys. Chem. Solids* **2015**, *81*, 100.
[120] a) F. Drymiotis, T. W. Day, D. R. Brown, N. A. Heinz, G. Jeffrey Snyder, *Appl. Phys. Lett.* **2013**, *103*, 143906; b) L. Zhao, X. Wang, F. F. Yun, J. Wang, Z. Cheng, S. Dou, J. Wang, G. J. Snyder, *Adv. Electron. Mater.* **2015**, *1*, n/a.
[121] L. Zou, B.-P. Zhang, Z.-H. Ge, C. Gao, D.-B. Zhang, Y.-C. Liu, *Phys. Status Solidi (a)* **2013**, *210*, 2550.
[122] B. Gahtori, S. Bathula, K. Tyagi, M. Jayasimhadri, A. K. Srivastava, S. Singh, R. C. Budhani, A. Dhar, *Nano Energy* **2015**, *13*, 36.
[123] P. L. Ying He, Xun Shi, Fangfang Xu, Tiansong Zhang, Gerald Geffrey Snyder, Ctirad Uher, Lidong Chen, *Adv. Mater.* **2015**, *27*, 3639.
[124] G. Dennler, R. Chmielowski, S. Jacob, F. Capet, P. Roussel, S. Zastrow, K. Nielsch, I. Opahle, G. K. H. Madsen, *Adv. Energy Mater.* **2014**, *4*, n/a.
[125] D. Tian, H. Liu, Y. Deng, Z. Du, J. Cui, *RSC Advances* **2014**, *4*, 34104.
[126] a) S. Yamanaka, M. Ishimaru, A. Charoenphakdee, H. Matsumoto, K. Kurosaki, *J. Electron. Mater.* **2009**, *38*, 1392; b) J. Cui, Y. Gao, H. Zhou, Y. Li, Q. Meng, J. Yang, *Appl. Phys. Lett.* **2012**, *101*, 081908.
[127] Y. Gao, P. Ying, J. Cui, S. Chen, Y. Li, *Procedia Engin.* **2012**, *27*, 156.
[128] a) M. Ohta, S. Hirai, *J. Electron. Mater.* **2009**, *38*, 1287; b) A. Charoenphakdee, K. Kurosaki, A. Harnwunggmoung, H. Muta, S. Yamanaka, *J. Alloys Compd.* **2010**, *496*, 53; c) J.-S. Rhyee, E. Cho, K. H. Lee, S. M. Lee, H.-s. Kim, Y. S. Kwon, *J. Appl. Phys.* **2010**, *107*, 053705; d) J. V. Zaikina, T. Mori, K. Kovnir, D. Teschner, A. Senyshyn, U. Schwarz, Y. Grin, A. V. Shevelkov, *Chem. A. Europ. J.* **2010**, *16*, 12582; e) O. Mayasree, C. R. Sankar, Y. Cui, A. Assoud, H. Kleinke, *Eur. J. Inorg. Chem.* **2011**, *2011*, 4037; f) C.-Y. Meng, H. Chen, P. Wang, L. Chen, *Chem. Mater.* **2011**, *23*, 4910; g) M. Ohta, S. Hirai, T. Kuzuya, *J. Electron. Mater.* **2011**, *40*, 537; h) X. Wang, R. Yang, Y. Zhang, P. Zhang, Y. Xue, *Appl. Phys. Lett.* **2011**, *98*, 222110; i) B. Kim, I. Kim, B.-k. Min, M. Oh, S. Park, H. Lee, *Electron. Mater. Letters* **2013**, *9*, 477; j) T. Kyratsi, M. Ioannou, *J. Electron. Mater.* **2013**, *42*, 1604; k) H. Lin, H. Chen, J.-N. Shen, L. Chen, L.-M. Wu, *Chem. A. Europ. J.* **2014**, *20*, 15401; l) M. Wu, Y. Xiao, Z. Fu, Z. Li, J. Xu, J. Jiang, H. Jiang, G. Xu, *J. Electron. Mater.* **2014**, *43*, 3087; m) W. Xie, S. Populoh, K. Gałązka, X. Xiao, L. Sagarna, Y. Liu, M. Trottmann, J. He, A. Weidenkaff, *J. Appl. Phys.* **2014**, *115*, 103707; n) H. Zhang, S. Li, D. Li, S. Jin, S. Shen, T. Ying, Z. Lin, K. Li, D. Yuan, H. Zhao, *Mater. Lett.* **2015**, *152*, 117; o) D. Parker, A. F. May, H. Wang, M. A. McGuire, B. C. Sales, D. J. Singh, *Phys. Rev. B* **2013**, *87*, 045205; p) J. Heo, G. Laurita, S. Muir, M. A. Subramanian, D. A. Keszler, *Chem. Mater.* **2014**, *26*, 2047; q) C. Uhlig, E. Guenes, A. Schulze, M. Elm, P. Klar, S. Schlecht, *J. Electron. Mater.* **2014**, *43*, 2362; r) D. Wu, Y. Pei, Z. Wang, H. Wu, L. Huang, L.-D. Zhao, J. He, *Adv. Funct. Mater.* **2014**, *24*, 7763; s) J. Corps, P. Vaqueiro, A. Aziz, R. Grau-Crespo, W. Kockelmann, J.-C. Jumas, A. V. Powell, *Chem. Mater.* **2015**, *27*, 3946.
[129] B. Yu, M. Zebarjadi, H. Wang, K. Lukas, H. Wang, D. Wang, C. Opeil, M. Dresselhaus, G. Chen, Z. Ren, *Nano Lett.* **2012**, *12*, 2077.
[130] a) M. Ibáñez, R. Zamani, S. Gorsse, J. Fan, S. Ortega, D. Cadavid, J. R. Morante, J. Arbiol, A. Cabot, *ACS Nano* **2013**, *7*, 2573; b) M. Ibáñez, R. Zamani, W. Li, D. Cadavid, S. Gorsse, N. A. Katcho, A. Shavel, A. M. López, J. R. Morante, J. Arbiol, A. Cabot, *Chem. Mater.* **2012**, *24*, 4615; c) F. Wu, W. Shi, X. Hu, *Electron. Mater. Letters* **2015**, *11*, 127.
[131] C. Han, Z. Li, G. Q. Lu, S. Xue Dou, *Nano Energy* **2015**, *15*, 193.

[132] C. Kim, D. H. Kim, Y. S. Han, J. S. Chung, S. Park, H. Kim, *Powder Technol.* **2011**, *214*, 463.
[133] K. Ding, H. Lu, Y. Zhang, M. L. Snedaker, D. Liu, J. A. Maciá-Agulló, G. D. Stucky, *J. Am. Chem. Soc.* **2014**, *136*, 15465.
[134] a) J. S. Son, H. Zhang, J. Jang, B. Poudel, A. Waring, L. Nally, D. V. Talapin, *Angew. Chem. Int. Ed.* **2014**, *53*, 7466; b) H. Z. Dmitriy S. Dolzhnikov, Jaeyoung Jang, Jae Sung Son, Mattew G. Panthani, Tomohiro Shibata, Soma Chattopadhyay, Dmitri V. Talapin, *Science* **2015**, *347*, 425.
[135] a) Y. G. Xu Sun, Changzheng Wu, Yi Xie, *Adv. Mater.* **2015**, *27*, 3850; b) K. M. Y. Joonki Suh, Deyi Fu, Xinyu Liu, Fan Yang, Jin Fan, David J. Smith, Yong-Hang Zhang, Jacek K. Furdyna, Chris Dames, Wladyslaw Walukiewicz, Junqiao Wu, *Adv. Mater.* **2015**, *27*, 3681.
[136] A. M. Ibrahim, D. A. Thompson, *Nuclear Instruments and Methods in Physics Research Section B: Beam Interactions with Materials and Atoms* **1985**, *7–8, Part 2*, 566.
[137] C. Wu, F. Feng, J. Feng, J. Dai, L. Peng, J. Zhao, J. Yang, C. Si, Z. Wu, Y. Xie, *J. Am. Chem. Soc.* **2011**, *133*, 13798.
[138] M. H. Lee, J.-S. Rhyee, M. Vaseem, Y.-B. Hahn, S.-D. Park, H. Jin Kim, S.-J. Kim, H. J. Lee, C. Kim, *Appl. Phys. Lett.* **2013**, *102*, 223901.
[139] Y. Min, G. Park, B. Kim, A. Giri, J. Zeng, J. W. Roh, S. I. Kim, K. H. Lee, U. Jeong, *ACS Nano* **2015**, *9*, 6843.
[140] Z.-Y. Li, M. Zou, J.-F. Li, *J. Alloys Compd.* **2013**, *549*, 319.
[141] Y. Pei, H. Wang, G. J. Snyder, *Adv. Mater.* **2012**, *24*, 6125.
[142] D. Vasilevskiy, R. A. Masut, S. Turenne, *J. Electron. Mater.* **2012**, *41*, 1057.
[143] B. Poudel, Q. Hao, Y. Ma, Y. Lan, A. Minnich, B. Yu, X. Yan, D. Wang, A. Muto, D. Vashaee, X. Chen, J. Liu, M. S. Dresselhaus, G. Chen, Z. Ren, *Science* **2008**, *320*, 634.
[144] a) S.-J. Jung, S. Kim, H.-H. Park, D.-B. Hyun, S.-H. Baek, J.-S. Kim, *J. Electron. Mater.* **2014**, *43*, 1726; b) V. Ponnambalam, D. Morelli, *J. Electron. Mater.* **2015**, *44*, 2089.
[145] A. Patyk, *J. Electron. Mater.* **2010**, *39*, 2023.
[146] M. Zebarjadi, B. Liao, K. Esfarjani, M. Dresselhaus, G. Chen, *Adv. Mater.* **2013**, *25*, 1577.
[147] a) Z. Lu, M. Layani, X. Zhao, L. P. Tan, T. Sun, S. Fan, Q. Yan, S. Magdassi, H. H. Hng, *Small* **2014**, *10*, 3551; b) D. Madan, Z. Wang, P. K. Wright, J. W. Evans, *Applied Energy* **2015**, *156*, 587; c) B. T. McGrail, A. Sehirlioglu, E. Pentzer, *Angewandte Chemie International Edition* **2015**, *54*, 1710; d) J. Y. Oh, J. H. Lee, S. W. Han, S. S. Chae, E. J. Bae, Y. H. Kang, W. J. Choi, S. Y. Cho, J.-O. Lee, H. K. Baik, T. I. Lee, *Energy Environ. Sci.* **2016**, DOI: 10.1039/C5EE03813H; e) K. V. Selvan, M. S. Mohamed Ali, *Renewable and Sustainable Energy Reviews* **2016**, *54*, 1035; f) Y. Sun, J. A. Rogers, *Adv. Mater.* **2007**, *19*, 1897; g) T. Wada, Y. Matsuo, S. Nomura, Y. Nakamura, A. Miyamura, Y. Chiba, A. Yamada, M. Konagai, *Phys. Status Solidi (a)* **2006**, *203*, 2593; h) C. Yan, P. S. Lee, *Small* **2014**, *10*, 3443; i) C. Yu, A. Murali, K. Choi, Y. Ryu, *Energy Environ. Sci.* **2012**, *5*, 9481; j) B. Zhang, J. Sun, H. E. Katz, F. Fang, R. L. Opila, *ACS Appl. Mater. Interface* **2010**, *2*, 3170; k) W. Zhao, H. T. Tan, L. P. Tan, S. Fan, H. H. Hng, Y. C. F. Boey, I. Beloborodov, Q. Yan, *ACS Appl. Mater. Interface* **2014**, *6*, 4940; l) C. Zhou, C. Dun, Q. Wang, K. Wang, Z. Shi, D. L. Carroll, G. Liu, G. Qiao, *ACS Appl. Mater. Interface* **2015**, *7*, 21015.
[148] a) A. Besganz, V. Zöllmer, R. Kun, E. Pál, L. Walder, M. Busse, *Procedia Technology* **2014**, *15*, 99; b) C. Cho, B. Stevens, J.-H. Hsu, R. Bureau, D. A. Hagen, O. Regev, C. Yu, J. C. Grunlan, *Adv. Mater.* **2015**, *27*, 2996; c) G. Delaizir, J. Monnier, M. Soulier, R. Grodzki, B. Villeroy, J. Testard, J. Simon, C. Navone, C. Godart, *Sensors and Actuators A: Physical* **2012**, *174*, 115; d) C. Dun, C. A. Hewitt, H. Huang, D. S. Montgomery, J. Xu, D. L. Carroll, *Physical Chemistry Chemical Physics* **2015**, *17*, 8591; e) S. Kim, J. H. Son, S. H. Lee, B. K. You, K.-I. Park, H. K. Lee, M. Byun, K. J. Lee, *Adv. Mater.* **2014**, *26*, 7480; f) S. J. Kim, J. H. We, B. J. Cho, *Energy Environ. Sci.* **2014**, *7*, 1959; g) K. Kusagaya, M. Takashiri, *J. Alloys Compounds* **2015**, *653*, 480; h) L.-X. Liang, Y. Deng, Y. Wang, H.-L. Gao, J. Cui, *J Nanopart Res* **2014**, *16*, 1.

[149] P. Jackson, D. Hariskos, E. Lotter, S. Paetel, R. Wuerz, R. Menner, W. Wischmann, M. Powalla, *Prog. Photovoltaics: Res. Appl.* **2011**, *19*, 894.
[150] D. Kraemer, B. Poudel, H.-P. Feng, J. C. Caylor, B. Yu, X. Yan, Y. Ma, X. Wang, D. Wang, A. Muto, K. McEnaney, M. Chiesa, Z. Ren, G. Chen, *Nat Mater* **2011**, *10*, 532.
[151] K. Kurosaki, H. Matsumoto, A. Charoenphakdee, S. Yamanaka, M. Ishimaru, Y. Hirotsu, *Appl. Phys. Lett.* **2008**, *93*, 012101.
[152] L. P. Bulat, V. T. Bublik, I. A. Drabkin, V. V. Karataev, V. B. Osvenskii, Y. N. Parkhomenko, G. I. Pivovarov, D. A. Pshenai-Severin, N. Y. Tabachkova, *J. Electron. Mater.* **2010**, *39*, 1650.
[153] K. Kim, K. Kim, G. Ha, *Electron. Mater. Letters* **2010**, *6*, 177.
[154] N. Keawprak, S. Lao-ubol, C. Eamchotchawalit, Z. M. Sun, *J. Alloys Compd.* **2011**, *509*, 9296.
[155] J. J. Shen, Z. Z. Yin, S. H. Yang, C. Yu, T. J. Zhu, X. B. Zhao, *J. Electron. Mater.* **2011**, *40*, 1095.
[156] X. Guo, X. Jia, K. Jie, H. Sun, Y. Zhang, B. Sun, H. Ma, *Chem. Phys. Lett.* **2013**, *568–569*, 190.
[157] J. Li, Q. Tan, J.-F. Li, D.-W. Liu, F. Li, Z.-Y. Li, M. Zou, K. Wang, *Adv. Funct. Mater.* **2013**, *23*, 4317.
[158] G. Lee, G. Ha, *J. Electron. Mater.* **2014**, *43*, 1697.
[159] P.-Y. Lee, J. Hao, T.-Y. Chao, J.-Y. Huang, H.-L. Hsieh, H.-C. Hsu, *J. Electron. Mater.* **2014**, *43*, 1718.
[160] K. Lee, S.-M. Choi, J. Roh, S. Hwang, S. Kim, W. Shin, H. Park, J. Lee, S. Kim, D. Yang, *J. Electron. Mater.* **2015**, *44*, 1531.
[161] F. Yu, J. Zhang, D. Yu, J. He, Z. Liu, B. Xu, Y. Tian, *J. Appl. Phys.* **2009**, *105*, 094303.
[162] Y. Zhou, X. Li, S. Bai, L. Chen, *J. Cryst. Growth* **2010**, *312*, 775.
[163] C. Kim, D. H. Kim, J. S. Kim, Y. S. Han, J. S. Chung, H. Kim, *J. Alloys Compd.* **2011**, *509*, 9472.
[164] C. E. Carlton, C. A. Kuryak, W.-s. Liu, Z. Ren, G. Chen, Y. Shao-Horn, *J. Appl. Phys.* **2012**, *112*, 093518.
[165] G.-E. Lee, A. Y. Eum, K.-M. Song, I.-H. Kim, Y. Lim, W.-S. Seo, B.-J. Choi, C.-W. Hwang, *J. Electron. Mater.* **2015**, *44*, 1579.
[166] Q. Zhang, X. Ai, L. Wang, Y. Chang, W. Luo, W. Jiang, L. Chen, *Adv. Funct. Mater.* **2015**, *25*, 966.
[167] B. Yu, Q. Zhang, H. Wang, X. Wang, H. Wang, D. Wang, H. Wang, G. J. Snyder, G. Chen, Z. F. Ren, *J. Appl. Phys.* **2010**, *108*, 016104.
[168] C. Kang, H. Wang, H. Kim, S.-J. Kim, W. Kim, *J. Electron. Mater.* **2014**, *43*, 353.
[169] S. N. Girard, J. He, C. Li, S. Moses, G. Wang, C. Uher, V. P. Dravid, M. G. Kanatzidis, *Nano Lett.* **2010**, *10*, 2825.
[170] H. Zhang, J. Luo, H.-T. Zhu, J.-K. Liang, L.-M. Ruan, Q.-L. Liu, J.-B. Li, G.-Y. Liu, *Acta Mater.* **2012**, *60*, 7241.
[171] J. Q. Li, X. X. Li, F. S. Liu, W. Q. Ao, H. T. Li, *J. Electron. Mater.* **2013**, *42*, 366.
[172] X. X. Li, J. Q. Li, F. S. Liu, W. Q. Ao, H. T. Li, L. C. Pan, *J. Alloys Compd.* **2013**, *547*, 86.
[173] A. Bali, H. Wang, G. J. Snyder, R. C. Mallik, *J. Appl. Phys.* **2014**, *116*, 033707.
[174] O. Falkenbach, D. Hartung, P. Klar, G. Koch, S. Schlecht, *J. Electron. Mater.* **2014**, *43*, 1674.
[175] P. K. Rawat, B. Paul, P. Banerji, *Appl. Mater. Interface* **2014**, *6*, 3995.
[176] Y. Lee, S.-H. Lo, C. Chen, H. Sun, D.-Y. Chung, T. C. Chasapis, C. Uher, V. P. Dravid, M. G. Kanatzidis, *Nat Commun* **2014**, *5*.
[177] H. Fan, T. Su, H. Li, B. Du, B. Liu, H. Sun, Y. Zhang, L. Li, S. Li, M. Hu, H. Ma, X. Jia, *J. Alloys Compd.* **2015**, *639*, 106.
[178] Q. Zhang, E. K. Chere, K. McEnaney, M. Yao, F. Cao, Y. Ni, S. Chen, C. Opeil, G. Chen, Z. Ren, *Adv. Energy Mater.* **2015**, *5*, n/a.
[179] L.-D. Zhao, S.-H. Lo, J. He, H. Li, K. Biswas, J. Androulakis, C.-I. Wu, T. P. Hogan, D.-Y. Chung, V. P. Dravid, M. G. Kanatzidis, *J. Am. Chem. Soc.* **2011**, *133*, 20476.
[180] L.-D. Zhao, J. He, C.-I. Wu, T. P. Hogan, X. Zhou, C. Uher, V. P. Dravid, M. G. Kanatzidis, *J. Am. Chem. Soc.* **2012**, *134*, 7902.

[181] Z. Ye, J. Young Cho, M. M. Tessema, J. R. Salvador, R. A. Waldo, H. Wang, W. Cai, *J. Solid State Chem.* **2013**, *201*, 262.
[182] J. Y. Cho, X. Shi, J. R. Salvador, J. Yang, H. Wang, *J. Appl. Phys.* **2010**, *108*, 073713.
[183] E. J. Skoug, J. D. Cain, D. T. Morelli, *J. Alloys Compd.* **2010**, *506*, 18.
[184] J. Fan, W. Carrillo-Cabrera, L. Akselrud, I. Antonyshyn, L. Chen, Y. Grin, *Inorg. Chem.* **2013**, *52*, 11067.
[185] J. Fan, H. Liu, X. Shi, S. Bai, X. Shi, L. Chen, *Acta Mater.* **2013**, *61*, 4297.
[186] R. Chetty, D. S. Prem Kumar, M. Falmbigl, P. Rogl, S. W. You, I.-H. Kim, R. C. Mallik, *Intermetallics* **2014**, *54*, 1.
[187] C. Raju, M. Falmbigl, P. Rogl, P. Heinrich, E. Royanian, E. Bauer, R. C. Mallik, *Mater. Chem. Phys.* **2014**, *147*, 1022.
[188] X. Y. Li, D. Li, H. X. Xin, J. Zhang, C. J. Song, X. Y. Qin, *J. Alloys Compd.* **2013**, *561*, 105.
[189] S. N. Guin, D. S. Negi, R. Datta, K. Biswas, *J. Mater. Chem. A* **2014**, *2*, 4324.
[190] R. Mohanraman, R. Sankar, K. M. Boopathi, F.-C. Chou, C.-W. Chu, C.-H. Lee, Y.-Y. Chen, *J. Mater. Chem. A* **2014**, *2*, 2839.
[191] K. Kurosaki, H. Uneda, H. Muta, S. Yamanaka, *J. Alloys Compd.* **2004**, *376*, 43.
[192] C. R. Sankar, S. Bangarigadu-Sanasy, A. Assoud, H. Kleinke, *J. Mater. Chem.* **2010**, *20*, 7485.
[193] C. Sankar, S. Bangarigadu-Sanasy, H. Kleinke, *J. Electron. Mater.* **2012**, *41*, 1662.
[194] S. Bangarigadu-Sanasy, C. R. Sankar, P. Schlender, H. Kleinke, *J. Alloys Compd.* **2013**, *549*, 126.
[195] Q. Guo, M. Chan, B. A. Kuropatwa, H. Kleinke, *Chem. Mater.* **2013**, *25*, 4097.
[196] H. Takahashi, N. Raghavendra, F. Gascoin, D. Pelloquin, S. Hébert, E. Guilmeau, *Chem. Mater.* **2013**, *25*, 1809.
[197] B. A. Kuropatwa, Q. Guo, A. Assoud, H. Kleinke, *Z. Anorg. Allg. Chem.* **2014**, *640*, 774.
[198] H. Fu, P. Ying, J. Cui, Y. Yan, X. Zhang, *J. Electron. Mater.* **2011**, *40*, 937.
[199] A. Banik, K. Biswas, *J. Mater. Chem. A* **2014**, *2*, 9620.
[200] L. D. Ivanova, V. G. Leontyev, L. I. Petrova, Y. V. Granatkina, E. S. Avilov, *Inorg. Mater.* **2014**, *50*, 124.
[201] Q. Tan, J.-F. Li, *J. Electron. Mater.* **2014**, *43*, 2435.
[202] Y. Li, X. Shi, D. Ren, J. Chen, L. Chen, *Energies* **2015**, *8*, 6275.
[203] B.-Z. Sun, Z. Ma, C. He, K. Wu, *RSC Advances* **2015**, *5*, 56382.
[204] X. Shi, J. Y. Cho, J. R. Salvador, J. Yang, H. Wang, *Appl. Phys. Lett.* **2010**, *96*, 162108.
[205] J. Cho, Y. Lim, S.-M. Choi, K. Kim, W.-S. Seo, H.-H. Park, *J. Electron. Mater.* **2011**, *40*, 1024.
[206] J. Cui, X. Liu, X. Zhang, Y. Li, Y. Deng, *J. Appl. Phys.* **2011**, *110*, 023708.
[207] J.-H. Yim, H.-H. Park, H. Jang, M.-J. Yoo, D.-S. Paik, S. Baek, J.-S. Kim, *J. Electron. Mater.* **2012**, *41*, 1354.
[208] G. Li, J. Yang, Y. Luo, Y. Xiao, L. Fu, M. Liu, J. Peng, *J. Am. Ceram. Soc.* **2013**, *96*, 2703.
[209] G. Li, J. Yang, Y. Xiao, L. Fu, J. Peng, Y. Deng, P. Zhu, H. Yan, *J. Electron. Mater.* **2013**, *42*, 675.
[210] J. Kim, J.-S. Rhyee, *Electron. Mater. Letters* **2014**, *10*, 801.
[211] G. Tewari, T. S. Tripathi, P. Kumar, A. K. Rastogi, S. K. Pasha, G. Gupta, *J. Electron. Mater.* **2011**, *40*, 2368.
[212] A. Kaltzoglou, P. Vaqueiro, T. Barbier, E. Guilmeau, A. Powell, *J. Electron. Mater.* **2014**, *43*, 2029.
[213] G. C. Tewari, T. S. Tripathi, H. Yamauchi, M. Karppinen, *Mater. Chem. Phys.* **2014**, *145*, 156.
[214] R. Bhatt, R. Basu, S. Bhattacharya, A. Singh, D. K. Aswal, S. K. Gupta, G. S. Okram, V. Ganesan, D. Venkateshwarlu, C. Surgers, M. Navaneethan, Y. Hayakawa, *Appl. Phys. A* **2013**, *111*, 465.
[215] S. G. Tan, L. J. Li, Y. Liu, P. Tong, B. C. Zhao, W. J. Lu, Y. P. Sun, *Phys. C: Supercond.* **2012**, *483*, 94.
[216] K. Zhang, C. Hu, X. Kang, S. Wang, Y. Xi, H. Liu, *Mater. Res. Bull.* **2013**, *48*, 3968.

[217] F. Drymiotis, T. Drye, D. Rhodes, Q. Zhang, J. C. Lashey, Y. Wang, S. Cawthorne, B. Ma, S. Lindsey, T. Tritt, *J. Phys.: Condens. Matter* **2010**, *22*, 035801.
[218] J. Xu, H. Li, B. Du, X. Tang, Q. Zhang, C. Uher, *J. Mater. Chem.* **2010**, *20*, 6138.
[219] B. Du, J. Xu, W. Zhang, X. Tang, *J. Electron. Mater.* **2011**, *40*, 1249.
[220] H.-j. Wu, S.-w. Chen, T. Ikeda, G. Jeffrey Snyder, *Acta Mater.* **2012**, *60*, 6144.
[221] J. Wu, J.-Y. Yang, J.-S. Zhang, G. Li, J.-Y. Peng, Y. Xiao, L.-W. Fu, Q.-Z. Liu, *J. Electron. Mater.* **2012**, *41*, 1100.
[222] S. Perlt, T. Höche, J. Dadda, E. Müller, B. Rauschenbach, *J. Electron. Mater.* **2013**, *42*, 1422.
[223] H.-j. Wu, T.-W. Lan, S.-w. Chen, Y.-Y. Chen, T. Day, G. J. Snyder, *Acta Mater.* **2015**, *93*, 38.
[224] X. Xin, Y. Jiang, D. Kong, H. Zhong, L. Chen, D. Yu, *Phys. Status Solidi (a)* **2010**, *207*, 163.
[225] P. F. P. Poudeu, A. Guéguen, C.-I. Wu, T. Hogan, M. G. Kanatzidis, *Chem. Mater.* **2010**, *22*, 1046.
[226] M. Zhou, J.-F. Li, H. Wang, T. Kita, L. Li, Z. Chen, *J. Electron. Mater.* **2011**, *40*, 862.
[227] H. Li, K. F. Cai, Y. Du, H. F. Wang, S. Z. Shen, X. L. Li, Y. Y. Wang, C. W. Zhou, *Curr. Appl. Phys.* **2012**, *12*, 188.
[228] Z.-Y. Li, J.-F. Li, *J. Electron. Mater.* **2012**, *41*, 1365.
[229] Z.-x. Yu, J.-F. Li, B.-P. Zhang, Z.-H. Ge, *J. Electron. Mater.* **2012**, *41*, 1337.
[230] Q. Zhang, Y. Lan, S. Yang, F. Cao, M. Yao, C. Opeil, D. Broido, G. Chen, Z. Ren, *Nano Energy* **2013**, *2*, 1121.
[231] L. Zhang, W. Wang, B. Ren, J. Guo, *J. Electron. Mater.* **2013**, *42*, 1303.
[232] B. Yu, W. Liu, S. Chen, H. Wang, H. Wang, G. Chen, Z. Ren, *Nano Energy* **2012**, *1*, 472.
[233] Y. He, T. Day, T. Zhang, H. Liu, X. Shi, L. Chen, G. J. Snyder, *Adv. Mater.* **2014**, *26*, 3974.
[234] L. Zou, B.-P. Zhang, Z.-H. Ge, L.-J. Zhang, *J. Mater. Res.* **2014**, *29*, 1047.
[235] L.-l. Zhao, X.-l. Wang, J.-y. Wang, Z.-x. Cheng, S.-x. Dou, J. Wang, L.-q. Liu, *Sci. Rept.* **2015**, *5*, 7671.
[236] H. Zhu, J. Luo, H. Zhao, J. Liang, *J. Mater. Chem. A* **2015**, *3*, 10303.
[237] J. Capps, F. Drymiotis, S. Lindsey, T. M. Tritt, *Philos. Mag. Lett.* **2010**, *90*, 677.

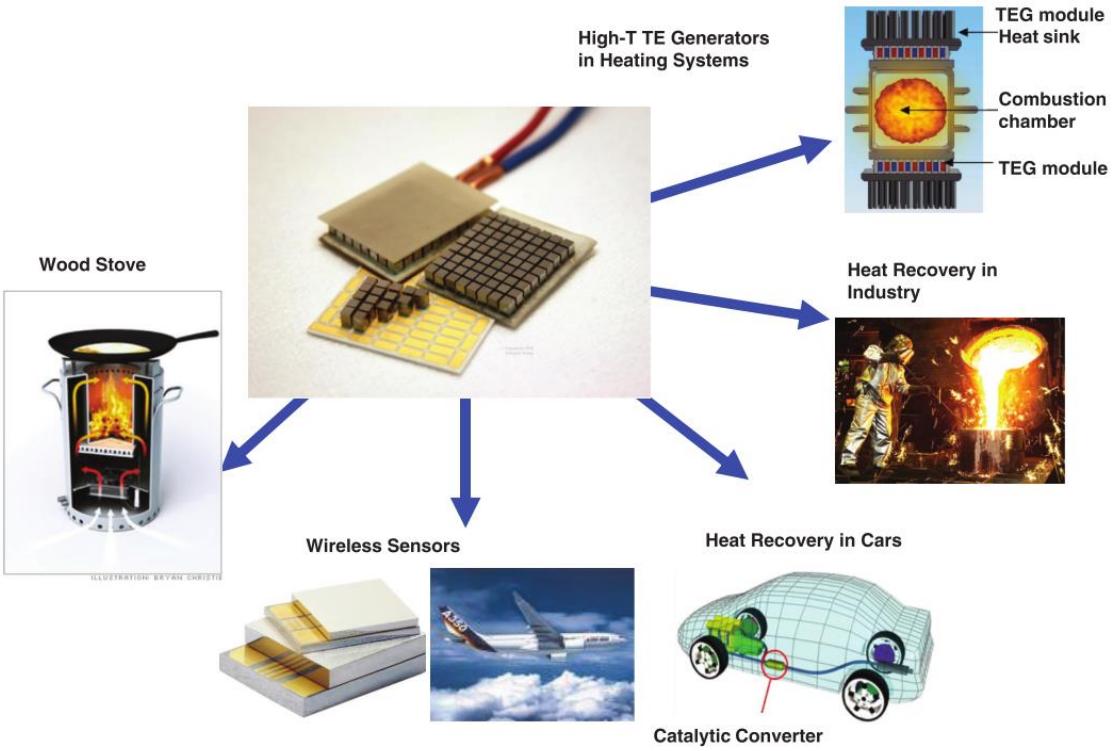

Figure 1. Typical applications of thermoelectric materials.[8a] Reprint with permission from WILEY-VCH Verlag GmbH & Co. KGaA, Weinheim.

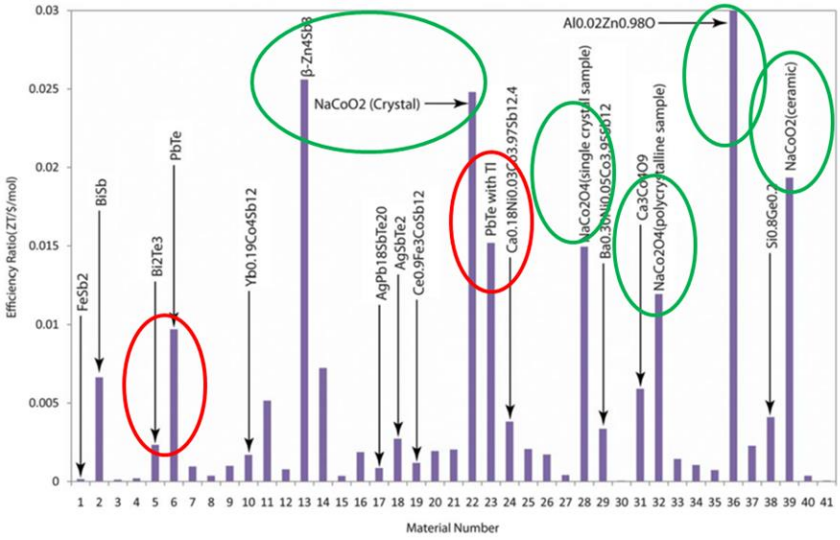

Figure 2. Efficiency ratios for various thermoelectric materials.[13] Reprint with permission from Royal Society of Chemistry.

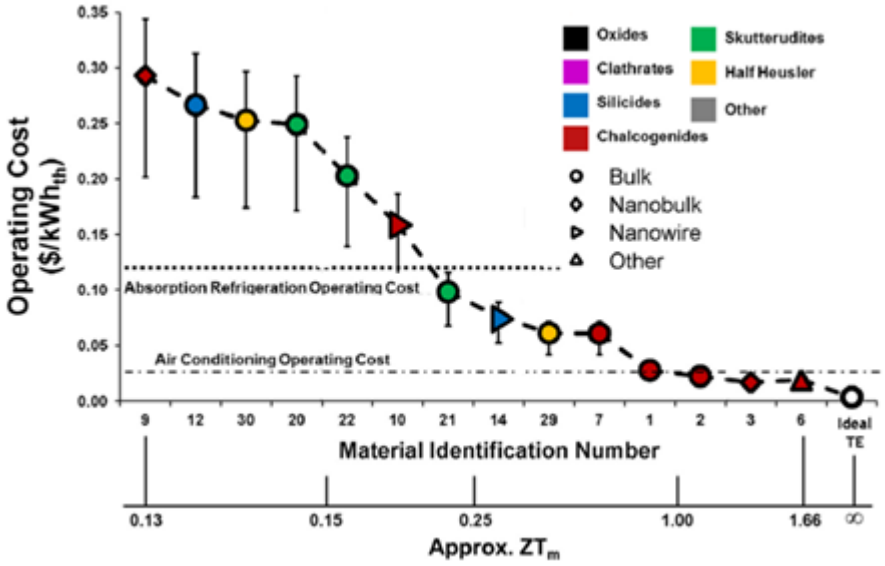

Figure 3. Operating costs of a thermoelectric cooler constructed from various materials.[14] Reprint with permission from Elsevier Ltd.

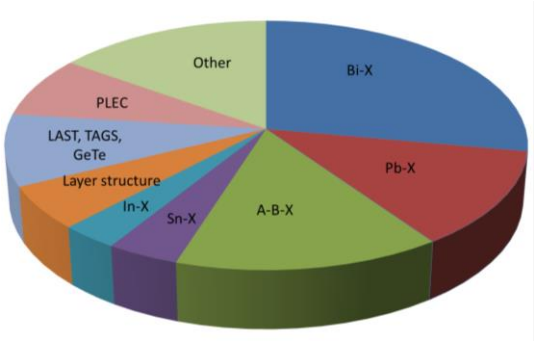

Figure 4. Shares of reports in the literature on different classes of metal chalcogenides.

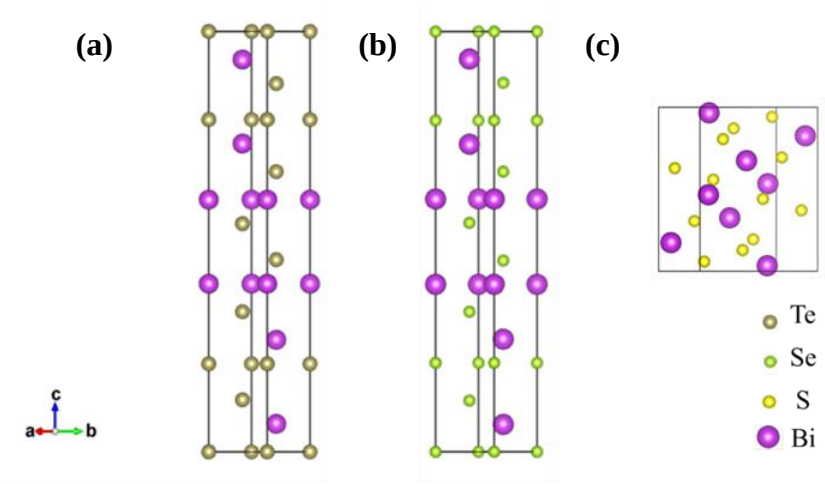

Figure 5. Crystal structures of (a) Bi_2Te_3; (b) Bi_2Se_3, and (c) Bi_2S_3.

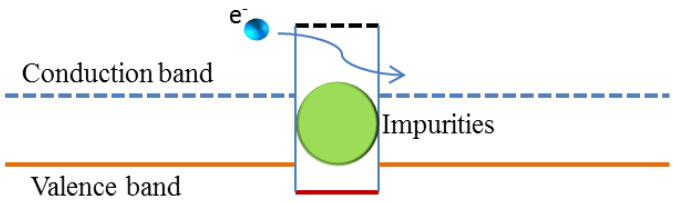

Figure 6. Schematic diagram of energy filtering effect (EFE).

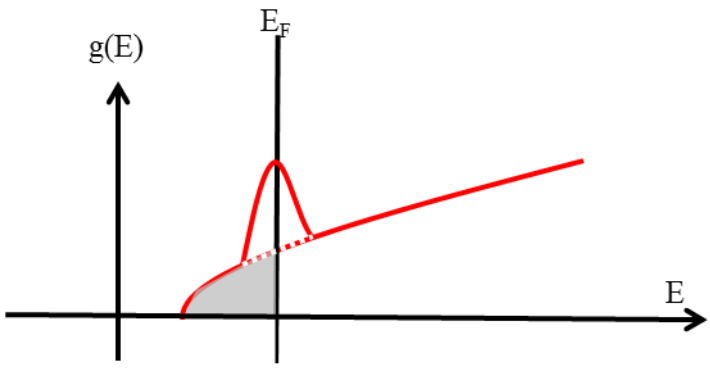

Figure 7. Schematic illustration of the density of states (g(E)) enhancement that can be achieved from the distortion caused by the resonant energy level. The dashed line corresponds to pure Bi_2Te_3, and the solid line corresponds to Sn-Bi_2Te_3 (with resonant energy levels from Sn).

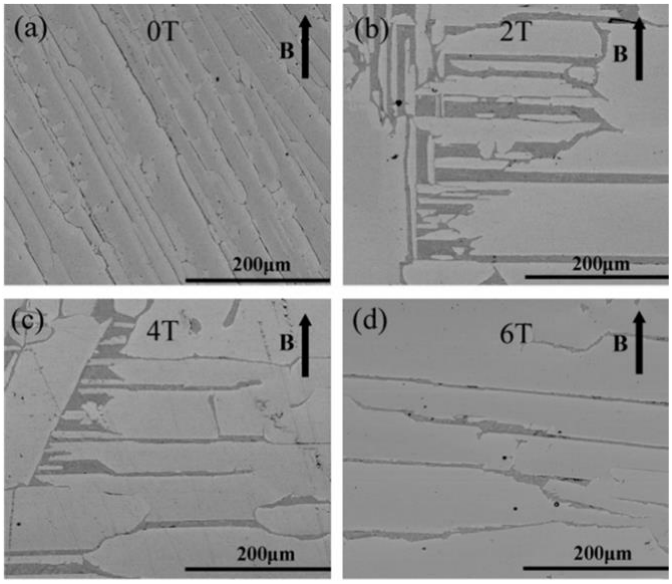

Figure 8. SEM images of a cross-section parallel to the magnetic field direction for *p*-type $Bi_{0.5}Sb_{1.5}Te_3$ samples prepared under 0 T (a), 2 T (b), 4 T (c) ,and 6 T (d).[33] Reprint with permission from Elsevier Ltd.

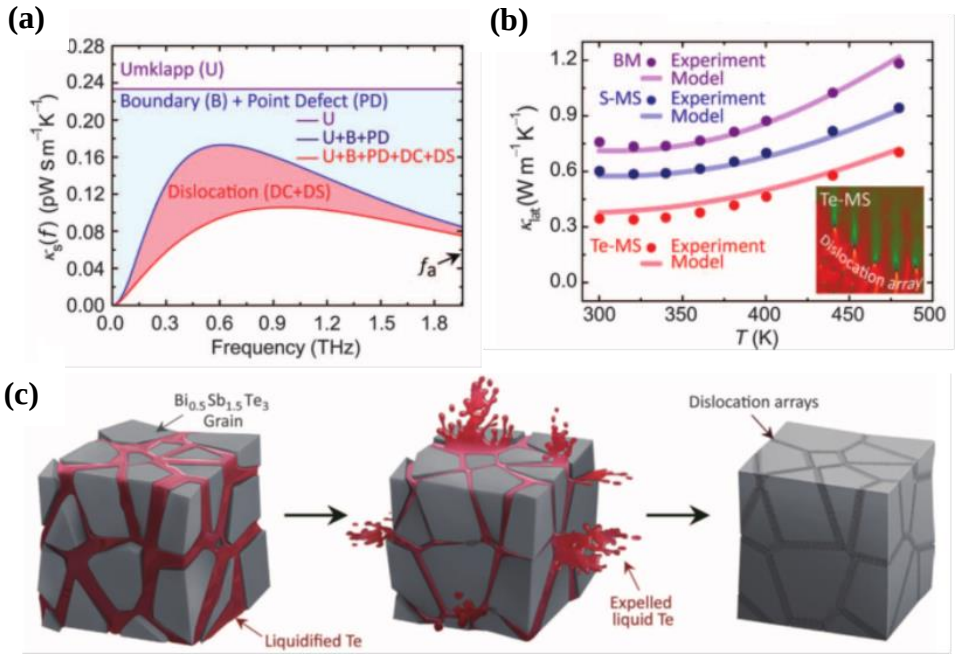

Figure 9. (a) The inclusion of dislocations for scattering is effective across the full frequency spectrum. Boundary and point defects are effective only at low and high frequencies. The acoustic mode Debye frequency is f_a. (b) Lattice thermal conductivity for $Bi_{0.5}Sb_{1.5}Te_3$ alloys produced by melt-solidification (ingot), solid-phase compaction (BM and S-MS), and liquid-phase compaction (Te-MS). (c) Schematic illustration of liquid-phase compaction using Te at 480°C.[20b] Reprint with permission from the American Association for the Advancement of Science.

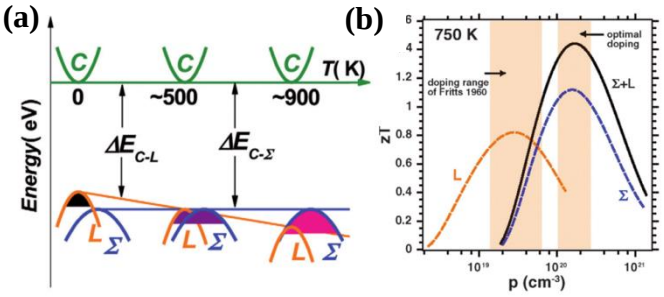

Figure 10. (a) Schematic illustration of two-band model for PbTe, and how the bands move with increasing temperature. The shaded areas schematically represent the hole population of each band. The orange line indicates the movement of the L band as the temperature increases; the Σ band refers to the heavy valence band. (b) The calculated *ZT* value as a function of carrier concentration for *p*-type PbTe, with a comparison of the results of transport from the L or the Σ band alone. The optimal carrier concentrations were proposed in the 1960s and very recently were also confirmed.[5] Reprint with permission from Elsevier Ltd.

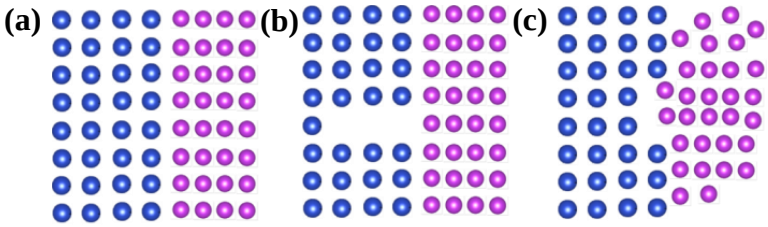

Figure 11. Schematic illustration of (a) coherent grain boundaries; (b) semi-coherent boundaries; (c) incoherent boundaries.

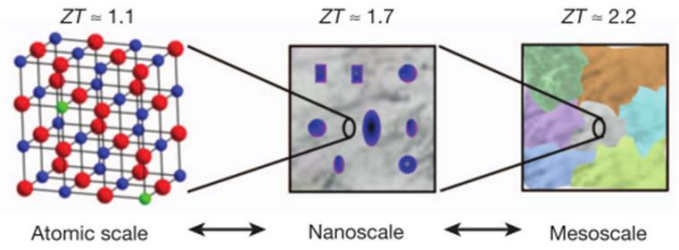

Figure 12. Maximum achievable *ZT* values for the respective length scales: the atomic scale (alloy scattering: red, Te; blue, Pb; green, dopant), the nanoscale (PbTe matrix, grey; SrTe nanocrystals, blue), and the mesoscale (grain-boundary scattering).[12] Reprint with permission from the Nature Publishing Group.

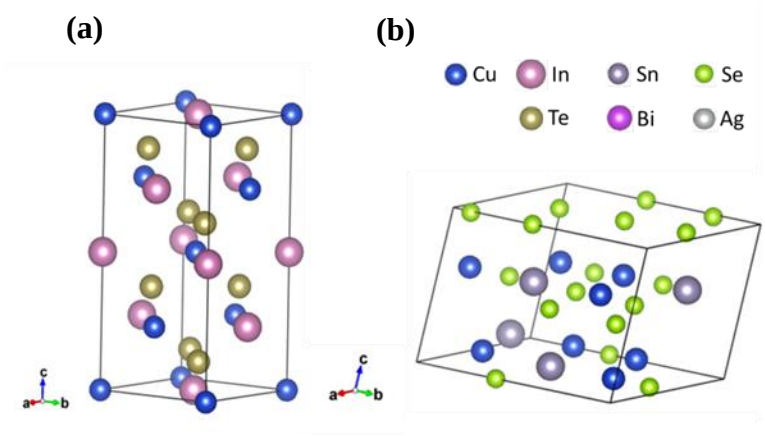

Figure 13. Crystal structures of some typical A-B-X based thermoelectric materials: (a) $CuInTe_2$ type; (b) Cu_2SnSe_3 type.

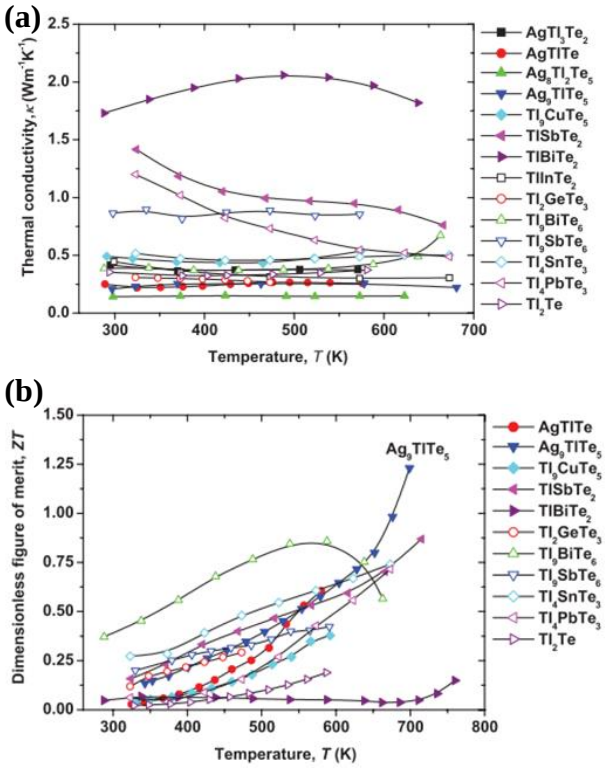

Figure 14. (a) Thermal conductivity and (b) *ZT* values of some typical compounds in the Tl-M-Te system.[74b] Reprint with permission from WILEY-VCH Verlag GmbH & Co. KGaA, Weinheim.

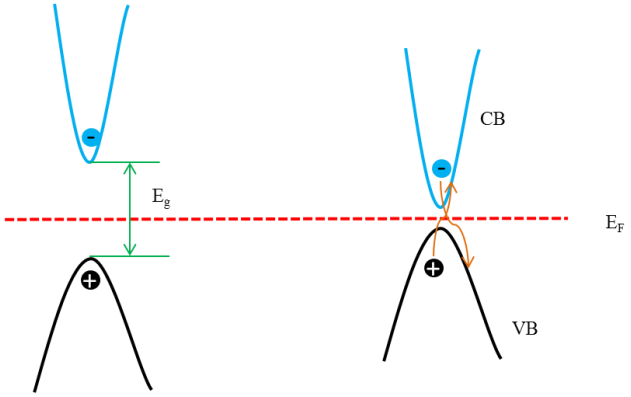

Figure 15. Bipolar effect of narrow-band-gap (right) semiconductor at high temperature. The situation for a large band gap (left) is also presented.

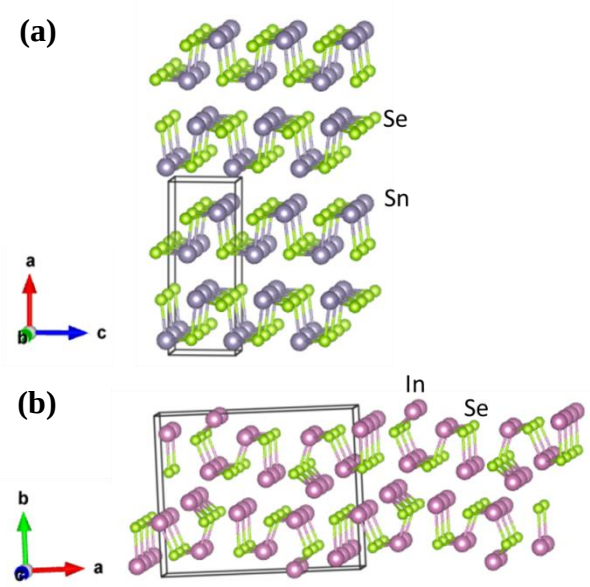

Figure 16. Crystal structure of (a) SnSe and (b) In_4Se_3.

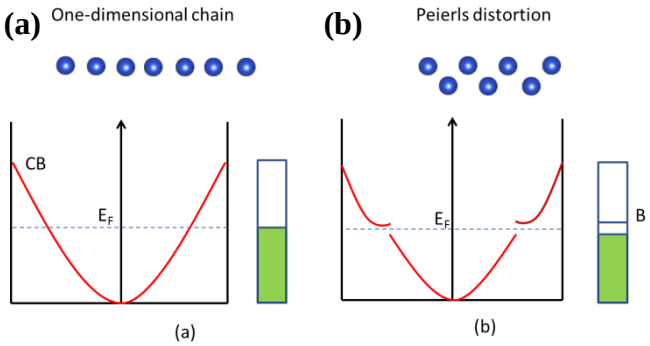

Figure 17. Effect of Peierls distortion: (a) Original state; (b) Peierls distortion state.

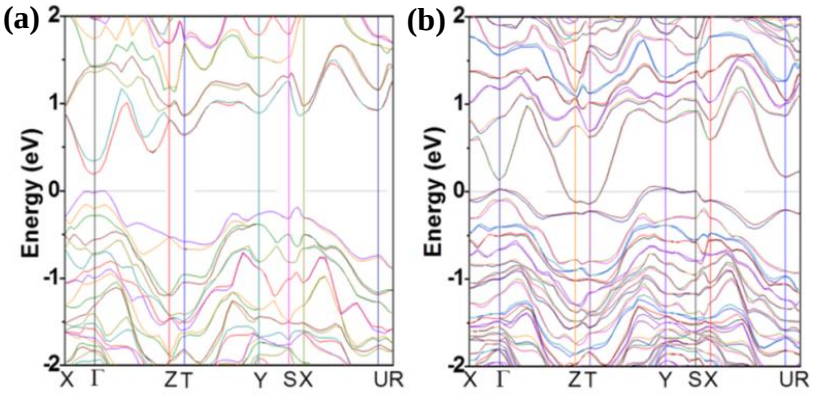

Figure 18. Band structure of In_4Se_3 (a) and $In_4Se_{2.75}$ (b).[81] Reprint with permission from AIP Publishing LLC.

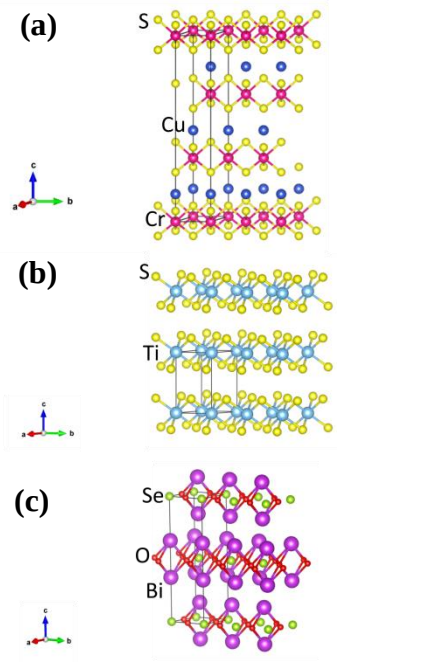

Figure 19. Crystal structures of (a) $CuCrS_2$; (b)TiS_2; (c) Bi_2O_2Se.

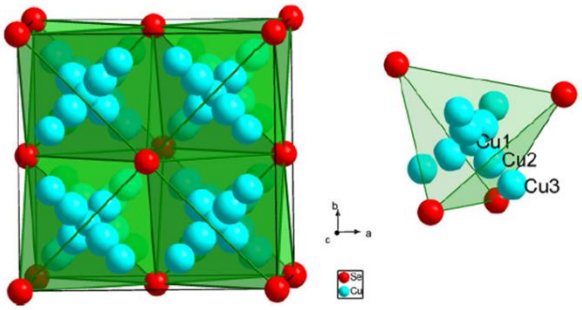

Figure 20. Crystal structure of the high temperature phase of Cu_2Se (left) and the structure of the Se_4 tetrahedron (right).[112] Reprint with permission from Ivan Franko National University of Lviv.

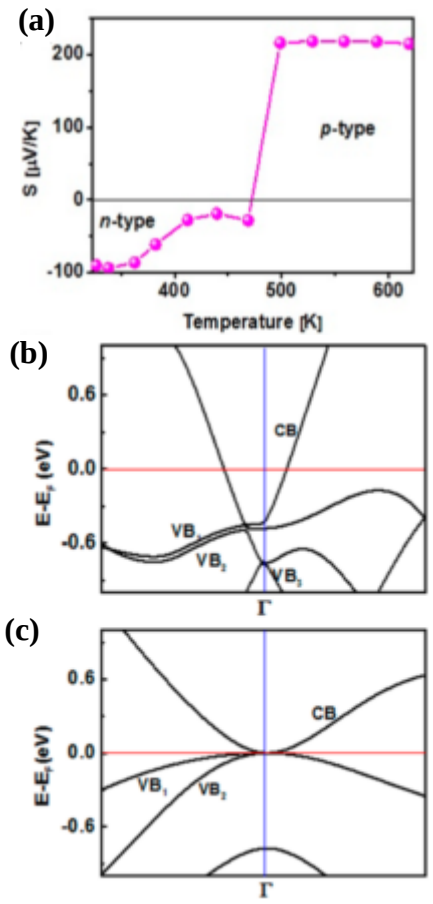

Figure 21. (a) Typical change in conduction type change for CuAgSe during the phase transition; band structures for the (b) low temperature phase and (c) high temperature PLEC status.[116b] Copyright 2014 from the American Chemical Society.

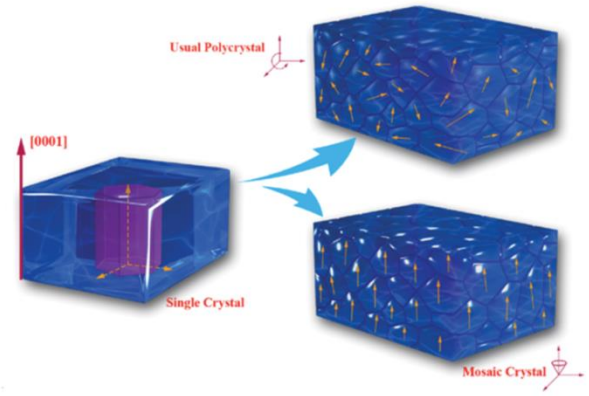

Figure 22. Schematic illustration of single crystal, polycrystal, and mosaic crystal.[123] Reprint with permission from WILEY-VCH Verlag GmbH & Co. KGaA, Weinheim.

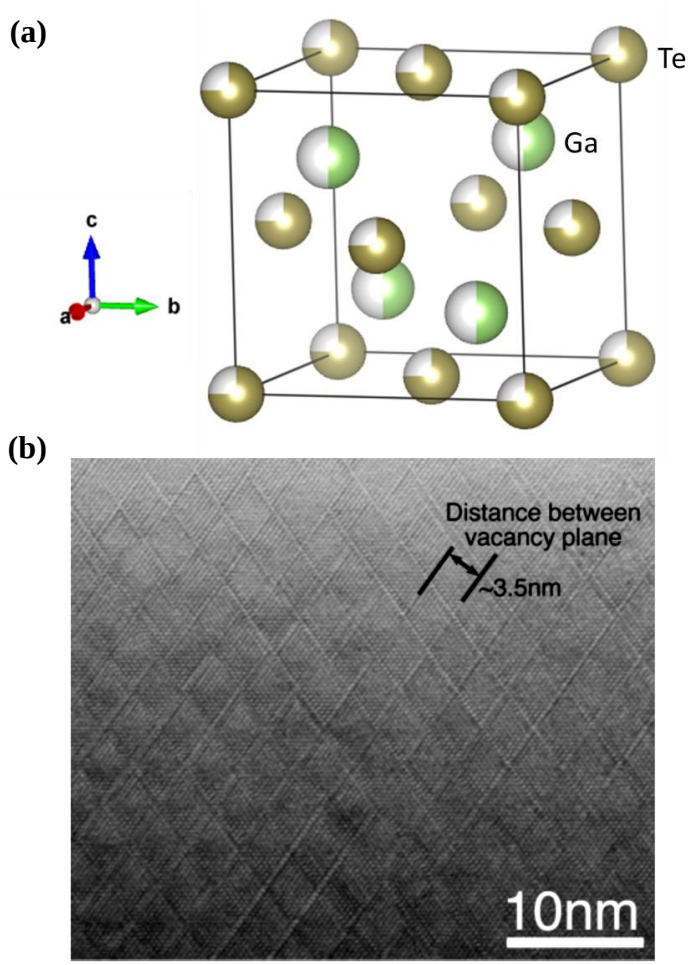

Figure 23. (a) Crystal structure of Ga_2Te_3, in which the white part is the vacancy; (b) high resolution transmission electron microscope (TEM) image of Ga_2Te_3, with the electron beam aligned along the [110] direction.[151] Reprint with permission from AIP Publishing LLC.

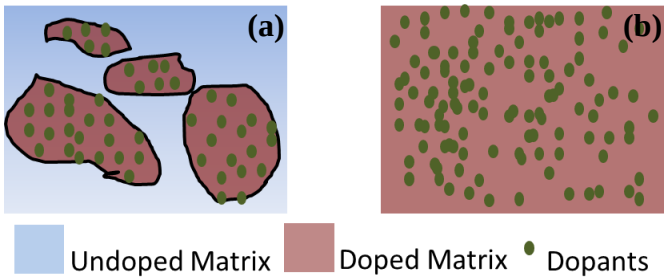

Figure 24. Schematic illustration of (a) modulation doping and (b) uniform doping.

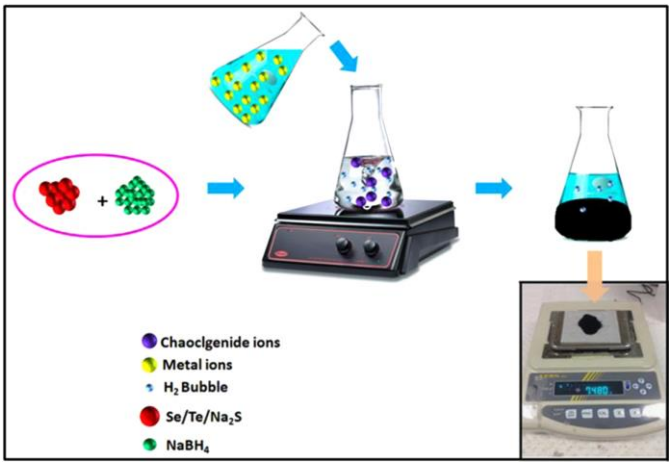

Figure 25. Schematic illustration of wet chemical synthesis route; the inset picture shows the weight of 40 mmol (theoretical yield) for the synthesized Cu_2Se powder.[358] Reprint with permission from Elsevier Ltd.

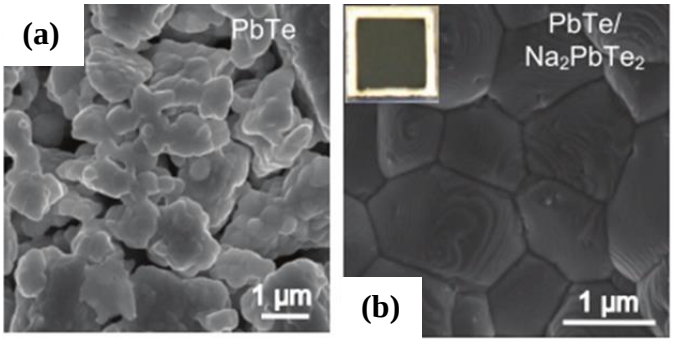

Figure 26. Microstructure of (a) ball-milled PbTe microparticles annealed at 500°C for 30 min, and (b) film of similar PbTe microparticles annealed in the presence of 5 wt % Na_2PbTe_2, with the inset showing a photograph of the sample.[134b] Reprint with permission from the American Association for the Advancement of Science.

Table 1. Recently reported *ZT* values of BiSbTe and BiSeTe based materials.

Materials	Type-ZT_{max}	Temperature (K)	Date	Ref.	Comments
$Bi_{0.5}Sb_{1.5}Te_3$	*p*-1.40	373	2008	[143]	Ball milling (BM), spark plasma sintering (SPS), preserved nanostructures
$Bi_{0.5}Sb_{1.5}Te_3$	*p*-1.56	300	2009	[22]	Melt spinning+SPS, nanostructures
$Bi_{0.4}Sb_{1.6}Te_3$	*p*-1.12	350	2010	[152]	Hot pressing (HP), nanograins
Bi_2Te_3	*p*-1.18	425	2010	[153]	Mechano-chemical process, nanograins
$Bi_{0.5}Sb_{1.5}Te_3$	*p*-1.40	300	2010	[38b]	Hot forging (HF), recrystallization formed nanograins
Bi_2Te_3	*p*-1.38	473	2010	[27c]	Nanopores in the bulk
$Bi_2Se_{0.36}Te_{2.67}$	*p*-1.20	300	2011	[154]	Optimized single crystal
$Bi_{0.5}Sb_{1.5}Te_3$	*p*-1.10	300	2011	[36a]	Slip-casting under high magnetic field
0.1 vol% $SiC+Bi_{0.5}Sb_{1.5}Te_3$	*p*-0.97	323	2011	[26]	Nanograins produced by *p*-type SiC
$Bi_{0.5}Sb_{1.5}Te_3$	*p*-1.11	300	2011	[155]	HF caused nanograins
$Bi_{0.5}Sb_{1.5}Te_3$	*p*-1.21	323	2012	[36b]	Slip casting under high magnetic field, SPS
$Bi_{0.5}Sb_{1.5}Te_3$	*p*-1.10	300	2012	[24a]	Wet chemical method
Bi_2Te_3	*p*-0.97	365	2013	[156]	Synthesis under high pressure
$Cr_{0.1}Bi_2Te_3$	*p*-0.80	325	2013	[29f]	Effect of Cr doping
$Bi_{0.5}Sb_{1.5}Te_3$+0.2 %Mn	*p*-1.47	310	2013	[27r]	Wet chemical method, metal nanoparticle decoration
0.5at% In+ $Bi_{0.4}Sb_{1.6}Te_3$	*p*-1.20	320	2013	[29g]	Effects of Ga and In doping: no effect on σ, but modified DOS
$Bi_{0.5}Sb_{1.5}Te_3$	*p*-1.79	373	2013	[25]	Improved parameters for ball-milling (BM)+SPS process, nanograins
0.4vol% $SiC+Bi_{0.3}Sb_{1.7}Te_3$	*p*-1.33	373	2013	[157]	Effect of SiC
5wt%Cu_7Te_4+$Bi_{0.4}Sb_{1.6}Te_3$	*p*-1.14	444	2013	[27h]	Composite, nanograins
$Bi_{0.5}Sb_{1.5}Te_3$+Te	*p*-1.05	425	2013	[27k]	In-situ formed Te nanoparticles
$Bi_{0.3}Sb_{1.7}Te_3$	*p*-1.30	380	2014	[20a]	Defect engineering
$Bi_{0.5}Sb_{1.5}Te_3$	*p*-1.60	323	2014	[35b]	HF, led to orientation of the polycrystals
$Bi_{0.5}Sb_{1.5}Te_3$	*p*-0.64	300	2014	[144a]	Effect of severe plastic deformation
$Bi_{0.5}Sb_{1.5}Te_3$	*p*-1.00	300	2014	[158]	BM+Reduction method,

					nanograins
$Bi_{0.4}Sb_{1.6}Te_3$	*p*-1.19	373	2014	[159]	Mixture of nanopowder and micropowder
$Bi_{0.4}Sb_{1.6}Te_3$	*p*-1.20	673	2014	[34e]	BM, hot extrusion (HE)
$Bi_{0.48}Sb_{1.52}Te_3$+4 mol% WSe_2	*p*-1.27	360	2014	[27m]	Composite, nanograins
$Bi_{0.48}Sb_{1.52}Te_3$	*p*-1.40	340	2014	[37]	In-situ exfoliation, SPS
$Bi_{0.42}Sb_{1.5535}Ga_{0.025}Ag_{0.0015}Te_3$	*p*-1.15	360	2015	[160]	Effect of co-doping
$Bi_{0.5}Sb_{1.5}Te_3$+1 vol% Cu_3SbSe_4	*p*-1.60	476	2015	[27o]	Carrier filtering effect, nanocomposite
$Bi_{0.5}Sb_{1.5}Te_3$	*p*-1.71	323	2015	[33]	Melt-solidification under high magnetic field
1at% Fe+$Bi_{0.48}Sb_{1.52}Te_3$	*p*-1.09	300	2015	[29i]	Effect of Fe doping
$Bi_{0.5}Sb_{1.5}Te_3$	*p*-1.86	320	2015	[20b]	Nanograins, dislocation arrays
$Ce_{0.1}Bi_{1.9}Te_3$	*p*-1.22	386	2015	[130c]	Wet chemical method, nanoflowers
$Bi_{0.4}Sb_{1.6}Te_3$	*p*-1.36	400	2015	[38f]	Zone melting, hot deformation
Bi_2Te_3	*n*-0.94	398	2009	[161]	BM+Hot press, nanograins
$Bi_2Se_{0.3}Te_{2.7}$	*n*-0.93	300	2010	[34b]	HE, orientation of the nanocrystals
$Bi_2Se_{0.3}Te_{2.7}$	*n*-1.04	398	2010	[34c]	Deformation induced defects, orientation of nanograins
$Bi_2Se_{0.21}Te_{2.79}$	*n*-1.14	300	2010	[162]	Grown in space, less defects
Bi_2Te_3	*n*-0.61	423	2011	[132]	Wet chemical method, nanoparticles
$Bi_2Te_ySe_{3-y}$	*n*-0.70	373	2011	[163]	Wet chemical method, nanoparticles
1vol%Al_2O_3+Bi_2Te_3	*n*-0.99	400	2011	[27d]	Dispersed nanoparticles
$Bi_2Se_{0.3}Te_{2.7}$	*n*-1.11	423	2011	[26]	Nanograins, SiC did not increase *ZT*
0.015 vol% MWCNTS+$Bi_2(Te_{0.9}Se_{0.1})_3$	*n*-0.98	423	2011	[27e]	Carbon nanotubes as electron donors, composite
$(Bi_{0.99}Ag_{0.04})_2(Te_{0.96}Se_{0.04})_3$	*n*-0.74	373	2011	[29c]	Effect of Ag doping
$Bi_2Se_{0.3}Te_{2.7}$	*n*-1.00	300	2012	[164]	BM, hot press, controlled nanostructures
$Bi_2Se_{0.3}Te_{2.7}$	*n*-0.54	300	2012	[24b]	Wet chemical method
Bi_2Te_2S/Se	*n*-0.80	573	2013	[45b]	Effect of alloying
Bi_2Te_3	*n*-1.00	430	2013	[21]	Wet chemical exfoliation, SPS
Bi_2Te_3	*n*-1.16	420	2013	[23]	Wet chemical method, flower-like nanostructure
$(In_4Se_3)_{0.03}$+(Bi_2T	*n*-1.00	500	2013	[27i]	Composite

$e_{2.7}Se0.3)_{0.97}$					
$Bi_2Te_{2.994}Cl_{0.006}$+0.5wt%In_2Te_3	*n*-0.94	300	2013	[27j]	Phase separation
$Bi_2Se_{0.3}Te_{2.7}$	*n*-1.20	445	2014	[20a]	Defect engineering
1.5vol% Ag NW+Bi_2Te_3	*n*-0.71	475	2014	[27n]	Effect of Ag nanowires
$Bi_2Te_3Se_{0.3}I_{0.0075}$	*n*-1.13	423	2015	[165]	Effect of I doping
$Bi_2Te_{2.4}Se_{0.6}$/CNT	*n*-0.80	425	2015	[27q]	BM, SPS, carbon nanotube (CNT) decrease grain size
$(Bi_2Se_3)_2(Bi_2Te_3)_8$	*n*-0.71	450	2015	[139]	Wet chemical method, multishell structure
2vol% Ag+Bi_2Te_3	*n*-0.77	475	2015	[166]	Ag nanoparticles

Table 2. Thermoelectric performance of Bi-Se and Bi-S systems.

Materials	Type-ZT	Temperature (K)	Date	Ref.	Comments
$Bi_{1.99}Ag_{0.01}S_3$	*n*-0.25	573	2011	[42a]	Ag doping
$Bi_{1.99}Ag_{0.03}S_3$	*n*-0.23	573	2012	[42c]	Ag doping
$Bi_2S_{2.7}Se_{0.3}$+0.5mol% $BiCl_3$	*n*-0.60	760	2012	[42b]	Alloy, Cl doping
$Bi_2S_{2.8}Se_{0.15}$	*n*-0.16	573	2013	[45c]	Alloy, deficiency of chalcogenides
Bi_2Te_3-Bi_2S_3	*n*-0.48	500	2013	[45a]	Wet chemical method, EFE, inorganic ligand capping
Bi_2SeS_2	*n*-0.80	773	2013	[45b]	Alloy effect, low thermal conductivity
Bi_2Se_3	*p*-0.41	533	2014	[40a]	Nanoplatelets, thermochemical method
1mol% $BiCl_3$+Bi_2S_3	*n*-0.60	675	2014	[42d]	BM, SPS, Cl doping
Bi_2S_3	*n*-0.50	723	2014	[41]	Wet chemical method, net-like structure
Bi_2Se_3	*n*-0.75	423	2015	[40b]	Single crystal
$Bi_2S_{2.5}$	*n*-0.10	300	2015	[44]	S deficiency
$Cu_{0.01}Bi_2Se_3$	*n*-0.54	590	2015	[42g]	Cu doping
$Cu_{0.02}Bi_2SeS_2$	*n*-0.70	723	2015	[42e]	Alloy, Cu doping
0.5mol% $CuBr_2$+Bi_2S_3	*n*-0.72	773	2015	[42f]	Cu intercalation and Br doping
1mol% ZnO+Bi_2S_3	*n*-0.66	675	2015	[43]	Composite, formation of ZnS

Table 3. Thermoelectric performance of the Pb-X system.

Materials	Type-ZT	Temperature (K)	Date	Ref.	Comments
$Pb_{0.98}TeTl_{0.02}$	*p*-1.50	773	2009	[32b]	Resonant doping of Tl
1.25% K+0.6% Na+PbTe	*p*-1.30	700	2010	[47a]	No resonant doping, K induced lattice expansion caused distortion of DOS, doping effect
$Pb_{0.98}TeTl_{0.02}$	*p*-1.30	673	2010	[167]	BM, Tl resonant doping
2%Na+PbTe+12%PbS	*p*-1.80	800	2011	[47b]	Na doping, PbS precipitation
$Na_{0.01}Tl_{0.02}Pb_{0.98}Te_{0.91}S_{0.08}$	*p*-1.60	675	2011	[31]	Tl resonant DOS, alloy, Na doping
Na doped PbTe/Ag_2Te	*p*-1.50	650	2011	[47c]	Band engineering, nanoprecipitation
Na doped $PbTe_{0.85}Se_{0.15}$	*p*-1.80	850	2011	[46]	Band convergence
$Pb_{0.97}Cd_{0.03}Te$	*p*-1.70	750	2012	[47e]	Modified DOS, in-situ precipitates
4mol% SrTe+2mol% Na+PbTe	*p*-2.20	915	2012	[12]	Full scale scattering of phonons
$Sm_{0.08}Pb_{0.92}Te$	*p*-0.84	300	2013	[47f]	Sm doping can increase Seebeck coefficient
1mol%Na+$(PbTe)_{0.65}(PbSe)_{0.1}(PbS)_{0.25}$	*p*-1.40	650	2014	[54a]	Na doping, alloy, precipitates
$Na_{0.05}Pb_{0.95}Te_{0.85}Se_{0.15}$	*p*-1.60	760	2014	[168]	Na doping, alloy
$(PbTe)_{0.84}(PbSe)_{0.07}(PbS)_{0.07}$+2%Na	*p*-2.00	800	2014	[52a]	Na doping, precipitation
$(Pb_{0.95}Na_{0.05}Te)_{0.95}(CoSe_2)_{0.05}$	*p*-1.20	723	2015	[144b]	Na doping, improved mechanical property
$Pb_{0.98}TeNa_{0.02}$	*p*-2.00	773	2015	[47g]	Controlled quench, hot pressing
3% Na-$(PbTe)_{0.8}(PbS)_{0.2}$	*p*-2.30	923	2015	[53]	Na doping, precipitates
$Na_{0.03}(PbTe)_{0.65}(PbS)_{0.25}(PbSe)_{0.1}$	*p*-2.00	850	2015	[54b]	Modulation doping, precipitates
PbTe+8% PbS	*n*-1.20	700	2010	[169]	In-situ precipitation by fast quench

$PbTeI_{0.0012}$	*n*-1.40	750	2011	[51b]	Accurate measurement of thermal conductivity
$Pb_{0.985}Te_{0.996}I_{0.004}In_{0.015}$	*n*-0.45	600	2012	[47d]	I doping, In doping modifies DOS
0.08 wt%SbI_3+ PbTe	*n*-0.99	653	2012	[142]	Hot extrusion, doping
0.03 Ag_2Te+$PbTe_{0.9}S_{0.1}$	*n*-1.20	773	2012	[170]	Ag_2Te nanoinclusions, alloy
$Sb_{0.004}Pb_{0.996}Te_{0.88}S_{0.12}$	*n*-1.20	773	2013	[171]	Sb doping, alloy
$(Bi_{0.001}Pb_{0.999}Te)_{0.88}(PbS)_{0.12}$	*n*-1.20	573	2013	[172]	Bi doping, alloy
Core-shell PbTe-PbS	*n*-1.10	710	2013	[130a]	Core shell structure, EFE
$Pb_{0.999}Te_{0.7}Se_{0.3}In_{0.001}$	*n*-0.66	800	2014	[173]	In doping, alloy
$Bi_{0.05}(PbTe)_{0.95}$	*n*-1.10	773	2014	[174]	Bi doping, Co-ball milling
2mol%ZnTe+0.025mol%PbI_2+PbTe	*n*-1.35	650	2014	[175]	EFE, nanocomposite, PbI_2 doping
PbSe+2mol%SrSe	*p*-1.30	923	2013	[56]	Full scale scattering
$Pb_{0.9975}Sb_{0.0025}Se$	*p*-1.50	820	2014	[176]	Sb rich-endotaxial precipitates
$(AgSb)_{0.03}Pb_{0.94}Se$	*p*-1.03	600	2015	[177]	Ag, Sb co-doping
$Pb_{0.99}SeAl_{0.01}$	*n*-1.30	850	2012	[51a]	Al resonant doping
$PbTe_{0.1}Se_{0.4}S_{0.5}$-Cl	*n*-0.94	700	2015	[52b]	HCl treated nanostructures, Cl doping
$Pb_{0.9925}Cr_{0.005}Se$	*n*-1.00	573	2015	[178]	Cr doping
PbS+1mol%Sb_2S_3+1mol%$PbCl_2$	*n*-1.10	923	2011	[179]	$PbCl_2$ doping, Sb_2S_3 nanoinclusions
PbSe+16%PbS	*n*-1.30	900	2011	[52c]	Nanoinclusions
$Pb_{0.975}Na_{0.025}S$+3%SrS	*p*-1.22	923	2012	[180]	Na doping, nanostructure

Table 4. Thermoelectric performance of MCs using crystal structure engineering.

Materials	Type-ZT	Temperature (K)	Date	Ref.	Comments
$Ag_{0.95}GaTe_2$	*p*-0.77	850	2011	[63a]	Deficiency of Ag
$AgIn_5Se_8$	*n*-0.72	863	2012	[64]	Microstructure modulation
$CuInTe_2$	*p*-1.18	850	2012	[58]	Crystal structure
$CuGaTe_2$	*p*-1.40	973	2012	[59]	Crystal structure
$CuGaTe_2$	*p*-1.69	950	2013	[61]	Calculation
$CuGaTe_2$	*p*-1.00	840	2013	[181]	Structure
$Cu_2Zn_{0.1}Ga_{3.9}Te_7$	*p*-0.46	770	2014	[62a]	Zn doping
$CuIn_{0.98}Cd_{0.02}Te_2$	*p*-0.27	600	2014	[62b]	Cd doping
$CuGaTe_2$	*p*-1.40	950	2014	[60]	BM, hot pressing
$CuIn_{0.98}Cd_{0.02}Te_2$	*p*-0.25	600	2014	[62c]	Cd doping
$Ag_{0.9}InZn_{0.1}Se_2$	*n*-1.05	815	2014	[62d]	Zn doping
$CuAg_{0.025}Ga_{0.975}Te_2$	*p*-0.31	950	2014	[62e]	Doping with Ag
$CuGaTe_2$+3vol% Cu_2Se	*p*-1.20	834	2014	[63b]	Composite
$Cu[In_{0.25}Ga_{0.75}]_{0.99}Zn_{0.01}Te_2$	*p*-1.30	865	2014	[62f]	Doping of Zn, alloy
$Cu_{0.985}Ni_{0.015}InTe_2$	*p*-0.35	635	2015	[62g]	Ni doping
$CuAl(S_{0.25}Se_{0.75})_2$	*p*-0.85	450	2015	[63c]	Alloy
$CuGa_{0.99}Cd_{0.01}Te_2$+0.7vol% Te	*p*-0.75	737	2015	[62h]	Cd doping, Te nano-inclusion
$Cu_2Ge_{1+x}Se_3$	*p*-0.30	700	2010	[182]	Crystal structure, optimized carrier concentration
$Cu_2Sn_{0.8}Ge_{0.2}Se_3$	*p*-0.04	300	2010	[183]	Crystal structure, alloy
$Cu_2Sn_{0.925}In_{0.1}Se_3$	*p*-1.14	850	2010	[66a]	In doping
Cu_2GeSe_3	*p*-0.27	750	2012	[130b]	Different crystal types
$Cu_2Sn_{0.925}In_{0.075}Se_{2.1}S_{0.9}$	*p*-0.62	760	2012	[66b]	Doping, alloy
Cu_2SnSe_3	*p*-0.33	650	2013	[184]	Crystal structure
$Cu_2Ga_{0.075}Sn_{0.925}Se_3$	*p*-0.43	700	2013	[185]	Structure, doping
$Cu_2In_{0.1}Ge_{0.9}Se_3$	*p*-0.23	723	2014	[186]	In doping
Cu_2SnSe_3	*p*-0.48	773	2014	[187]	Structure
$AgBiS_2$	*n*-0.23	705	2013	[68b]	Structure, phase change
2mol% Bi+$AgSbSe_2$	*p*-1.15	680	2013	[68a]	Structure, doping
$Cu_4Sn_7S_{16}$	*n*-0.20	600	2015	[67]	Complex structure
$Cu_3Sb_{0.98}Se_3Bi_{0.02}$	*p*-0.70	600	2013	[188]	Structure, doping
$AgBi_{0.08}Sb_{0.95}Te_2$	*p*-1.04	570	2013	[98]	Energy filtering effect
$Ag_{0.96}Nb_{0.04}BiSe_2$	*n*-1.00	773	2013	[115]	Doping with Nb
$Cu_{15}As_{30}Te_{55}$	*n*-0.14	365	2013	[71a]	Controlled crystallinity of amorphous structure

$AgSbSe_2$+2mol%ZnSe	*p*-1.10	635	2014	[189]	Carrier engineering, nanodomains
$Ag(Sb_{0.93}In_{0.07})Te_2$	*p*-1.35	650	2014	[190]	In doping
$Cu_3Sb_{0.94}Ge_{0.06}S_4$	*p*-0.10	323	2014	[69a]	Doping with Ge
$Cu_{2.95}SbSe_4$	*p*-0.50	673	2014	[69b]	Cu deficiency
Cu_3SbSe_4+5vol% Zn_4Sb_3	*p*-1.37	648	2014	[69c]	EFE, composite
Cu_7PSe_6	*p*-0.35	575	2014	[70]	Extremely low thermal conductivity
Tl_9BiTe_6	*p*-1.20	500	2001	[75a]	Structure
$TlSbTe_2$	*p*-0.87	715	2005	[191]	Structure
Tl_4ZrTe_4	*p*-0.16	420	2010	[192]	Narrow band gap
$TlGdTe_2$	*p*-0.50	550	2012	[193]	Structure
$Tl_{8.98}Nd_{1.02}Te_6$	*p*-0.20	550	2013	[194]	Structure
$Tl_9Bi_{0.98}Te_6$	*p*-1.10	500	2013	[195]	Deficiency of element
Ag_9TlTe_5	*p*-1.20	700	2013	[74b]	Structure
$Tl_xCr_5Se_8$	*p*-0.5	800	2013	[196]	Structure
$Tl_{10-x-y}Sn_xBi_yTe_6$	*p*-0.90	500	2014	[197]	Doping
$Ni_{0.06}Mo_3Sb_{5.4}Te_{1.6}$	*p*-0.93	1023	2007	[76a]	Complex structure
$Mo_3Sb_{5.4}Te_{1.6}$	*p*-0.60	1000	2010	[76b]	Complex structure
$Fe_{0.05}Mo_3Sb_{5.4}Te_{1.6}$	*p*-0.31	673	2010	[77]	Complex structure
$Cr_{1.3}Mo_6S_8$	*p*-0.17	973	2010	[78a]	Complex structure
$Ag_{3.8}Mo_9Se_{11}$	*p*-0.70	800	2011	[78b]	Chevrel phase, Ag rattling
$Ag_2Tl_2Mo_9Se_{11}$	*p*-0.60	800	2014	[78c]	Complex structure

Table 5. Thermoelectric performance of Sn-X and In-X systems.

Materials	Type-ZT	Temperature (K)	Date	Ref.	Comments
$(In_{1.9}Al_{0.1}Te_3)_{0.08}+(SnTe)_{0.92}$	*p*-0.28	668	2011	[198]	Doping
0.25at%In+SnTe	*p*-1.10	873	2013	[32a]	Resonant doping with In
1.5at% In+ $SnTe_{0.85}Se_{0.15}$	*p*-0.80	860	2014	[199]	In doping, alloy
$Pb_{0.2}Sn_{0.8}Te$	*p*-0.13	570	2014	[200]	Thermal decomposition
$SnCd_{0.03}Te$+2%CdS	*p*-1.30	873	2014	[83]	Self-compensation of Sn and Cd, Band engineering, endotaxially nanostructured CdS
SnS	*p*-0.16	823	2014	[201]	Layer structure
SnSe	*p*-2.60	923	2014	[11]	Single crystal
SnSe	*p*-0.50	800	2015	[202]	Polycrystals
SnS	*p*-1.61	1080	2015	[203]	Calculation
SnSe	*n*-3.10	770	2015	[85]	Calculation
In_4Se_{3-x}	*n*-1.48	705	2009	[15]	Peierls distortion, charge wave density (CDW), Se deficiency, single crystal
In_4Se_3	*n*-0.60	700	2010	[204]	Polycrystals
$In_4Se_{2.95}$	*n*-0.60	700	2011	[84a]	Deficiency of Se
80wt% In_4Se_3+In_4Te_3	*n*-0.56	672	2011	[205]	Diffusion of Se into In_4Te_3
$In_{1.8}Cu_{0.2}Se_3$	*n*-0.55	846	2011	[206]	Formation of Cu_2Se slab, band engineering
$In_4Se_{2.67}Cl_{0.03}$	*n*-1.53	700	2011	[84b]	Cl doping, Se deficiency, single crystal
$In_4Se_{2.35}$	*n*-1.00	698	2011	[84c]	Polycrystals, BM, SPS
$In_4Se_{2.65}$	*n*-0.93	700	2012	[84d]	BM, hot pressing, Se deficiency
$In_4Se_{2.35}$	*n*-0.84	673	2012	[207]	Se deficiency
$SrTiO_3$+$InSe/In_4Se_3$ composite	*n*-0.25	600	2013	[138]	Composite
0.3 wt%Cu+In_4Se_3	*n*-0.97	723	2013	[208]	BM, Cu doping

$Fe_{0.05}In_{3.95}Se_3$	*n*-0.44	723	2013	[209]	Fe doping
$In_{1.25}Sn_{0.05}Se$	*n*-0.66	700	2013	[84e]	Sn doping, structure
$In_4Se_{3-x}Cl_y+BaIn_2Se_4$	*n*-0.75	675	2014	[210]	Phase separation
$In_4Pb_{0.01}Sn_{0.03}Se_{2.9}$	*n*-1.20	723	2014	[84f]	Doping

Table 6. Thermoelectric performance of metal chalcogenides with layered structure.

Materials	Type-ZT	Temperature (K)	Date	Ref.	Comments
$CuCrS_2$	*p*-2.00	300	2010	[88a]	Structure
$AgCrSe_2$	*p*-1.00	848	2011	[88b]	Structure, PLEC
$CuCrS_2$	*p*-0.90	350	2011	[211]	Structure
$CuCrS_2$	*p*-0.11	673	2012	[90]	Structure
$(AgCrSe_2)_{0.5}(CuCrSe_2)_{0.5}$	*p*-1.40	773	2014	[89]	Nanocomposite
$NiCrS_2$,$CuCrS_2$	*n*-0.024, *p*-0.023	313	2014	[212]	Structure
$CuCrSe_2$	*p*-0.17	300	2014	[213]	Structure
$(SnS)_{1.2}(TiS_2)_2$	*n*-0.37	700	2010	[91e]	Misfit layer structure
$Cu_{0.1}TiS_2$	*n*-0.50	800	2011	[91a]	Intercalation of Cu
$Co_{0.3}Ti_{0.7}S_2$	*n*-0.03	310	2011	[91b]	Intercalation of Cu
$Ti_{1.008}S_2$	*n*-0.34	663	2012	[92]	Near stoichiometric
$Cu_{0.11}TiSe_2$	*n*-0.15	650	2013	[214]	Intercalation of Cu
Li_xZrSe_2	*n*-0.26	300	2013	[91f]	Electrical chemical insertion of Li
$Ti_{1.025}S_2$	*n*-0.48	700	2014	[93]	Intercalation of Ti
$(LaS)_{1.2}NbS_2$	*n*-0.15	950	2014	[91g]	Misfit layered structure
TiS_2	*n*-0.28	373	2015	[91d]	Flexible, electrical, chemical insertion of organics
$Cu_{0.05}TiSe_{0.5}S_{1.5}$	*n*-0.54	700	2015	[91c]	Alloy, intercalation of Cu
Bi_2O_2Se	*n*-0.20	800	2010	[95]	Structure
$Bi_4O_4S_3$	*n*-0.03	300	2012	[215]	Structure
Bi_2O_2Se	*n*-0.0073	460	2013	[216]	Structure
$Bi_{1.9}O_2Se$	*n*-0.12	773	2015	[96]	Deficiency of Bi

Table 7. Thermoelectric performance of spinodal systems.

Materials	Type-ZT	Temperature (K)	Date	Ref.	Summary
$Cu_{0.2}Ag_{2.8}SbSeTe_2$	*p*>1.50	675	2010	[217]	In-situ precipitation, Cu doping
$Ag_{0.84}Sb_{1.16}Te_{2.16}$	*p*-1.53	500	2010	[97]	In-situ Ag_2Te precipitate
$(Ag_2Te)_{50}(Sb_2Te_3)_{50}$	*p*-1.55	533	2010	[218]	Wet chemical method, nanostructure
$(Ag_2Te)_{50}(Sb_2Te_3)_{50}$	*p*-1.22	593	2011	[219]	Nanodomain, EFE
$Cu_{0.2}Ag_{2.8}SbSeTe_2$	*p*>1.50	675	2010	[217]	In-situ precipitation, Cu doping
$Ag_{0.84}Sb_{1.16}Te_{2.16}$	*p*-1.53	500	2010	[97]	In-situ Ag_2Te precipitate
$Ag_{20}Pb_5Sb_{25}Te_{50}$	*p*-0.80	425	2012	[220]	Nanodomains
$AgPb_9Sn_9SbTe_{20}$	*p*-0.70	675	2012	[221]	Nanodomains
$AgPb_{18}SbTe_{18}$	*p*-1.10	573	2013	[222]	Ag/Sb ratio
$Ag_{25}Sb_{25}Se_{10}Te_{40}$	*p*-1.40	680	2015	[223]	Nanodomains
$Ag_{0.8}Pb_{18}SbTe_{20}$	*n*-1.02	673	2010	[224]	Nanodomains
$K_{0.95}Pb_{20}Sb_{1.2}Te_{22}$	*n*-1.60	750	2010	[225]	Nanodomains, Sb resonant doping, K substitution
$Ag_{0.4}Pb_{22.5}SbTe_{20}$	*n*-1.50	700	2011	[226]	Composition control
$Ag_{0.4}Pb_{22.5}SbTe_{20}$	*n*-1.50	700	2011	[226]	Nanodomains
$AgPb_{18}SbTe_{18}Se_2$	*n*-0.82	523	2012	[227]	Hydrothermal, composition control
$AgPb_{20}SbTe_{20}$	*n*-1.20	675	2012	[228]	BM+Oxygen level control
$Ag_{0.8}Pb_{22.5}SbTe_{18}S_2$	*n*-0.97	673	2012	[229]	S substitution
$AgPb_{18}SbSe_{19.928}Cl_{0.072}$	*n*-1.30	873	2013	[230]	Cl doping
$AgPb_{22.5}SbTe_{20}$	*n*-1.54	723	2014	[100]	Repeated BM, SPS
$Ge_{12}Sb_2Te_{14}$	*p*-1.00	673	2013	[106a]	Nanodomains
$(GeTe)_{11}(LiSbTe_2)_2$	*p*-1.00	723	2013	[107]	Nanodomains
$(GeTe)_{0.82}(Mn_{0.6}Sn_{0.4}Te)_{0.15}(Bi_2Te_3)_{0.03}$	*p*-1.54	700	2013	[231]	Composite with nanostructured Bi_2Te_3
$(Pb_{0.9}Yb_{0.1}Te)_{0.15}(GeTe)_{0.85}$	*p*-1.40	723	2014	[104a]	Yb doping
$Ge_{0.95}Mn_{0.05}Te$	*p*-1.30	773	2014	[104b]	Mn doping
$Ge_{0.75}Pb_{0.25}Te_{0.5}Se_{0.5}$	*p*-1.60	673	2014	[109]	Nanodomains
$Ge_{12}Sb_2(Te_{0.2}Se_{0.8})_{10}$	*p*-1.20	698	2014	[105]	Se substitution
$(GeTe)_{85}(Ag_{0.6}SbTe_{1.8})_{15}$	*p*-1.50	700	2014	[101]	Nanodomains
$Ge_{0.85}Te(Pb_{0.9}Yb_{0.1})_{0.15}$	*p*-1.40	723	2015	[103]	Yb doping

$(Ge_{0.8}Pb_{0.2})_{0.9}Mn_{0.1}Te$	*p*-1.30	723	2015	[104c]	Nanodomains
GeSbTe	*p*-1.48	670	2014	[106b]	Nanodomains
$(CoGe_2)_{0.2}(GeTe)_{17}Sb_2Te_3$	*p*-1.90	723	2015	[108]	Herringbone-like nanostructure

Table 8. Thermoelectric performance of PLEC materials.

Materials	Type-ZT	Temperature (K)	Date	Ref.	Comments
$Cu_{2-x}Se$	*p*-0.38	750	2011	[118]	PLEC
Cu_2Se	*p*-1.50	1000	2012	[16]	PLEC
Cu_2Se	*p*-1.60	973	2012	[232]	PLEC
$Cu_{1.97}Ag_{0.03}Se$	*p*-1.00	400	2013	[116a]	Phase transition
Cu_2SeI_x	*p*-2.30	400	2013	[17]	Critical scattering
$5wt\%SiO_2+Cu_{1.8}S$	*p*-0.28	623	2013	[121]	Nanocomposite
CuAgSe	*p*-0.80	623	2014	[116b]	Structure
$Cu_{1.97}S$	*p*-1.70	1000	2014	[233]	PLEC
CuAgSe	*p*-0.95	623	2014	[116c]	Structure
$Cu_{1.85}S$	*p*-0.11	623	2014	[117a]	Percolation effect
Cu_2Se	*p*-1.35	900	2014	[119b]	Wet chemical method
$Cu_{1.75}Te$	*p*-0.04	650	2014	[114]	Wet chemistry method
$Cu_{1.96}Se$	*p*-1.23	773	2014	[234]	PLEC
$Cu_{2-x}Se$	*p*-0.30	723	2015	[119c]	Wet chemical method, nanowires
Cu_2Se	*p*-2.10	973	2015	[122]	Full scale scattering
Cu_2Se	*p*-1.40	973	2015	[119d]	BM, SPS, Cu deficiency
CuAgSe	*p*-0.60	450	2015	[117b]	Element deficiency
$Cu_2S_{0.5}Te_{0.5}$	*p*-2.20	1000	2015	[123]	Mosaic crystal
$Cu_{1.97}S$	*p*-1.90	970	2015	[113]	PLEC
$Cu_{2-x}Te_{0.16}Se_{0.84}$	*p*-1.00	973	2015	[120b]	Alloying
$Cu_{2-x}Se$	*p*-1.80	973	2015	[235]	Quench method
$Ag_{1.37}Cu_{0.6}Te$	*p*-1.39	832	2015	[236]	Substitution of Cu
Ag_2Te	*n*-0.64	575	2010	[237]	High purity raw materials, high density
Ag_2Se	*n*-0.60	300	2011	[119a]	Hydrothermal, SPS
$Ag_2Se_{0.5}Te_{0.5}$	*n*-1.00	520	2013	[120a]	Alloying
$Ag_2Se_{1.08}$	*n*-1.00	400	2014	[116d]	Deficiency of Ag
$AgBiSe_2$	*p*-1.50	700	2012	[111]	Phase change

Table 9. Thermoelectric performance of other metal chalcogenides.

Materials	Type-ZT	Temperature (K)	Date	Ref.	Comments
Ga_2Te_3	*p*-0.16	850	2009	[126a]	2D-vacancy plane
$Ga_2Cu_{0.05}Sb_{0.2}Te_{2.75}$	*p*-0.50	700	2012	[126b]	Tuning of vacancy plane
$Cu_{0.05}Sb_{0.1}Ga_{1.9}Te_{2.95}$	*p*-0.21	631	2012	[127]	Band engineering, doping
$Ga_{1.9}Cu_{0.05}Sb_{0.1}Te_3$	*p*-0.41	750	2014	[125]	Engineering of vacancy plane
Au_2Te	*n*-0.09	450	2010	[128b]	Telluride
Ce_3Te_4	*p*-13.5	1200	2011	[128h]	Calculation
$Mn_{0.51}Te_{0.49}$	*p*-0.41	773	2013	[128i]	Broad band semiconductor
$MnTe_{0.9}S_{0.1}$	*p*-0.65	773	2014	[128m]	Solid solution
$TmCuTe_2$	*p*-0.81	745	2014	[128k]	Layer structure
$CdTe_{0.97}Cl_{0.03}$	*n*-0.20	630	2014	[128l]	Cl doping
$BaCu_{5.7}Se_{0.6}Te_{6.4}$	*p*-0.13	650	2011	[128e]	Complex structure
$Cs_xLaCu_{6-x}Te_6$	*p*-0.26	614	2011	[128f]	Complex structure
$Ce_{0.9}Cu_{0.1}Se_2$	*p*-0.18	800	2010	[128c]	Band engineering, CDW
$K_2Bi_8Se_{13}$	*n*-0.58	673	2013	[128j]	Complex structure
$Ba_{0.7}Cu_{0.3}Cu_2Se_2$	*p*-0.32	800	2015	[128n]	Layer structure
$LaGd_{1.02}S_3$	*n*-0.4	953	2011	[128g]	Self-doping
$NdGd_{1.02}S_3$	*n*-0.51	950	2011	[128a]	Self-doping
CoFeS	*n*-0.35	773	2013	[128o]	Complex structure
$Cu_{11}MnSb_4S_{13}$	*p*-1.13	575	2014	[128p]	Tetrahedrite structure
5% Co+FeS_2	*n*-0.02	600	2014	[128q]	Low cost
$(BiAgSeS)_{0.5}(BiAgSeS_{0.97}Cl_{0.03})_{0.5}$	*n*-1.23	773	2014	[128r]	Modulation doped
$Co_3Sn_{1.6}In_{0.4}S_2$	*n*-0.32	673	2015	[128s]	Structure

The table of contents

Metal chalcogenides, with extremely complex compositions and structures, usually feature both lower cost and higher performance than other thermoelectric materials. This paper provides a comprehensive review on the different kinds of metal chalcogenides as heat-electricity conversion materials. Several new strategies to further enhance their performance are also summarized.

Keywords: metal chalcogenides, thermoelectrics, enhancement of ZT, new strategies

Chao Han, Qiao Sun, Zhen Li,* and Shi Xue Dou

Thermoelectric enhancement of different kinds of metal chalcogenides

ToC figure